

Българско списание за **Инженерно ПРОЕКТИРАНЕ**

брой: 3 ноември 2009

ЦЕЛ И ОБХВАТ

„Българско списание за инженерно проектиране” е периодично научно списание с широк научен и научно-приложен профил. Целта му е да предостави академичен форум за обмен на идеи между учените, изследователите, инженерите, потребителите и производителите, работещи в областта на машиностроенето, транспорта, логистиката, технологиите, съвременното компютърно проектиране, а също така и в областта на различни интердисциплинарни научни и научно-приложни проблеми. Издателите приветстват научни публикации с високо качество и значими научни, научно-приложни и творчески приноси.

РЕДАКЦИОННА КОЛЕГИЯ

Почетен председател

Любомир Димитров Технически Университет-София, България

Председател

Божидар Григоров Технически Университет-София, България

Зам. председател

Милчо Георгиев Технически Университет-София, България

Членове

Димчо Чакърски Технически Университет-София, България

Димитър Ралев Технически Университет-София, България

Георги Дюкенджиев Технически Университет-София, България

Мирослав Денчев Технически Университет-София, България

Марин Георгиев Технически Университет-София, България

Веско Панов Технически Университет-София, България

Георги Тодоров Технически Университет-София, България

Николай Николов Технически Университет-София, България

Викенти Спасов Висше техническо училище „Тодор Каблешков”, България

Виктор Иванов Одески национален политехнически университет, Украйна

Vadea Lepadatescu Transilvania University of Braşov, Romania

Редактор

Росен Митрев Технически Университет-София, България

Издател: Машиностроителен факултет, Технически университет-София.

ISSN 1313-7530

Адрес на редакцията: София, бул.Климент Охридски №8, Технически Университет-София, бл.4, Машиностроителен факултет.

За контакти: bsip@abv.bg; **Електронна версия:** mf.tu-sofia.bg

Печат: Дейликонт ЕООД

Bulgarian journal for **Engineering Design**

No. 3 november 2009

AIM AND SCOPE

Bulgarian Journal of Engineering Design is a periodical scientific issue covering wide scientific and application areas of engineering activities. The aim of the journal is to provide an academic forum for exchange of ideas and information between scientists, engineers, manufacturers and customers working in the spheres of mechanical engineering, transport, logistics, modern computer – aided design and technology and solving different interdisciplinary scientific and applied problems. The editors welcome articles of substantial quality bearing significant contribution to the engineering knowledge.

EDITORIAL BOARD

Honorable chairman

Lubomir Dimitrov Technical University-Sofia, Bulgaria

Chairman

Bozhidar Grigorov Technical University-Sofia, Bulgaria

Deputy chairman

Milcho Georgiev Technical University-Sofia, Bulgaria

Members

Dimcho Chakarski Technical University-Sofia, Bulgaria

Dimitar Ralev Technical University-Sofia, Bulgaria

Georgi Diukendzhiev Technical University-Sofia, Bulgaria

Miroslaw Denchev Technical University-Sofia, Bulgaria

Marin Georgiev Technical University-Sofia, Bulgaria

Vesko Panov Technical University-Sofia, Bulgaria

Georgi Todorov Technical University-Sofia, Bulgaria

Nikolay Nikolov Technical University-Sofia, Bulgaria

Vikenti Spasov University of transport " Todor Kableskov", Bulgaria

Viktor Ivanov National Polytechnic University of Odessa, Ukraine

Badea Lepadatescu Transilvania University of Braşov, Romania

Editor

Rosen Mitrev Technical University-Sofia, Bulgaria

Publisher: Машиностроителен факултет, Технически университет-София.

ISSN 1313-7530

Publisher Address: Sofia, Kliment Ohridski blvd. №8, Technical University-Sofia, Mechanical engineering faculty.

Contact us: bsip@abv.bg; **Electronic version:** mf.tu-sofia.bg

Print: Deilikont Ltd.

СЪДЪРЖАНИЕ/CONTENTS

Numerical simulation of tensile mechanical behavior of lap welded reinforcing steel bar joints	5
Ch.Alk. Apostolopoulos, D. Michalopoulos, L. Dimitrov	
Experimental determination of test piece temperature intended for strength testing at increased temperatures	12
V. Tsonev, N. Nikolov	
Мегаметод „Фокуси” за решаване на евристични задачи	16
М.Лепаров	
Изследване на заварени конструкции с Solidworks Simulation	25
С.НИКОЛОВ	
CAD документиране на механично изделие за автоматизиран монтаж	31
Г.Динев, Х.Недев, Е.Чалъкова	
Измерване на покрития	36
Н.Цонев, В.Иванов	
Изследване на гъвкавия тръбопровод на перисталтичните помпи	40
В.Иванов	
Studies on the suspension stiffness control	44
M. Clinciu, L. Gaceu, D. Thierheimer, W. Thierheimer ,F. Popescu	
Research on optimizing of automatic ABS regulator	47
V. Cojocaru, F. Popescu, D. Thierheimer, D. Ola, W. Thierheimer	
Pneumatic mechatronic system for load simulation on toothed the rack heads	50
V.Cojocaru, N. Tane, D. Thierheimer, C. Mihai, W. Thierheimer	
Simulation of the braking process at the stroke end of linear hydraulic motors	54
I. Cristian	
Calculation of natural elastic compensators configurations	58
M. Urdea, E. Scheibner	
Mathematical modeling of the experimental data for the deep drawing force	63
I. Neagoe, A. Filip	
Improving energy efficiency of thermal to the neighborhood by mounting of solar collectors intended for the domestic hot water	68
Cristian Mugea, Buzatu Constantin, Lepadatescu Badea	

Energy Efficiency and Sustainable Development. Energy efficient material in a building system with real example	70
Crutescu Ruxandra, Crutescu Marin, Nicolaie Costache, Ismail Ozgur, Viorel Badescu, Dragos Hera, Florin Iordache, Liviu Drughean, Gabriel Ivan, Anica Ilie, Nadine Laaser	
An algorithm for optimization of a power distribution network	75
G. Sorea	
Инженерен анализ и симулация на 3D модел на стифираща машина, като част от АЛ за дребногабаритни бетонови изделия	79
И.Янакиев	
Синтезиране на система от графични символи за рационализиране проектирането на производствени системи	84
Р.Петкова	
Анализ на динамичното поведение на системата „Мостов кран-сграда” с метода на крайните елементи	89
К.Радлов, Н.Коцев	

NUMERICAL SIMULATION OF TENSILE MECHANICAL BEHAVIOR OF LAP WELDED REINFORCING STEEL BAR JOINTS

Ch.Alk. Apostolopoulos D. Michalopoulos L. Dimitrov
lubomir_dimitrov@tu-sofia.bg

Lap welded splices of reinforcing steel bars suffer from eccentricity problems and probable failures of the surrounding concrete due to the kinematic behavior of the end connections. After compliance with the demanding antiseismic regulations the adequacy and reliability of such splices and also structural reinforced concrete members becomes questionable. In the present investigation the tensile mechanical behavior of lap welded steel splices is examined, by applying loading up to the yield point region of the reinforcing steel. The results of the numerical simulation and analysis raise questions about the reliability of such types of joints.

1.Introduction

This article investigates the mechanical behavior of welded splices between new and existing reinforcement of concrete structures during addition of new columns and beams, a practice which is very common during building expansion. Common and cost effective practices of connecting rebar during reinforced concrete member expansion are:

- by lap splicing the old with the new steel bars, providing that there is adequate steel length, and
- by use of mechanical connectors and welded splices if the steel length is inadequate.

Mechanical connections are cost effective and they are usually made with proprietary splice devices of which the effectiveness and application is on a piece meal basis, providing that they satisfy the code requirements ^[1-4]. In Greece this procedure is governed by the ELOT 971 the ELOT 1421-3 standards, and 2008 code ^[5-7], using lap welded joints of new or new and pre-existing steel bars in a vertical upward or overhead position. Properly designed and well-executed splices are of vital importance in the construction industry. Where space limitations permit and when all requirements are satisfied lap splice is generally the predominant method of splicing and forming rebar connections. When lap splices, are impractical, or when their use is prohibited by the design codes, mechanical or welded connections are used to splice the reinforcing bars ^[8]. The weldability of reinforcing steel is encountered from the steel industry that produces

such steels. The codes are very specific about the welding methodology, as shown in Fig. 1.

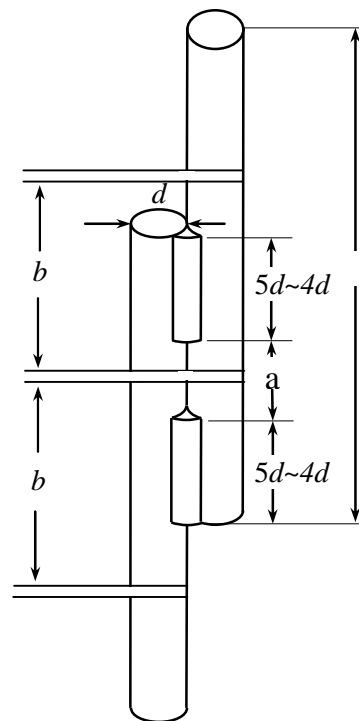


Fig. 1. Schematic of welded lap joint of reinforcing steel specimens ^[5-7].

As it may be realized from Fig. 1 eccentricity problems are likely to arise in lap joints which can be intensified especially during the installation of reinforcing steel bars, primarily in columns, where

luck of contact with the stirrups is frequently observed.

The luck of connectivity between the plain or welded main rebar of a column and the stirrups is met quite frequently. This is due to the extended use of ready made rebar cages. Therefore it is often observed that the distance between the main reinforcing bars and stirrups exceeds 50 mm. For this reason it is interesting to know the displacement of the ends of

the connections when the distance b has values between 500-1000 mm.

2. Welding of Reinforcing Steel and Methods

In the present study non corroded B500c steel rebar specimens were welded according to codes, as shown in Fig. 1 and 2, with two welding beads on one side only of $5d$ length and free space of a in between them^[5-7].

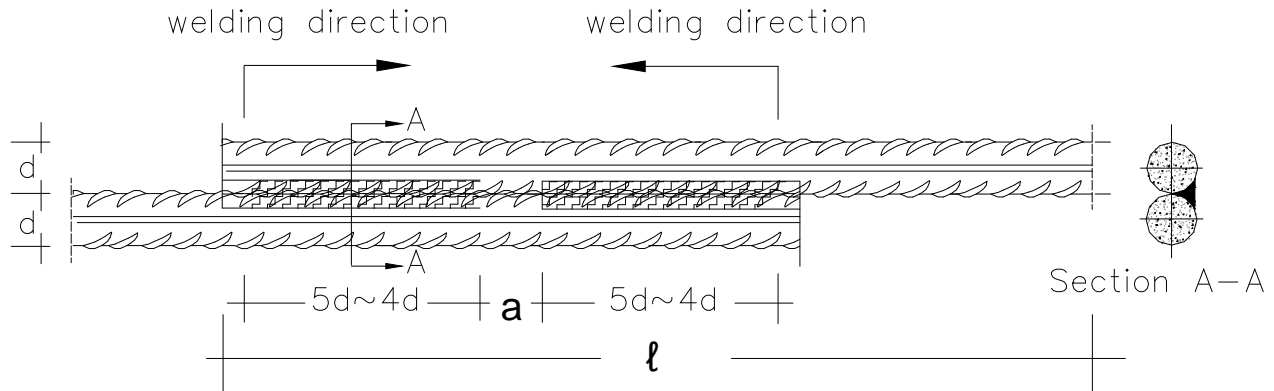


Fig. 2. Welded specimens

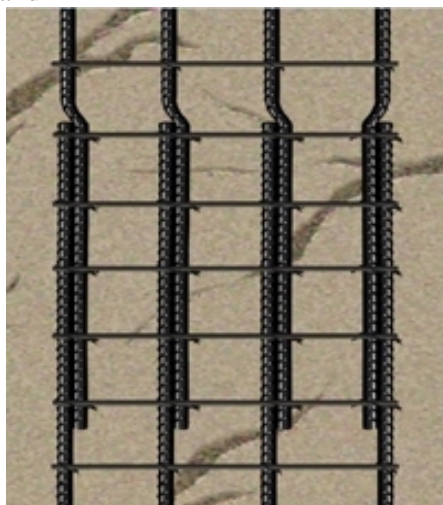
Figure 3, shows typical splicing of rebar and mechanical connectors.

Even though the traditional method of lap splicing is quite popular for joining old with new steel, due to its simplicity, it appears that it can create functional problems due to:

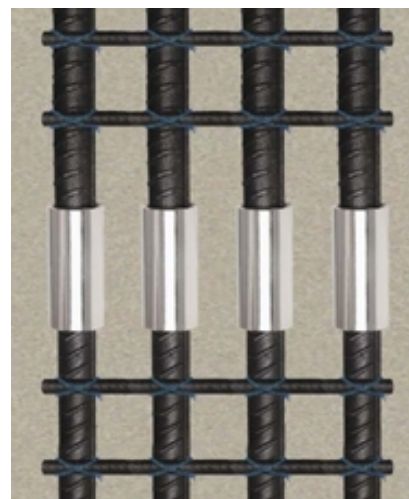
a) unequal tensile and compressive behavior of the joint and development of additional eccentric stresses^[9], and

b) side movement of the end connections in the region of the welded joints.

Such connection errors of lengthwise rebar with stirrups create reduced mechanical efficiency during earthquakes and reduced structural safety.



(a) Traditional lap splicing



(b) Mechanical splicing

Fig. 3. Rebar splicing

In this article an investigation was conducted in order to determine the mechanical and kinematic behavior and merit, of the ends of the connections of the lap-welded splices between new and existing B500c steel reinforcing bars which is produced during the last 4 years as an improved steel and was initiated due to the need for higher yield strength steel required in seismogenic regions like Greece, Romania, Turkey, and East Bulgaria. These types of joints are used in concrete structures during addition of new elements such as columns and beams. This is a practice very commonly used during building expansion. A numerical analysis was used in this process, and loading of the elastic model of the lap welded steel joint up to the point of yield strength (500 MPa) in the outer steel fiber, was examined.

Parameters considered during the analysis were:

- i) The rebar diameter,
- ii) the welding bead length $4d$ and $5d$ between the ends of the lap welded joints and the free length of the bars, as shown in Fig. 1.

The analysis of the lap welded steel joint without the influence of the concrete is legitimate since the concrete cover is of small thickness and can not affect the welded joint behavior. The eccentric loading mode of lap welded steel reinforcing bars was the incentive for further investigation of this issue^[9,10].

3. Numerical Simulation

In order to study the tensile mechanical behavior of the lap welded joints, the influence of the various geometric characteristics of the steel bars and of the welds, along with the appearing sideways movements of the ends of the bars, were examined through linear and non-linear analyses.

For the geometric mesh discretization of the welded bars, assuming smooth outer bar surface, the SOLID45 element of the ANSYS finite element analysis program (FEA) was used. This 8- nodes element with 3-degrees of freedom at each node is shown in Fig. 4a, while in Fig. 4b the 3-dimensional beam element LINK8 is presented, which was used to discretize the stirrups.

A typical finite element model of the lap welded rebar is presented in Fig. 5. The model sizes, concerning the number of nodes and elements for each case depend on the examined for each case geometry. Thus the number of nodes ranged between 14000-33000 and the corresponding elements between 12500-30000.

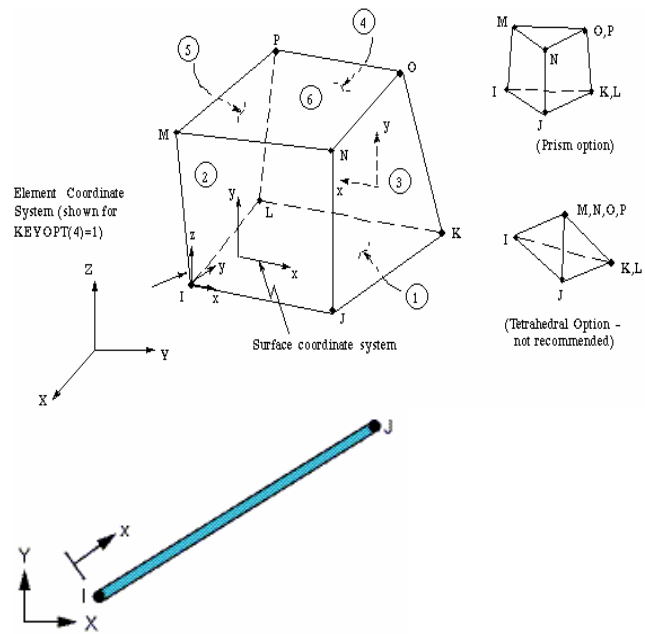


Fig. 4. Finite Element types : SOLID45 and LINK8

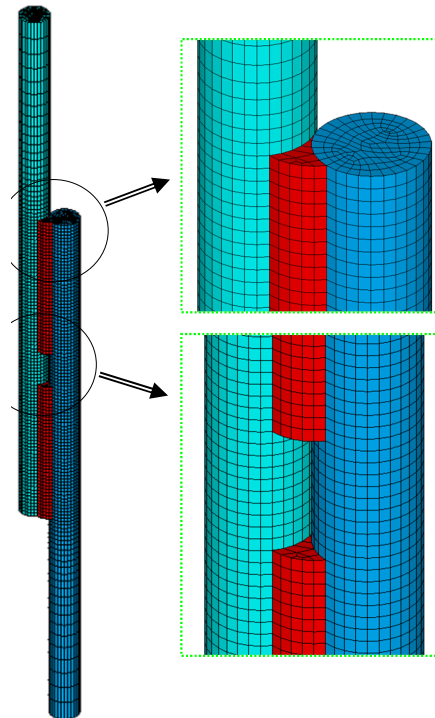


Fig. 5. Lap welded steel reinforcing bars finite element model

The bar and weld material were assumed to be steel with modulus of elasticity $= 210$ GPa and Poisson ratio $= 0.3$. The boundary conditions applied to the model concern the complete restraint of

all the degrees of freedom of the nodes that are found in the lower end of the bottom bar.

On the nodes of the upper end of the top bar, restrictions were applied on all degrees of freedom except of the vertical bar motion. At the same time on these nodes the same displacement was assigned also in the vertical direction. Figure 6 shows the boundary conditions applied on the finite element model.

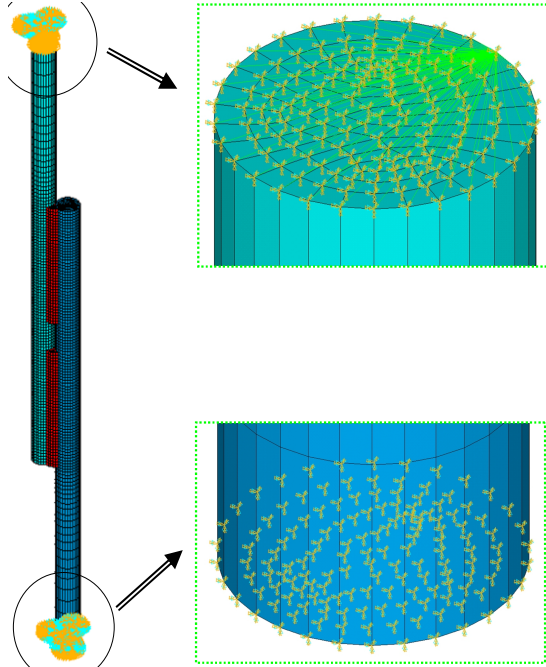


Fig. 6. Boundary conditions at the ends

4. Results

In the case of normal tension of the lap welded steel joints, the geometry is altered as it is expected, resulting in the dislocation of the edges of the bars. This dislocation is causing initially spot damage of the concrete which will evolve as a local explosion of the overlapped surrounding concrete. At this point it is necessary to accept an elastic behavior from the steel reinforcing bars until yielding of their external fibers occurs.

Analysis No. 1

Figure 1 indicates the variation of the lap welded bar ends of the maximum displacement for bar length $l = 300$ mm and welding bead length of $5d$ by varying the dimension "a" between 8-80 mm.

A linear elastic analysis was implemented with external tensile loading of 500 MPa in the model of Fig. 1. A combination of values of the parameters (l , d , a) of Table 1 were used and the results are

presented in Figures 7-9.

Table 1 shows the variables used for the geometry of No1 analyses.

Table 1. Values of geometric variables for analyses No. 1

variables	Values (mm)
l	500, 750, 1000
d	8, 10, 12, 16, 20, 24
a	8, 16, 24, 32, 40, 48, 56, 64, 72, 80

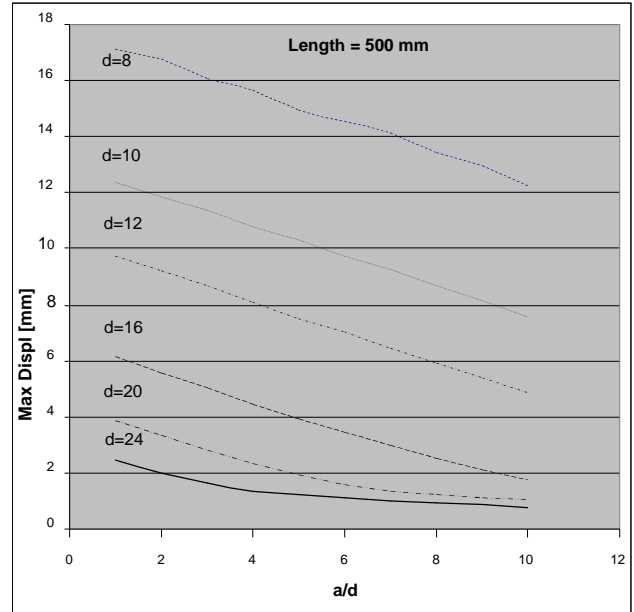


Fig. 7. Maximum lateral displacements of the lap welded bars as a function of the ratio a/d for different diameter values d and bar length of 500 mm

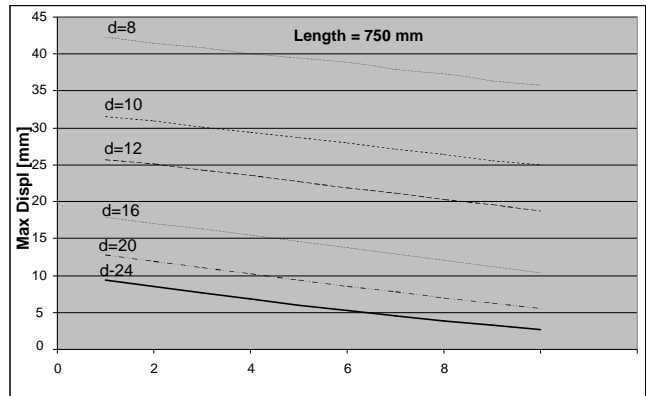


Fig. 8. Maximum lateral displacements of the lap welded bars as a function of the ratio a/d for different diameter values d and bar length of 750 mm.

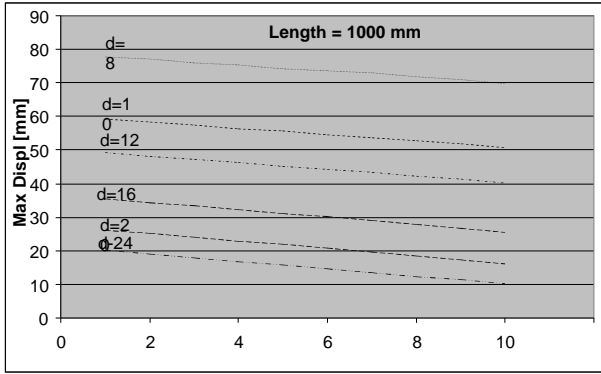


Fig. 9. Maximum lateral displacements of the lap welded bars as a function of the ratio a/d for different diameter values d and bar length of 1000 mm.

The following conclusions are drawn from the above analysis:

- a) The use of ready made rebar cages, where the length of the free length of the rebar may assume values between 500-1000, it might create considerable displacements of the ends of the lap-welded splices of the rebar.
- b) By increasing the free end of the larger diameter (20-24 mm) bars even though the end displacement is between 1-4 mm for 500 mm, or 3-13 mm for 750 mm, and 10-26 mm for 1000 mm, these types of displacements may create undesirable failures of the surrounding concrete of the column.
- c) By increasing the free end of the smaller diameter (8-10 mm) bars even though the end displacement is between 8-17 mm for 500 mm, or 25-42 mm for 750 mm, and 50-79 mm for 1000 mm, these types of displacements will definitely cause great failures to the surrounding concrete of the column. In addition lack of bonding between concrete and steel rebar will develop with all the negative consequences.

d) For the same length, the change of the above mentioned displacement values of the end connections progresses diminishing by increasing the value of the a/d ratio.

Analysis No. 2

Table 2 presents the values of the variables of the geometry of analyses No. 2 that were used.

Table 2. Geometric variable values of analyses No. 2

Variables	Values (mm)
l	300, 400, 500, 600, 700, 800, 900, 1000
d	8, 10, 12, 14, 16, 18, 20

In Fig. 10 and Table 3 the calculated maximum lateral displacements of the ends of the lap welded bars are presented as a function of the variables of Table 2. It is noted that these values were equal both for tension and compression.

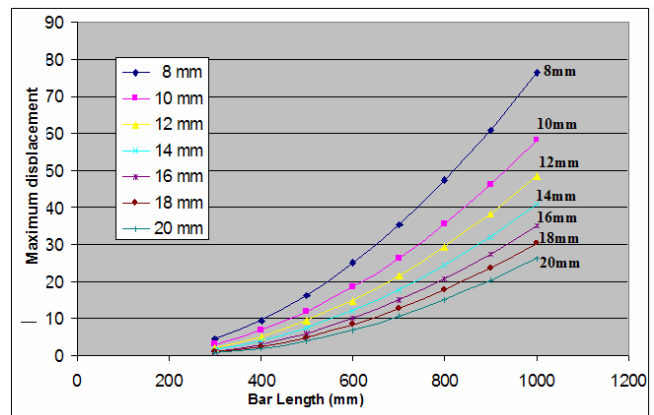


Fig. 10. Maximum lateral displacements of the lap welded bars as a function of the length of each bar for different diameter values.

Table 3. Maximum lateral displacements of the ends of the lap welded bars (No.2 Analyses).

Bar diameter (mm)	Bar length (mm)								
	a=20mm	300	400	500	600	700	800	900	1000
8 mm		4,30	9,40	16,28	24,88	35,19	47,21	60,93	76,36
10mm		2,83	6,63	11,83	18,39	26,31	35,59	46,22	58,20
12mm		1,98	5,05	9,35	14,84	21,50	29,31	38,28	48,41
14mm		1,38	3,85	7,45	12,11	17,79	24,49	32,19	40,91
16mm		0,99	2,97	6,03	10,07	15,04	20,92	27,70	35,39
18mm		0,81	2,25	4,83	8,29	12,60	17,72	23,65	30,39
20mm		0,71	1,71	3,86	6,84	10,58	15,06	20,27	26,20

The following conclusions (a=20mm) are drawn from the above analysis:

For 300 mm bar length the end displacement progresses diminishing

a) For 300 mm bar length the end displacement progresses diminishing from 4.30–0.70 mm for 8–20 mm diameter areas accordingly.

b) On the other hand when the bar length becomes 1000 mm the end displacement jumps to a range of values between 76.3-26.2 mm for 8–20 mm diameter areas accordingly.

Analysis No. 3

Table 4 presents the values of the variables of the geometry of analyses No. 3 that were used.

Table 4. Geometric values of the variables for No. 3 analyses

Variable	Values (mm)
l	300,400,500,600,700,800,900,1000
d	8,10,12,14,16,18,20
a	20,30,40,50,60,80,100,150,200

Figures 11 and 12 present the calculated maximum lateral displacements of the welded bars as function of the variables of Table 4.

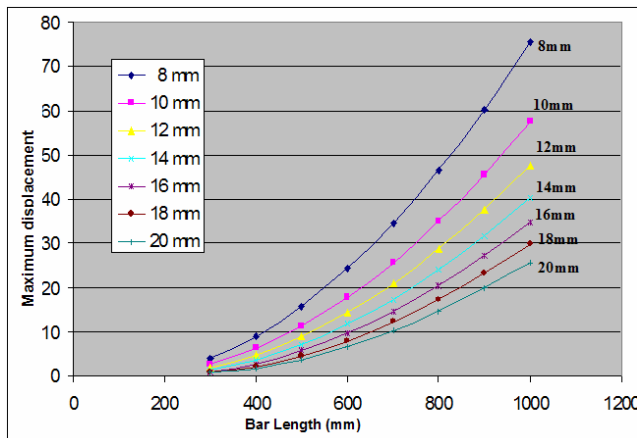


Fig. 11. Maximum lateral displacements of the lap welded bars as a function of the length of each bar for different diameter values and 30 mm distance between beads.

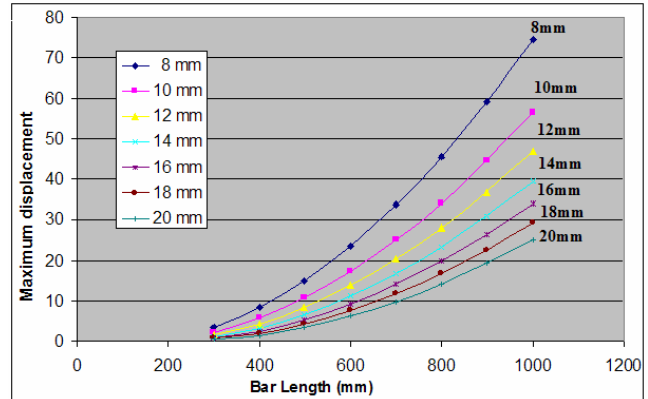


Fig. 12. Maximum lateral displacements of the lap welded bars as a function of the length of each bar for different diameter values and 40 mm distance between beads.

The results of analysis No. 3 are similar to those of analysis 2.

5. Conclusions

Lap welded splices of steel rebar are susceptible to eccentricity problems and probable failures of the surrounding concrete due to the kinematic behavior of the end connections.

The mechanical characteristics of maximum sustained load and elongation at maximum force between joints of new and existing reinforcement of concrete structures during addition of new columns and beams, has shown that:

- a) Lap welded joints of larger diameter bars appear as a rule to cause smaller displacements of their end sections versus the smaller diameter bars.
- b) An increase in the “a/d” ratio creates as a rule a decrease in the displacements of the ends of the same diameter bars.
- c) A reevaluation of the existing design codes, treating complex tensile or compressive behavior of welded splices, is mandatory.

Further investigation is required on the welding methods in order to promote and secure the safety of reinforced concrete structures and especially during expansion and addition of new elements.

References:

1. ACI code, AWS D1 4-92 ,American Welding Society, Structural welding code reinforcing steel, D1, 4-92.
2. Metal Arc Welding of Steel for Concrete Reinforcement, CEN 247/BS 7123, 1989.

3. Welding of Reinforcing bars in reinforced concrete structures, W186-M 1990, 1998.
4. Welding of Reinforcing Steel, prEN ISO 17660, 2002.
5. Weldable Steels for the Reinforcement of Concrete, ELOT 971, Hellenic Standard, Athens, 1994.
6. Steel for the Reinforcing of Concrete-Weldable Reinforcing Steel-Part 3, ELOT 1421-3, Hellenic standard, Technical class B500c, Athens, 2005.
7. Reinforced Concrete Steel Code Technology, 2008 (Government Gazette No. 1416 / / 17.07.2008), Hellenic Ministry of Public Works.
8. Hellenic Reinforced Concrete Code, EKOS 2000, Athens, 2000.
9. Ch.Alk.Apostolopoulos, D. Michalopoulos, L.Dimitrov, The Impact of Corrosion on the Mechanical Behavior of Welded Splices of Reinforcing Steel S400 and B500_c, Journal of Materials Engineering and Performance, pp.70-79, 2008.
10. C.A. Issa, An Experimental Study of Welded Splices of Reinforcing Bars, Building and Environment, 2006, 41(10), p 1394–1405.

Ch.Alk. Apostolopoulos , University of Patras

D. Michalopoulos , University of Patras

L. Dimitrov , Technical University of Sofia

EXPERIMENTAL DETERMINATION OF TEST PIECE TEMPERATURE INTENDED FOR STRENGTH TESTING AT INCREASED TEMPERATURES

Veselin Tsonev
tzonev@tu-sofia.bg

Nikolay Nikolov
nyky@tu-sofia.bg

This article describes the methodology and presents the results of temperature measurement in different points of a test piece, intended for strength testing at increased temperatures. The aim is to check the temperature field homogeneity and the work temperature deviation from the given values in specialized device for strength testing at increased temperatures. It is concluded that the device answers the requirements for making such tests.

Key words: temperature measurement, high temperature strength test

1. Introduction

In order to estimate the material working capacity, a test piece of the material is subjected to strength testing in normal and extreme conditions. The purpose is to determine the different strength material properties, which are of utmost importance to the exploitation –yielding limit, ultimate strength, creep limit etc. These limits represent critical stress values for the material, causing plastic strain or rupture. As these phenomena are inadmissible in practice, the details are designed with allowable stress, which is part of the critical stress.

Various material strain properties are normally defined in the course of the strength testing. More often these are the Young's modulus E of the material, representing the relation between the normal stress and the engendered by it longitudinal strain in the same direction, and the coefficient of the transversal strain μ , (known as the Poisson's coefficient), representing the relation between the transversal and longitudinal strains [1].

The main stress-strain properties of the materials are standardized. So are also the requirements towards the methods and the means for their definition [2]. In the matter of strength testing at increased temperature, the standard specifies the allowable deviations from a specified test temperature . For the different temperature ranges they are as follows:

$\pm 3^\circ$	for	600°	
$\pm 4^\circ$	for	$600^\circ <$	800°
$\pm 5^\circ$	for	$800^\circ <$	1000° .

Three thermocouples, situated at equal distance along its working length (the length of the test piece part with minimal cross-section area), are enough to control the test piece temperature. The thermocouples shall make good thermal contact with the surface of the test piece and their sensitive point shall be screened from direct radiations from the furnace walls.

The temperature measuring device shall have a resolution of at least 1° and a precision of $\pm 2^\circ$.

In order to be able to carry out strength testing at increased temperatures, the "Strength of materials" department of the Technical University - Sofia, has designed and developed a special device, consisting of a specialized furnace and clamping elements, made of heat-resistant steel [3]. The device has been designed to work together with a standard testing machine ZD 20, allowing a load of up to 20 tons (fig.1). The purpose of the present research is to verify whether the developed device can maintain the test piece working temperature within the range, set by the standard.

2. Furnace's special features

The specialized furnace represents an enclosed heat-insulated space with electric heater mounted on its walls [4]. The maximum working temperature of the furnace is 1100° . There are 16 electric heaters in total, grouped along the height of the furnace walls in two sections, each with an active power of 1500 W. In order to maintain the working temperature within the required range, each section has got an independent programmable temperature controller, receiving

information about the working space temperature in the corresponding section from a special type “ ” thermocouple. The operator can set the testing

working temperature, as well as the heaters’ switching on and off temperatures.



Fig.1 Heating module for material strength testing at increased temperatures



Fig.2 Thermocouples position and numbering

The dimensions of the furnace’s working space are 170 330 230 mm. There are two cylindrical apertures on the back side, letting pass the controlling thermocouples. A cylindrical aperture on the upper and one on the lower part, let pass the clamping elements. A door on the front allows placing or replacing the test piece. Next to this door there is a rectangular opening, through which pass strain measurement system elements. In our case these are the control thermocouples, necessary for the present research. All furnace apertures are made tight with insulating wadding in order to reduce the heat losses.



Fig.3 Temperature measurement device

The clamping elements are details made of high-alloy steel, ensuring the connection between the test piece, placed in the middle of the furnace working space, and the clamps of the testing machine. The material of the clamping elements allows a maximum working temperature of 1250° at a relatively low thermal conductivity. Nevertheless, as these elements are made of steel and are in contact with the furnace working space, as well as with the atmosphere and the cold details of the testing machine, it is supposed that there will be considerable heat losses through them. The present research will verify whether these losses will lead to inhomogeneous heating of the test piece, or even to lower temperature of the test piece compared to the furnace working space temperature.

3. Test piece temperature measurement

The experiment has been carried out in the following sequence:

3.1. Holes 2 mm deep are driven in the working part of the test piece.

3.2. The clamping elements and the test piece are mounted in the furnace.

3.3. Three thermocouples type TSSB() - NiCrNi (7/ 8) with work temperature up to 1100° are placed in the driven holes (3, 4 and 5 on fig. 2).

3.4. A thermocouple of the same type (2 on fig.2) is placed near the sensitive point of the thermocouple, controlling the heaters' upper section (1 on fig.2), in order to determine whether there is a difference between the indications of both thermocouples.

3.5. The values of both temperature controllers are set to the desired work temperature and the furnace is put in operation.

3.6. After the work temperature in both sections is reached, the furnace is left working for three hours in order to steady the process.

3.7. Using a portable temperature measuring device HS 700 (fig.3) the test piece temperature is observed in the three points of its working part.

The measurement is made at a work temperature of 1000° . The temperature controllers are programmed so that to switch on the heaters at 996° and switch them off at 1000° . After reaching 1000° the temperature continues to increase, due to the process inertness, and reaches $1001-1002^{\circ}$ before decreasing again. The work temperature variations lead to constant changes in the test piece temperature.

A periodicity of the furnace operation was established in the course of the measurement. The

temperatures, measured with the five thermocouples for one furnace working cycle are given in Table 1. The curves of the five temperatures changes in time are shown on fig.4.

Table 1. Measured temperatures

time, s	1, °	2, °	3, °	4, °	5, °
0	1000	993	996	996	997
10	1001	994	997	997	998
20	1002	995	997	998	999
30	1001	997	999	999	1001
40	1000	999	1000	1002	1003
50	1000	1001	1002	1003	1004
60	998	1003	1004	1004	1004
70	995	1004	1004	1003	1002
80	995	1004	1003	1001	1000
90	996	1001	1001	999	999
100	997	997	999	998	998
110	998	994	997	997	997
120	1000	993	996	996	996

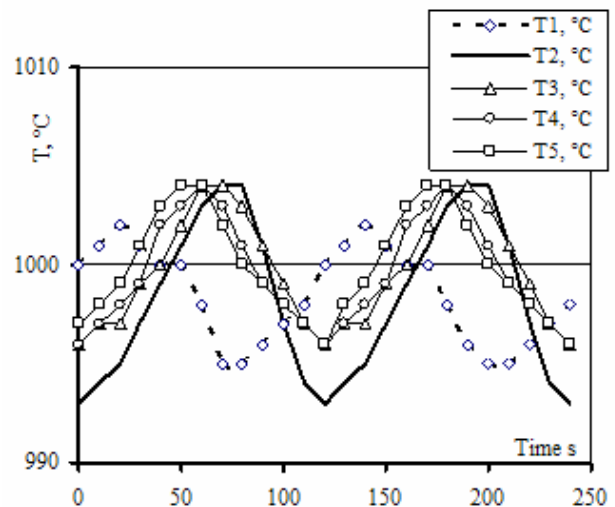


Fig.4 Temperature variations with time

The results obtained show that there is little difference and dephasing in the temperatures, measured by both types of thermocouples. This is due to the different construction of their bodies - that of the controlling thermocouple has greater diameter, which makes it more inert. That's why the measured temperatures with thermocouple 1 are within the range of $995-1002^{\circ}$, and those measured with thermocouple 2 - are within the range of $993-1004^{\circ}$.

The results obtained show that the highest test piece temperature measured is 1004° , and the lowest – 996° .

4. Inferences

1. The developed experimental device provides test piece heating up to 1000° .

2. The measured temperatures of the test piece are within the allowable limits according to the standard EN 10002-5.

3. For one heaters' work cycle the test piece temperature in the three controlled points does not differ with more than 3° . This difference follows the

temperature variation cycle within the working field. This shows that the temperature field in the vicinity of the test piece has got the necessary homogeneity for the needs of the planned strength testing at high temperatures.

5. Conclusion

The developed experimental device answers the necessary requirements for running tests at temperatures within the range of 800-1000° and it can be used to determine the materials' stress-strain properties at such temperatures.

References:

[1] Silva V.D., Mechanics and Strength of Materials, Springer, Netherlands, 2006.

[2] EN 10002-5 5: -

[3] Nikolov N., Tsonev V., "Reconstruction of a heating device for brief material testing at high temperature". Proceedings of "TechSys 2009", Plovdiv, Bulgaria, 2009.

[4] , Sofia, Bulgaria, 1982.

Assist.Prof. Veselin Tsonev, Technical University- Sofia
Assist.Prof. Nikolay Nikolov, Ph.d, Technical University- Sofia

” ”

mleparov@tu-sofia.bg

1.

()

[1-3]

$p_i, i=1,2,\dots,N.$

$p_{ij}, j=1,2,\dots,N_i.$

$p_{ijk}, k=1,2,\dots,N_{ij}.$

[p]-

().

(. .I) ,, ” ;

2.

[p_{ij}]-

[p_{ijk}]-

(),

()

, , , , : (.2.1 3.1)
 (.1.1 1.1' .1), (.3.2), , ,
 (.1.2 .1.2') , (.1.3 ; (.3.3), .
 .1.3'), ;
 , . , .

2

” ”			
		, ,	3
		, , , ,	5
		,	2
		, , , , , , .	6 ⁺
		, ,	3
		,	2
		1, 2, 3, 4	4
		, , , , ,	5
		,	2
		, , , , , , ,	5
		, , , , , , ,	6 ⁺
		2 , , 1 , , , ,	5
		, ,	3
		, , , , , ,	5
		, , , , , , ,	6 ⁺
		1 , , , , ,	4
		, , , , , , ,	6
		,	2
		,	2
		3, 4	2
		,	2

	(.1)	(.1)	(.1)	(.1)
1	1.1, 2.1, 3.1, 5.1	1.1', 2.1', 3.1', 5.1'	4.1	6.1
2		1.1', 2.1', 3.2', 5.1'		
3		1.1', 2.1', 3.3', 5.1'		
4		1.1', 2.2', 3.1', 5.1'		
5		1.1', 2.2', 3.2', 5.1'		
6		1.1', 2.2', 3.3', 5.1'		
7		1.1', 2.3', 3.1', 5.1'		
8		1.1', 2.3', 3.2', 5.1'		
9		1.1', 2.3', 3.3', 5.1'		
10		1.2', 2.1', 3.1', 5.1'		
11		1.2', 2.1', 3.2', 5.1'		
12		1.2', 2.1', 3.3', 5.1'		
13	1.3, 2.1, 3.1, 5.1	1.3', 2.3', 3.1', 5.1'	4.2	6.1
14	1.2, 2.1, 3.1, 5.1	1.3', 2.1', 3.1', 5.1'		
15	1.1, 2.2, 3.1, 5.1	1.1', 2.1', 3.1', 5.1'		
16	1.1, 2.2, 3.2, 5.1	1.3', 2.1', 3.1', 5.1'		
17	1.1, 2.1, 3.1, 5.2	1.1', 2.1', 3.2', 5.2'		
18	1.1, 2.1, 3.1, 5.1	1.2', 2.1', 3.2', 5.2'		
19	5.1	1.3', 2.3', 3.1', 5.1'		
20		1.1', 2.3', 3.2', 5.1'		
21	1.2, 2.1, 3.1, 5.1	1.1', 2.3', 3.1', 5.1'		
22	1.1, 2.1, 3.1, 5.1	1.1', 2.1', 3.1', 5.1'		
23		1.1', 2.1', 3.2', 5.1'		
24		1.2', 2.1', 3.1', 5.1'		
25		1.1', 2.2', 3.1', 5.1'		

P_{11} [, ,];
 P_{12} [, ,];
 P_{13} [, ,];
 P_{14} [, ,];
 P_{21} [, ,];
 P_{22} [, ,];
 P_{23} [, ,];

.1: 1, 2, 3, 5; 1', 2', 3', 5'
 - 4. 4 25

p1 p2: " "-
 :
 , . . . P₁₁ [, ,]
 ,] -

p24 [, ,];

5

(.4)	(.3)		(.3)	
1				
2			()	
3			()	
4				
5			()	
6			()	
7				
8			()	
9			()	
10			()	
11			()	
12			” ” ()	
13				
14			” ”	
15				
16			()	
17				
18				
19				
20				
21				
22				
23	()			
24				
25				

1.

3.

a :

1.

2.

[1-3].

4. .1, “ ” (

5. () “ ” ();

6. .5 “ ” (, , ,

(), () ;

7. “ ” (“ ”);

” [1-3] “ ” (

” ” ;

“ ” (,

);

” ” ”;

“ ” ();

“ ” (

;

.3 “ ”);

“ ” (- ,);

;

;

(-) “ ” (,

1. “ ” ”);

2. “ ”

3. (“ ”);

.2. “ ” ();

“ ” (“ ”);

“ ” (“ ”);

.3. (“ ” , ..);

4-7. .4 25 “ ”

” .5

” ”

6.1 1.1, 2.1, 3.1, 5.1; 1.1', 2.2', 3.1', 5.1'; 4.1;

6.1 1.1, 2.2, 3.2, 5.1; 1.2', 2.3', 3.1', 5.1'; 4.1;

” ”;

() - ;
 () - ; “ ” /);
 () - ; “ ” / ();

1.1, 2.1, 3.1, 5.1; 1.1', 2.3', 3.1', 5.1'; 4.1; (

6.1

; ,
 ; ;
 - ; ;
 () - ;
 () - ; “ ” / ();
 () - ; “ ” / ();
 () - ; “ ” / ();
 ; “ ” / ();

1.1, 2.1, 3.1, 5.1; 1.3', 2.3', 3.1', 5.1'; 4.1; (

6.1

; ,
 , ((),
); “ ” /);
 , (();
); “ ” /);
 , (();
 ” ” (); “ ” /
 , (, / ((;
 , (”); “ ” , (;
 , ” (”); “ ” , “ ?” .);
 , (“ ” /);
); (“ ” /);

1.1, 2.1, 3.1, 5.1; 1.3', 2.1', 3.1', 5.1'; 4.1;

6.2

“ ” ” / 180°);
 “ ” / (;
 / (-);
);
 “ ” / 1,
 / (, - .

-
- [1] „...”, 2008.
- [2] „...”, 2008.
- [3] : , , , “ - ”, ..1995.
- [4] . . “ ” , 16 . - . .
 . ” 2007, ., 2007.

MEGAMETHOD “FOCUSES” FOR HEURISTIC TASKS SOLVING

M. Leparov

bstract

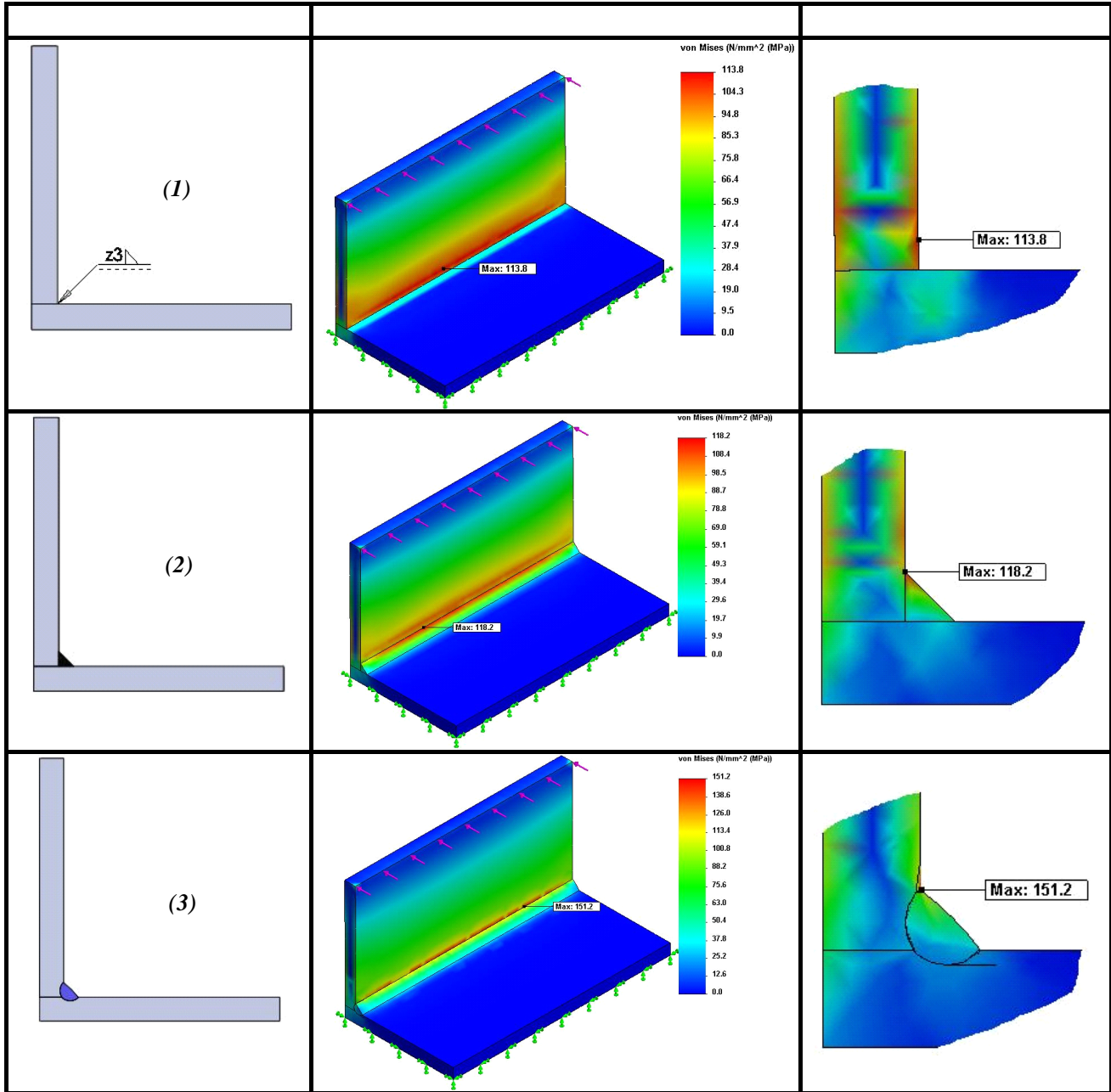
Problems, that cannot be formalized and for what no methods to solve them are known, are called heuristic problems. There are many heuristic methods for solving them, which represent a set of guiding steps. The objective of the present work is to propose a new method named megamethod designed for the cteation of heuristic methods through which heuristic problems can be solved.

Key words: heuristics, heuristic methods, megamethods, heuristic tasks

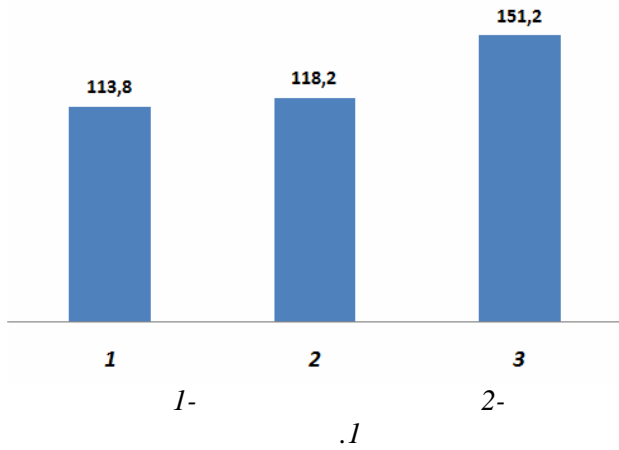
Prof. Mihail Leparov, PhD, Technical University – Sofia

(2) (3) -

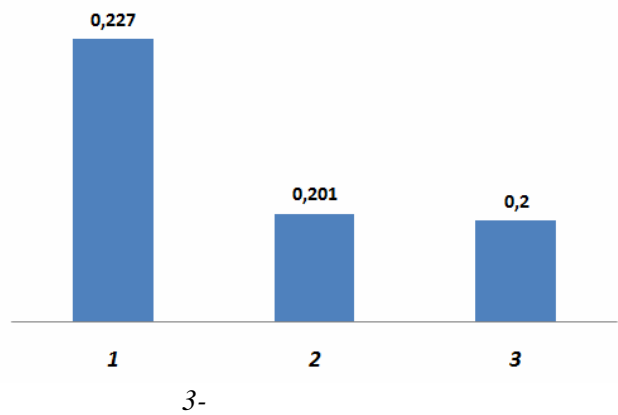
1



Получавани максимални напрежения по von Mises [MPa]



Получавани максимални еластични премествания [mm]



2.

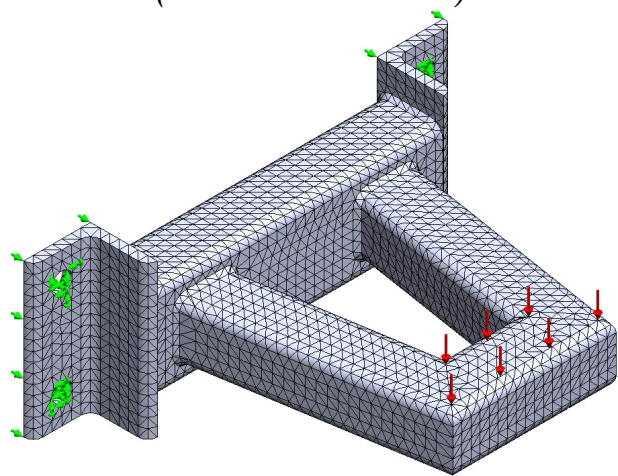
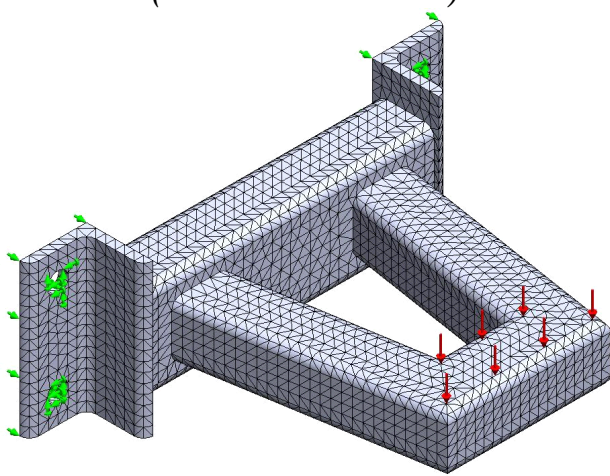
1

3D

.2

1

2



.2

SolidWorks

3.

Simulator

.3

.4

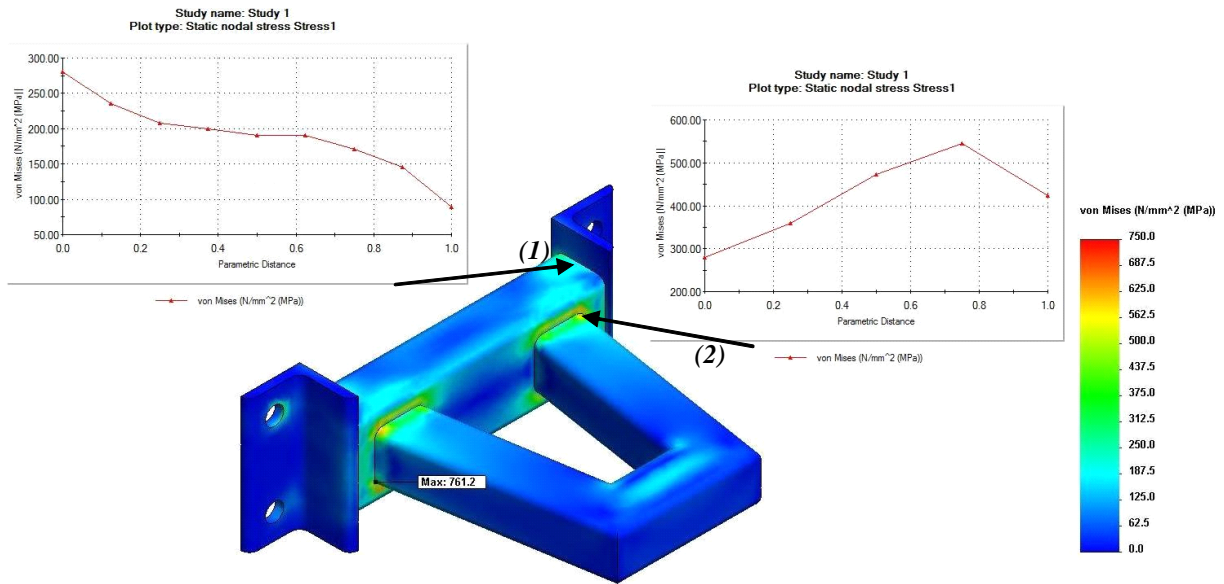
von

[1]

Mises

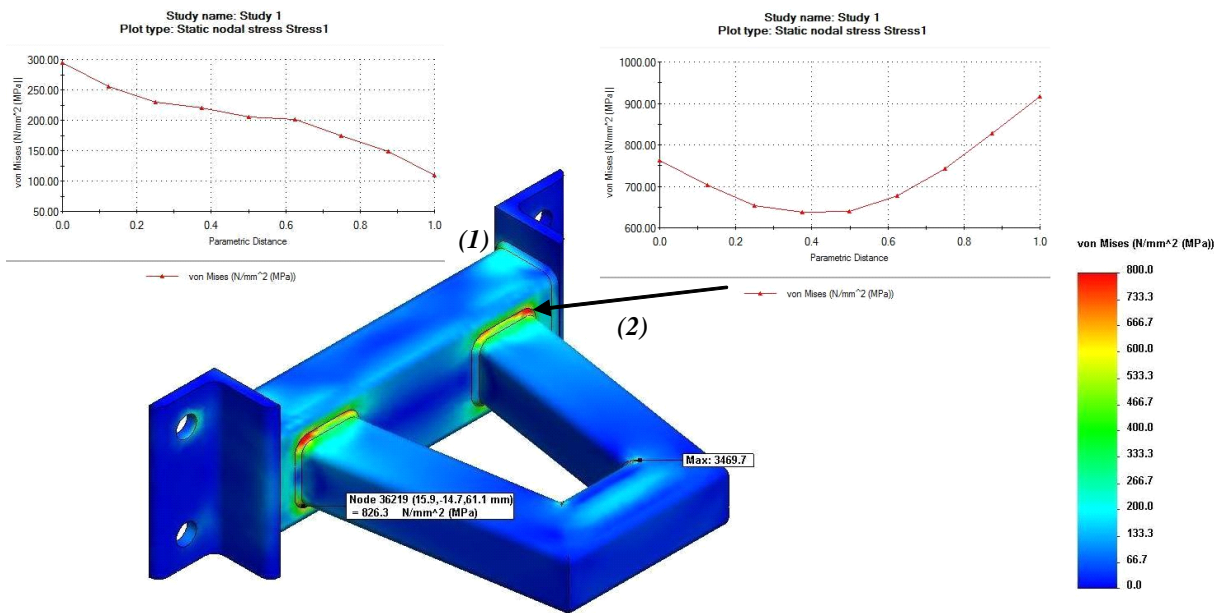
/ mesh).

(Bonded / Incompatible



.3

von Misses 1



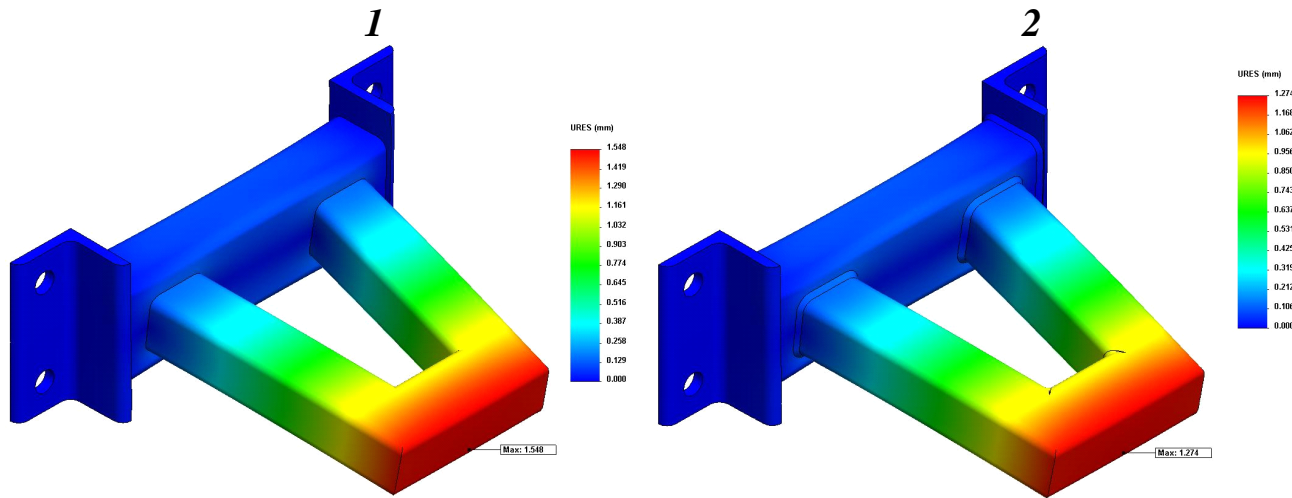
.4

von Misses 2

[MPa]	761,2 [MPa]	1''	3469,7	826,3 [MPa].	1''	2''	8,5%.	-
	2'',				1''			-
					2''		4%.	-
			2''.					-

1" 750/910 [MPa] „ 2 (290/420 [MPa] „ 2").

.5



.5

.5

[mm] „ 1" 1,274 [mm] „ 20% (1,548 2").

4.

[2]

5.

3D

1. :
„ SolidWorks Simulation, VI,
. 2(112), 2009 ., ISSN-13 10-3946, (513-519)
2. „ „ VI, . 2(112), 2009 ., ISSN-13 10-3946,
(533-539)
3. SolidWorks 2009 Online User’s Guide, SolidWorks Corp., 2008
4. SolidWorks Simulation 2009 Online User’s Guide, SolidWorks Corp., 2008

STUDYING WELDED CONSTRUCTIONS BY SOLIDWORKS 3D SIMULATION

S. Nikolov

Abstract

Welded constructions find wide application in different engineering products. The possibilities of 3D welds introduction given by CAD systems when 3D modeling parts is considered in this paper. The differences which result from that when making static analysis of welded constructions by the CAE system SolidWorks Simulation are studied.

Keywords: *welded constructions, static analysis, CAD, CAE, SolidWorks Simulation*

Assist. prof. Stiliyan Nikolov, Ph.d, Technical University-Sofia

CAD

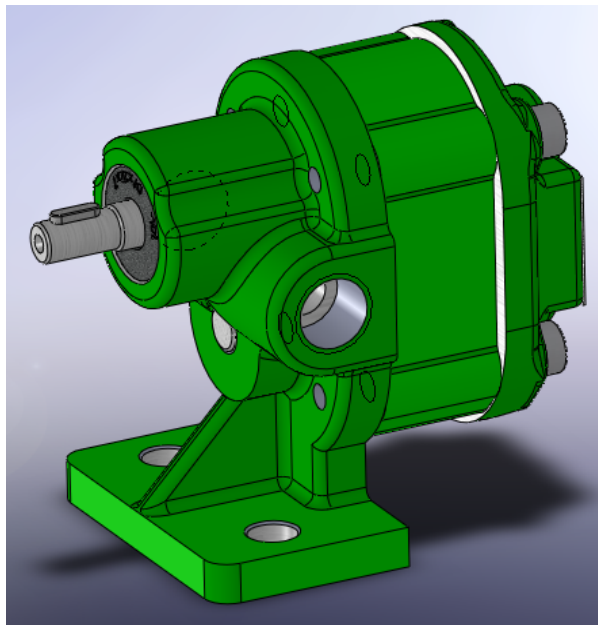
[3].

[10].

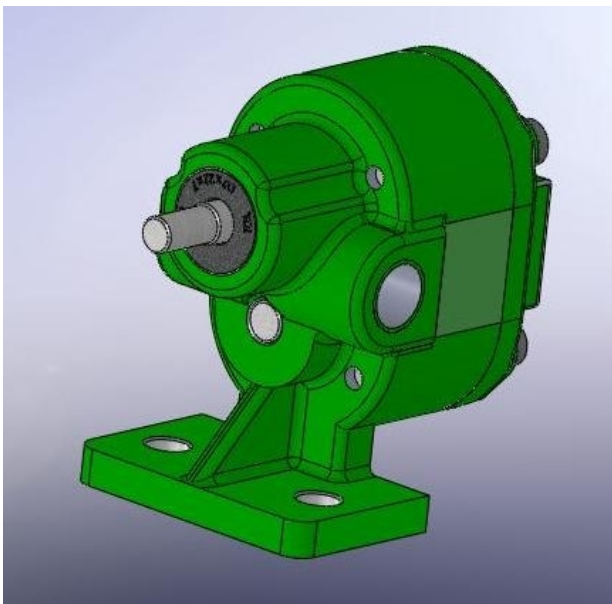
3D

2D

AutoCad.



.1



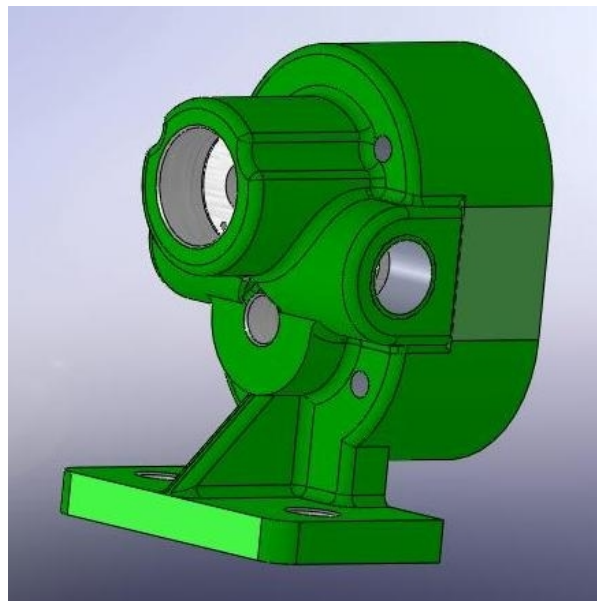
.2

[4]

“EXTRUDE”.

CAD

.3.



.3

().

3D

AutoCAD,

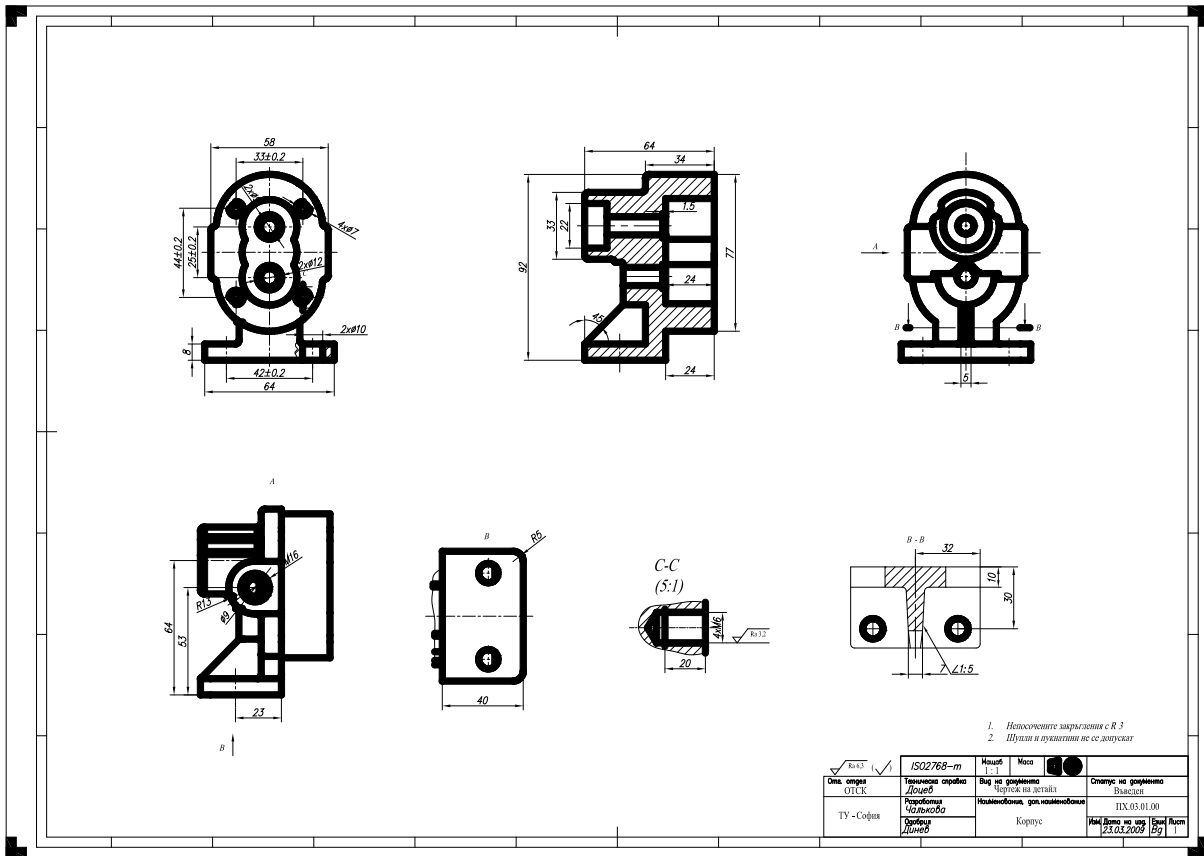
.4.

.6.

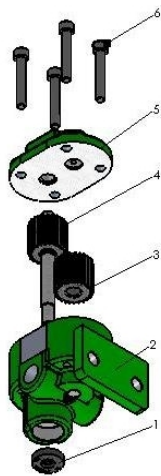
(.5),

CAD

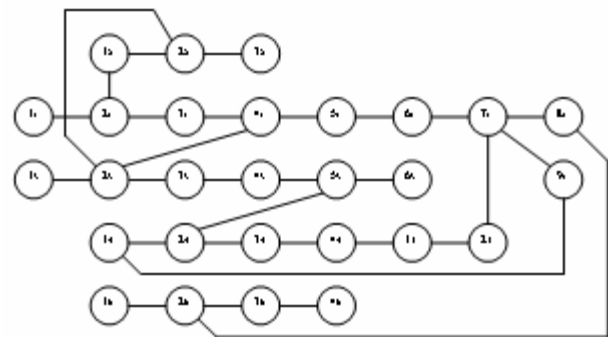
.7.



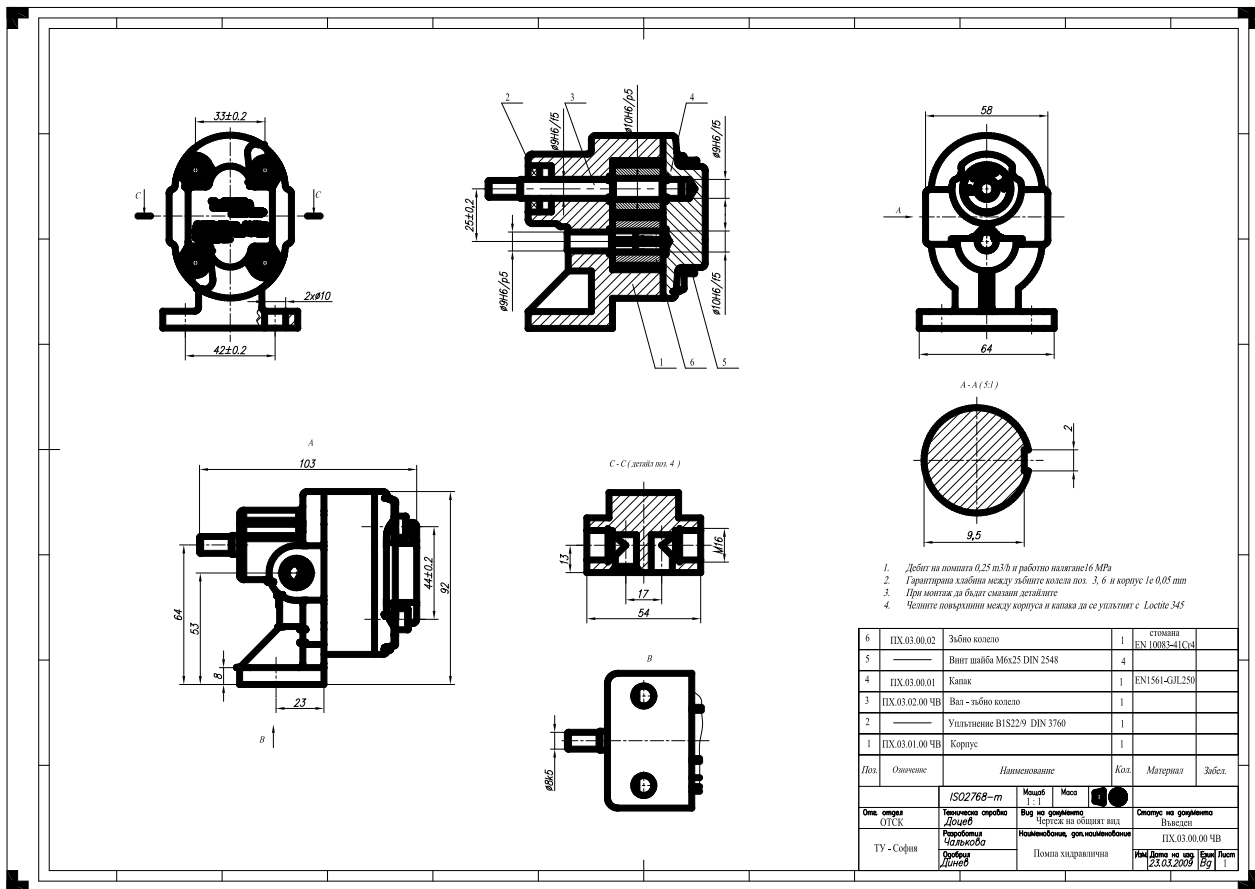
.4



.5



.6



.7

3.

CAD

1. „...“, 1978. .2-
2. „...“, 2009.
3. „...“, 2009, 117-120.
4. „...“, 2009.
5. „...“, 2009. CAD



ygi@tu-sofia.bg

1.

2.

1a

[2].

2

1

3,

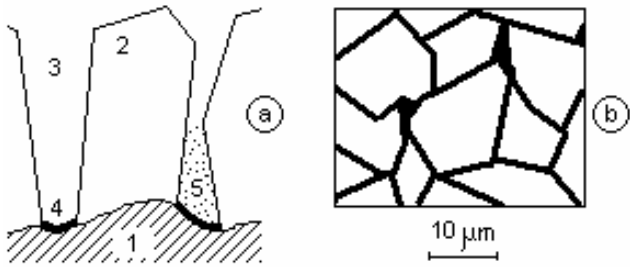
4

5.

1b

[1]

(Znph)



. 1

0,01 0,1 μm.

r 2 μm 50 μm, 90°

3.)

h

$$\frac{a}{h} \geq 2 + 1,64 \frac{r}{a} \quad (1)$$

2. ÷ [8],

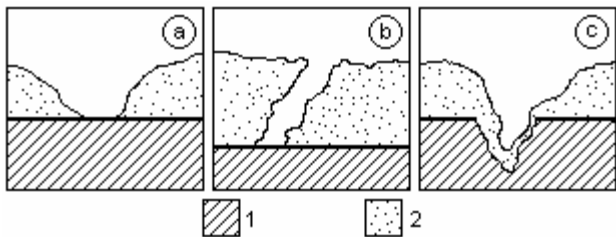
2,

1 (a,b) (a,c)

(b) (c); (a,c) (b);

(c),

(a,b).



. 2

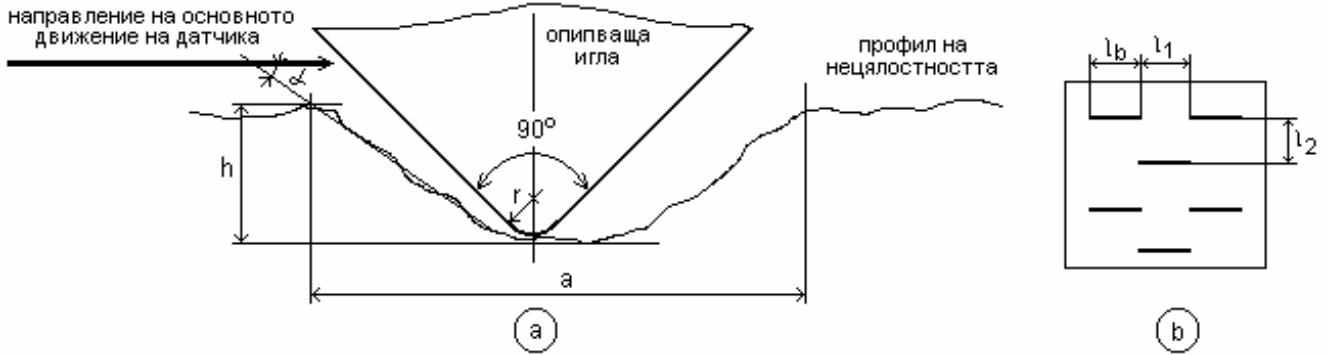
45°.

10 mN (r 2 μm 50 μm), 0,7 mN

(Znph, Mnph)

3.

l_1 l_2 (l_b . 3.b)



. 3

$$t_p - t_p' = 100\%$$

$$l_b = 30\%$$

$$R_{max} e$$

$$b_i, l_b \quad \%$$

100

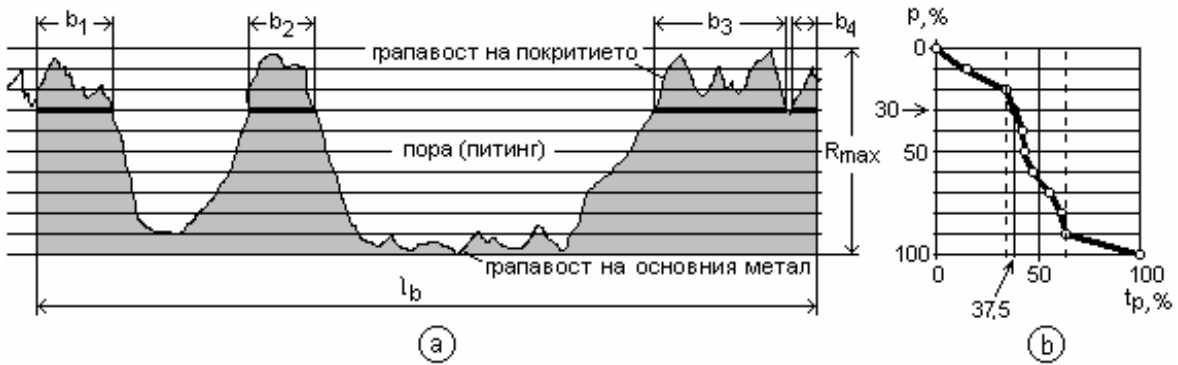
. 4b

$$(t_{25}' = 44\%)$$

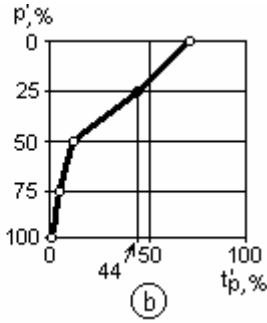
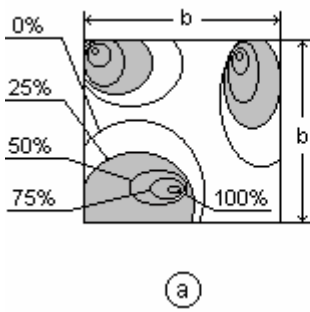
p'

$$t_p = \frac{\sum b_i}{l_b} \cdot 100, \% \quad (2)$$

$$t_{30} = 37,5\%$$



. 4



100 μm²

160 000

4.

.5.

196 mm² - 50 000

1. Freeman, Dennis B. Phosphating and metal pre-treatment. A guide to modern processes and practice. Industrial Press Inc., New York, 1986.
2. Lorin, Gue. Phosphating of metals. Constitution, physical chemistry and technical applications of phosphating solutions. FINISHING PUBLICATIONS LTD, Middlesex, England,1974.
3. Roobol, Norman R. Industrial Painting. Principles and Practices. Gardner Publications inc., Cincinnati, U.S.A., 1988.
4. , , , , 1981.

MEASUREMENT OF COATINGS

N. Tsonev V. Ivanov

Abstract

The phosphate conversion coatings of different metals and alloys are use wide for protection of corrosion, electric isolation, rising on the antifriction characteristics, like base for lay of varnishes and paints and etc. Basic index of the quality on like coatings is their uninterrupted. It can to use and like criterion to define of the technology for plating on phosphate coatings. Those indexes don't accepted united methods.

The authors on the base literary studying and known experience, in the report are analyzing the applicability of profilometric method for valuation on the uninterrupted of the phosphate coatings. Recommendations are made for the used of that method to define regime of plating on the duly coatings.

Keywords: *quality of coatings, measurement on quantities on coatings, profilometric method*

Assoc.prof. INikola TsonevI, PhD, Technical University-Sofia
 Assist. prof. Valentin Ivanov, Technical University-Sofia

vgi@tu-sofia.bg

1.

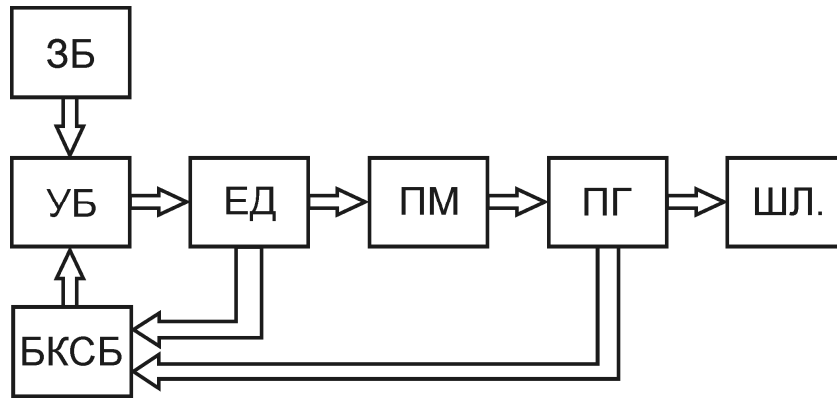
(0,85%), Marlow ISMATEC. MASTERFLEX, Watson-
0.06-3400 ml/min.

[3].

2.

[1].

.1.



.1.

() .

() ,

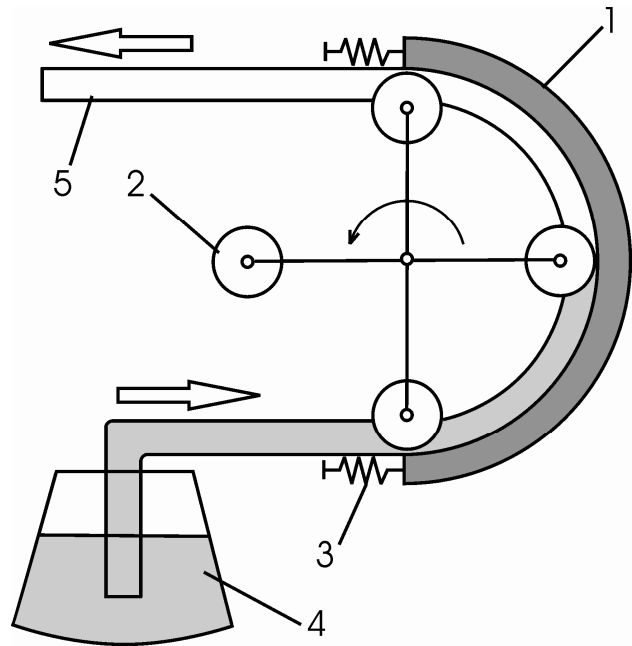
() ,

() .

() ,
()

() -

() .



.2.

.2

5

1,

3.

4,

4

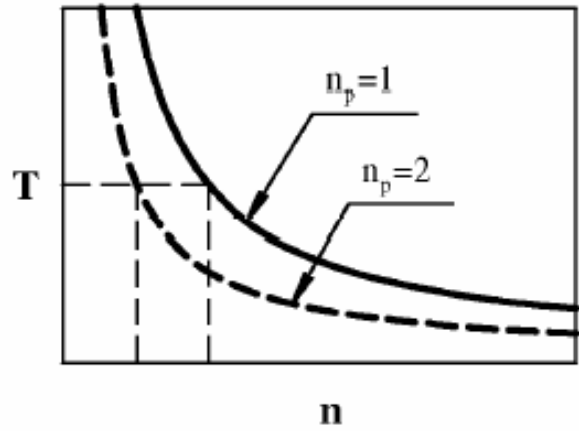
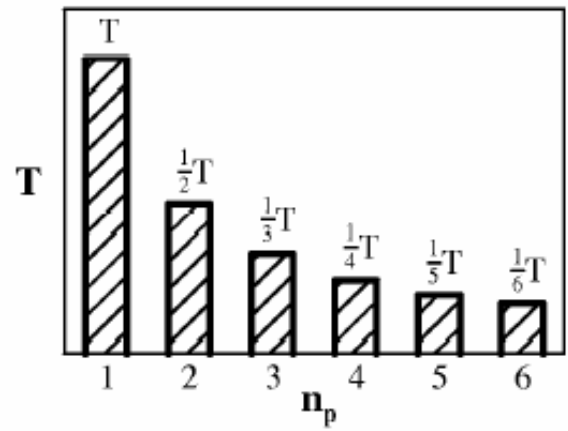
[2].

3.

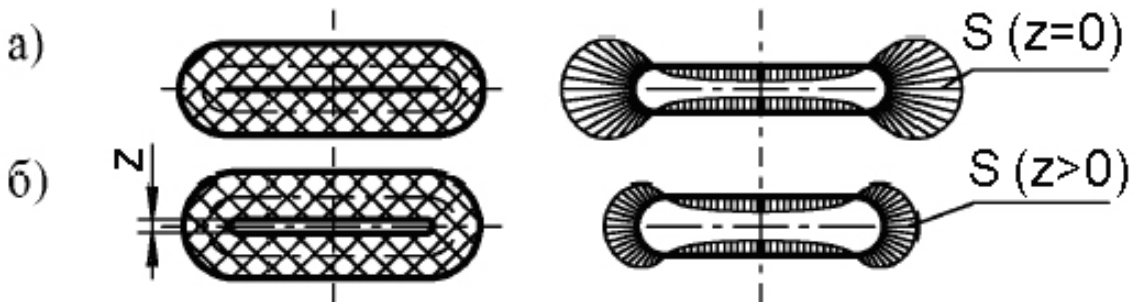
()

$$T = \frac{U}{n \cdot n_p \cdot 60} \quad (1)$$

T — ();
 U — ;
 n — (;
 n_p —);



(.5).



$(z=0)$ $(z>0)$
 $z e$

- z
- 4.
1. :
, 7-8/2005, . 26-29 .
 2. ,, “ , XV - ‘2006’, , 12-16 , 2006.
 3. : www.ismatec.com, www.masterflex.com, www.instechlabs.com

RESEARCH OF FLEXIBLE TUBE IN PERISTALTIC PUMPS

V. Ivanov

Abstract

In this work are examine design and principle of peristaltic pumps. Wear and pressure was investigated of the flexible tube.

Keywords: *pump, peristaltic, volume proportioning device, infusion, flexible tube*

Assist. prof. Valentin Ivanov, Technical University-Sofia

STUDIES ON THE SUSPENSION STIFFNESS CONTROL

Mihai-Constantin Clinciu Liviu Gaceu Diana Thierheimer Walter Thierheimer Florentin Popescu
mihaiclinciu@yahoo.com gaceul@unitbv.ro boldor@vega.unitbv.ro thierheimer@unitbv.ro

In this paper, the important error induced by wheel suspending mechanism from rolling movement is reduced by means of solution proposed. The cinematic model, the dynamic one and mathematical models the dynamic behavior of the vehicle at the moment of passing to the another way of driving and the turning motion. The results data accomplished by theoretical and experimental tests confirm all the hypothesis refers to the dynamic behavior of the vehicle.

Key words: control, hydraulic system, stability, maniability.

1. Introduction

The active influence of stabilizers, who must be compatible with this principle of action, must be realized by stabilizer mechanism or by an equivalent system.

Accordingly, stabilizers' active influence, which must be compatible with this driving principle, should be achieved in the stabilizer, steering mechanism unit or in an equivalent constructive solution.

The operation of stabilizer bar doesn't produce stress between body structure and bar, because these bars are mounted on the body by means of rolling bearing. In this way we are sure that stabilizer bars react only on perturbation resulting from the road and from unequal action of suspension.

One must also take into consideration the fact that the output regulator used to correct angular lags based on constructive achievement conventional elements is achieved quite easy and cost-effectively, with the use of the electro-mechanical and mechatronic devices [2].

2. The influence of stabilizer bars on dynamic behavior

The most convenient solution for safety in motion of the vehicle would be the transfer of an angular difference of rotation $\Delta\varphi$ between two positions of action, compress-detent, of the spin bar. It must be direct that one element of angular differences correction who has basics on the conventional elements structures, may be realized with very low costs, by means of electro-mechanics and mechatronics elements.

To fulfill of the angular differences $\Delta\varphi$ as a result of spinning of the stabilizer, lead on angular displacement of the stabilizer end proportionate to $\Delta\varphi$, that is $\Delta c = c_s \cdot \Delta\varphi$, based on the longitudinal axis of the vehicle. This dimension combines geometrical parameters of suspension mechanism and stabilizer bar and is adequate to the next approach, figure 1. Following the findings on analyzed rolling movement, and taking account to the rebound movement, the result of rolling k^s of the vehicle is:

$$\Delta k(a_y) = \frac{k_s + k_w}{k_g} \quad k^s = \left(\frac{h_g - h_w}{k_w + k_g} + \frac{h_g}{c_z E_s^2 / 2} \right) \cdot m a_y \quad (1)$$

Where k_w , k_1 and k_2 are elastic characteristic of the suspension, stabilizer bars and wheels, for front and rear axle respectively, figure 1.

If we want to totally reduce the rolling movement, the ends of stabilizers must be rearranging, taking account on the Δc .

On suppression the rolling movement, is necessary to know only the change of transversal acceleration of the vehicle a_y . To realize a minimum of shimming, 1 – 2 Hz, and high dumping of the transversal oscillatory movement, the parameters of work must be in the prescribed field [1].

The strategy of mathematical model for adaptive suspension mechanism, vary depending on design process of the control law, from using a simplified model of movement, with only one degree of freedom for testing algorithms of control with high degree of complexity, to drawing up a extended model of movement, with seven and more degree of freedom, for representing much better the comfort

performances and safety for the development results. In the next sections, I'll analyze the basic models,

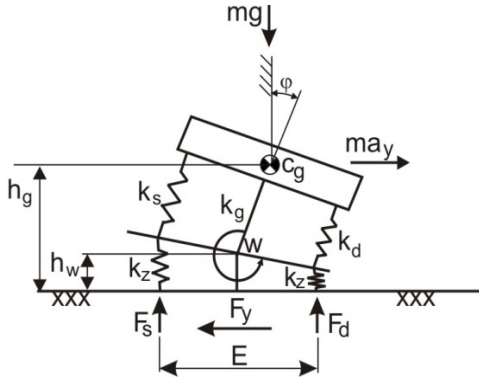


Figure 1

3. Model with two degree of freedom

The most common model used remains the model of suspended axle, named quarter of the vehicle, with two degree of freedom, figure 2. This model doesn't contain any representation of the fact that vehicle has four wheels: doesn't offer the possibility of studying for the longitudinal interconnection, neither study of rolling or pitching movement, neither using, by control, of data refers to the suspension mechanism state for the rear axle to utilize on the front axle suspension. Therefore, that model contains the basic principle to analyze the solution according to the experimental tests.

More, the model has the advantage of o relative small parameters.

SA - active servomechanism, CC - conventional compensatory.

Technical considerations regarding the introduction of the roundabout lines are the necessity to find the servomechanism equations in the state system of equations. Numerical considerations are made to resolve the Riccati matrix equations. Another variant with five states is obtained by ignoring the dynamics of electro hydraulic element; indeed, it must be possible to assess, by comparison, sharing of actuator dynamics within the model with two degrees of freedom.

$$\begin{aligned} M\ddot{x}_M + c_1(\dot{x}_M - \dot{x}_m) + k_1(x_M - x_m) + u &= 0 \\ m\ddot{x}_m - c_1(\dot{x}_M - \dot{x}_m) - k_1(x_M - x_m) - u + k_2(x_m - \xi) &= 0 \\ \ddot{\xi} + \alpha_a \dot{\xi} &= w \end{aligned} \quad (2)$$

4. Basics for semi active control

The cycle of evolution for semi active control is ended by appearance the sequential logics of balancing forces, named balance logic. By this

both physical and mathematical, of the movement equations.

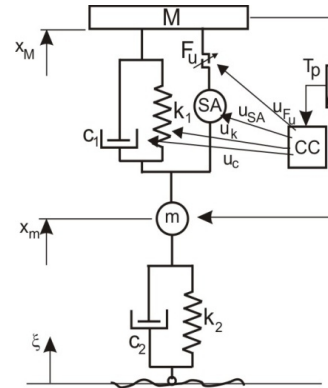


Figure 2

technique is possible to balance the elastic force from elastic elements by controlling the angular differences from the ends of stabilizer bars $(|\psi_s - \psi_d|)$ from figure 3. Considering the system with two degrees of freedom, presented in figure 2 end described by (2).

The fundamental principle for semi active control is:

$$\begin{aligned} u(\dot{x}_M - \dot{x}_m) &\geq 0 \\ |M\ddot{x}_M| &= |c(\dot{x}_M - \dot{x}_m) + k(x_M - x_m)| \end{aligned} \quad (3)$$

Like modus operandi, the semi active control strategy is consistent in all four variants, taking account to definition (4), but overstressing the following reasoning is risky.

Because the harmonically evolution of dissipative force $F_d = c \cdot (\dot{x}_M - \dot{x}_m)$ and elastic $F_s = k \cdot (x_M - x_m)$, illustrates in figure 3 and equation, in absence of control u, the quadrant 1 and 3 is distinguished from quadrant 2 and 4, from the point of view of contribution of those two forces to increasing, respectively decreasing of the acceleration modulus \ddot{x}_M , who is an indicator of comfort [1].

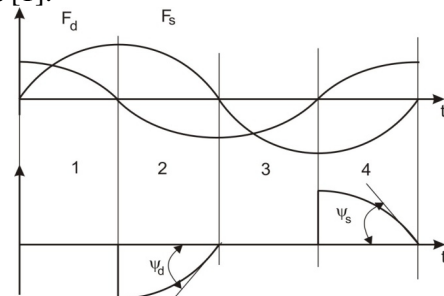


Figure 3

5. Experimental analysis

The two sets of weights mentioned - the control weight being equal to the unit each time - illustrate the flexibility if the focus is on improving Safety.

In this hypothetical case, to decreasing the acceleration modulus, so that improving the comfort performance, generally, and safety in particular, is proposed the strategy of induction in system of a resistive force, which has the evolution from figure 3: the diminution to a maximum possible of the rebounds, by alteration the angles from the ends of stabilizer bars ψ_s and ψ_d , in quadrant 1 and 3, respectively by modulation of this force, like in quadrant 2 and 4.

6. Conclusions

It may be concluded that the linear-squared compensator from hydraulic regulator RHLP has a

good robustness, in the case of solution proposed, having the evidence on self values of the system in closed loop, if this robustness depends more on model.

The detailed researches on RHLP hydraulic regulator accentuate interesting facts, figure 4 a, b. The incidence of prevision data exclusively on the rear axle assure to the system important advantages referring to the classical suspension as reference guide. The simultaneous reception of data for both axles doesn't seem to assure a real advantage to situation when those data are received only from the front axle. All the data are obtained from mean results of two simulations, with different sampling rate for three sets of noise data, one on the state and two on the measured values, displacement and velocity of the suspension.

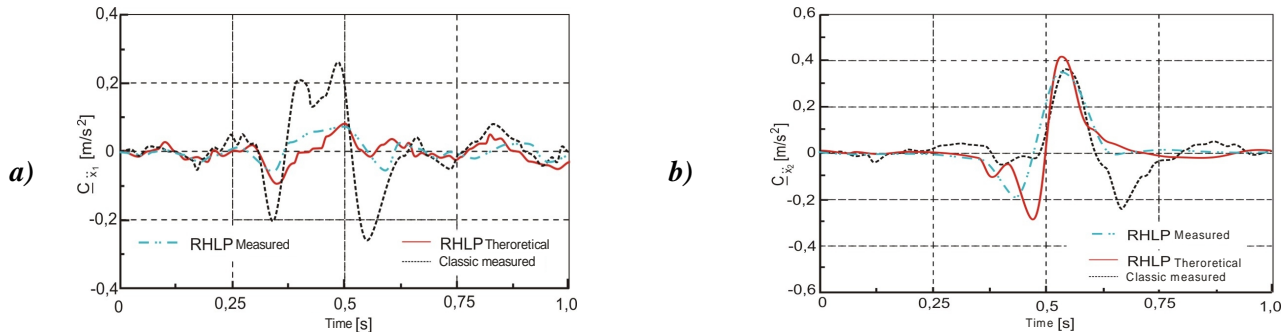


Figure 4

References

- [1] Tane, N.; Cojocaru, A.; Turea, N.; Thierheimer, D.; Thierheimer, W. (2008) The optimization of the suspension and rolling mechanisms of the vehicles – vol I, Transylvania University of Brasov, ISBN 978-973-598-421-2, Romania.
- [2] Thierheimer, W. (2001) The theory of tehcnical systems of agriculture and food industry, Transylvania University of Brasov Publishing House, ISBN 973-8124-76-X.
- [3] Thierheimer, W.; Tane, N.; Thierheimer, D.; (2008) Studies concernering the rolling motion reduction by controlling the steering and gear and the spring rigging correlation, In: Annals of DAAAM for 2008 & Proceedings of the 19th International DAAAM Symposium, Katalinic, B. (Ed.), pp. 1383-1384, ISBN 978-3-901509-68-1, ISSN 1726-9679, Published by DAAAM International, Vienna, Austria

Mihai - Constantin CLINCIU, drd.-eng., Transilvania University of Brasov

Liviu Gaceu, assoc.prof.dr.-eng., Transilvania University of Brasov

Diana C. Thierheimer, drd.-eng., Transilvania University of Brasov

Walter W. Thierheimer, assoc.prof.dr.-eng., Transilvania University of Brasov

Florentin Popescu, drd.-eng., University of Craiova

RESEARCH ON OPTIMIZING OF AUTOMATIC ABS REGULATOR

Vasile-Valerian Cojocaru Florentin Popescu Diana Thierheimer Daniel Ola Walter Thierheimer
gva_tgv@yahoo.com florinbebepopescu@yahoo.com boldor@vega.unitbv.ro danielola@unitbv.ro

Abstract: In this paper is presented a structure solution of elastic element from electromagnetic valve that has the roll to reduce the noise and vibrations from brake pedal. At the same time, this solution improve the dynamic of ABS regulator of the vehicle, allowing an increase of frequency of work and, implicit the reducing the braking space. The performances of constructive solution depending on achieving own resonance frequency are presented and confirmed in this paper by means of results obtained experimentally.

Key words: control, adjustment, diaphragm elastic element

1. Introduction

In construction of braking systems, beside technical, functional and the reliability parameters, must be taking account of the influence of braking on the stability of the vehicle, occupants and goods transported [2].

The braking, with or without locking the wheels, is strictly relate to complex system driver-vehicle-road-environment.

The assessment and comparison of braking quality of the vehicles are realized by means of maximum deceleration both absolute and relative, time and minimum braking space, as function of velocity state of movement of the wheel.

Braking system influence the active safety of the vehicle.

Braking process by achieving a minimum of braking space is optimal in the moment when the sideslip of the braked wheel would have the values corresponding to maximum of drag factor [3].

2. Independent adjustment

In figure 1 is presented the main loop of adjustment for braking system with ABS, from the point of view of wheel. The longitudinal sideslip of the wheel s_{ref} is replaced by wheel speed ω_{ref} , but it may be used another variable, who characterize the wheel speed as command parameter. The variable s_{ref} is generated by the superior stage of ABS adjustment strategy, which has the objective the dynamic behavior of the vehicle during braking [3].

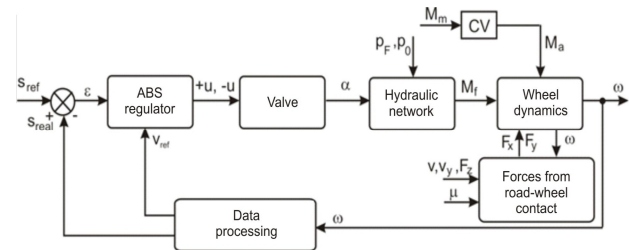


Figure 1

The adjustment loop, particular to the wheel, is composed by an ABS automat regulator (controller) with high dynamicity, who generate the measures for command, like electrical signals $+u(t)$, $-u(t)$ for the electromagnetic valves, with the aim of increasing or decreasing of the pressure in the system.

2.1 The physical modeling of the valve

By electromagnetic dynamics of the valve, described by equations (1), (2) the command signals are transcribed in corresponding opening of the valve [2].

In the contact track are dissipated the effects of the pulling moment of the wheel M_a , received by means of drive train from the engine M_m , longitudinal and transversal velocity of the tyre v_x , v_y , the momentary load on the wheel F_z and the drag factor ω . The wheel speed and velocity v are acquired by means of measures elements and introduced in the adjustment loop, after a previous analyses and processing of the signal in real time, resulting the reference velocity v_{ref} and the error ϵ .

To exemplifying the electromagnetic properties, in figure 2 is presented the ABS valve response from a perturbation like impulse form with fixed time.

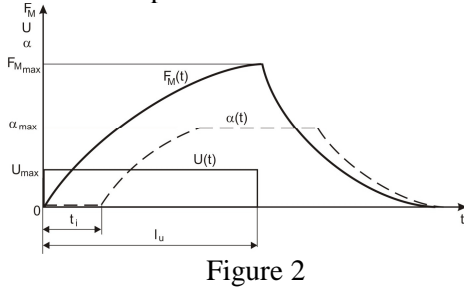


Figure 2

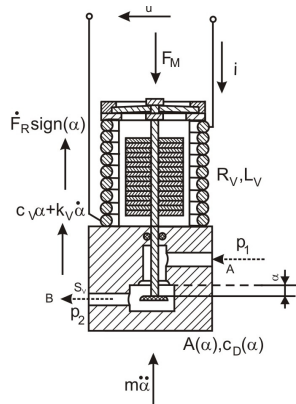


Figure 3

The passing section is maximum only in the case when magnetic force F_M surmounts the toughness of the elastic element of the valve and another force who lead on sitting of the mobile element on his seat. This is the reason why the opening of the valve $\alpha(t) > 0$ is realized with a time delay t_i , but reach quickly his maximum value α_{max} , meanwhile the electromagnetic force F_M is still rising. The response characteristic on the closing stage of the valve, results from cutting the command signal $u(t) \rightarrow 0$, would be distortional and delayed because of inertia, in the same way like the opening stage $\alpha(t) > 0$.

The relationship between acting voltage of the valve $u(t)$ and the passing section resulting from displacement of the valve $\alpha(t)$ are analyzed taking account by electromagnetic components of the valve.

In figure 3 are represented the construction and important parameters of the electromagnetic valve, proposed for the ABS system. The dynamics of opening electromagnetic valve is described by means of a equivalent system, electro-mechanical, nonlinear of the hydraulic element 3/2 (two ways and three positions).

The construction and dynamic characteristics for the electromagnetic valve with diaphragm like elastic element.

Because of technical limitations of the input and output measures, the modeling of the valve dynamics would be described integrally by means of references measures:

$$\frac{\dot{f}}{\omega_M} + f = f_u \cdot u^*(t); \quad u^*(t) = \frac{u(t)}{u_{max}} \quad (1)$$

$$f_m \ddot{\alpha} + f_d \dot{\alpha} + f_c \alpha + f_R \cdot \text{sign}(\dot{\alpha}) + f_0 = f; \quad (2)$$

$$\alpha(t) = \frac{x(t)}{x_{max}}$$

$u^*(t)$ represent the voltage of the command measure for the valve, who is in the range $0 \leq u^*(t) \leq 1$. The f_u parameter is used in studying of different amplitudes of voltage for command; generally $f_u = 1$. The characteristic value $\omega_M = R_v / L_v$ describe the inertial delay of electrical circuit. From experimental research and speciality reviews results an existence between nominal magnetic force $f(t) = F_M(t) / F_{Mmax}$ and the opening state α of the valve. The effect is generated by the inductivity alteration on opening, and in this case must act by altering the frequency parameter ω_M .

The parameters from mechanical differential equations may be identical with the ones on the opening stage, $0 \leq \alpha \leq 1$, where f_u describe the mass inertia, f_d – te viscous damping (generally neglected) and f_c the characteristic factor for the elastic element, f_R – frictions between valve, f_0 – pre-tensioning of elastic element.

3. Experimental analysis

The closing and opening times of the electromagnetic valve depend on the commuting mode, pressure, the necessary flow used in braking process, depend also with liquid temperature. These times may be modified by changing the characteristic of elastic element, the work section, etc.

The sealing up from the rod and the cap piece of the electromagnetic valve is realized with special adhesive and O-ring element, to eliminate the influence on the dynamics of commuting process. The pieces in movement were carefully accomplished (rod coupling mobile element, cylinder bore act element sensor).

For the proposed electromagnetic valve, the forces of liquid jet for a certain displacement $\bar{\alpha}$ of the mobile element, between 0 ... 1 mm have a maximum. For these reason the resultant force on the mobile element increases to the end of displacement of the closing event.

For the opening event, notice the small dependency from stiffness of the elastic element. If consider the closing event, it may be noticed a clearly reduction of that, together with increasing the force of spring. This is the result of importance of the spring forces, noticed above, in closing process, representing at the beginning an important part from main forces for the acceleration phase of the mobile element. As a result from testing the system, is obtained the next characteristic, figure 4.

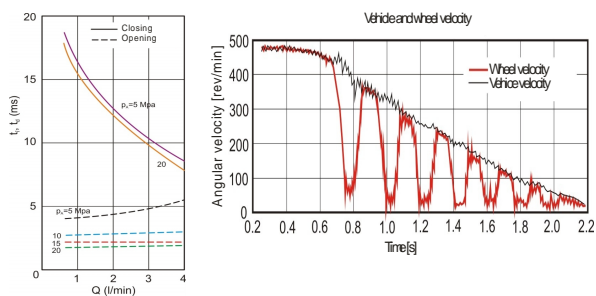


Figure 4

4. Conclusions

These solutions proposed for elastic element construction is realized for increased of efficiency of braking process.

Frequently, besides commutation functions of elastic elements, like closing maintains of electromagnetic forces, the opening forces due that, will be done by corresponding choice of stiffness of

References

- [1] Deac, D. (2008), Researches regarding the improvement of vehicle active safety, Ph.D. thesis, October, Transilvania University Brasov.
- [2] Tane, N.; Cojocaru, A.; Turea, N.; Thierheimer, D.; thierheimer, W. (2008) The optimisation of the suspension and rolling mechanisms of the vehicles – vol I, Transylvania University of Brasov, ISBN 978-973-598-421-2, Romania.
- [3] Thierheimer, W. (2001) The theory of tehcnical systems of agriculture and food industry, Transylvania University of Brasov Publishing House, ISBN 973-8124-76-X.

Vasile - Valerian COJOCARU, drd.-eng., Transilvania University of Brasov
 Florentin Popescu, drd.-eng., University of Craiova
 Diana C. Thierheimer, drd.-eng., Transilvania University of Brasov
 Daniel Ola, assist.prof.dr.-eng., Transilvania University of Brasov
 Walter W. Thierheimer, assoc.prof.dr.-eng., Transilvania University of Brasov

PNEUMATIC MECATRONIC SISTEM FOR LOAD SIMULATION ON TOOTHED THE RACK HEADS

Vasile - Valerian Cojocaru Nicolae Tane Diana Thierheimer Clinciu Mihai Walter Thierheimer
gva_tgv@yahoo.com nictan54@vega.unitbv.ro boldor@vega.unitbv.ro mihaiclinciu@yahoo.com

Abstract: *The dynamic behaviour of pneumatic actuator systems is dominant by nonlinear functions. First, a mathematical model for the pneumatic system is derived. Secondly, we investigate the mathematical properties of this model and show boundedness and positiveness of certain variables. Thirdly, we prove that a proportional output feedback controller with saturation achieves practical tracking a wide class of reference trajectories. We verify the theoretical results and the effectiveness of the control by experiments.*

Key words: *pneumatic cylinder, modeling, force control.*

1. Introduction

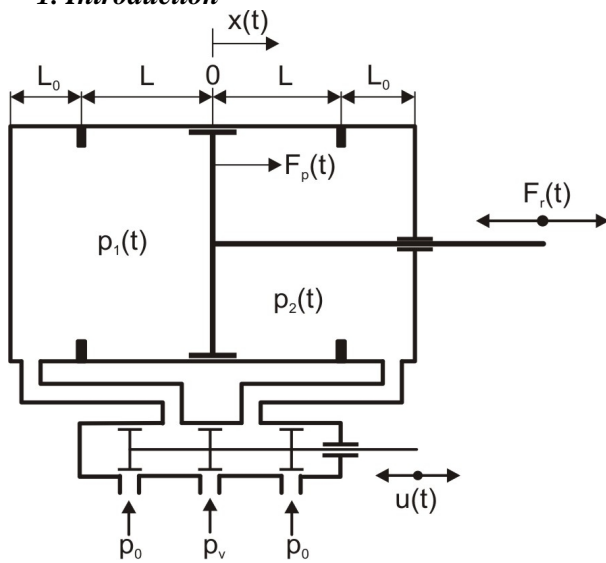


Figure 1

In this paper, we model, analyse, and control an experimental set-up of a pneumatic actuator as illustrated in Figure 1.

Up to now, adequate applications are mostly control tasks with modest requirements on position and force accuracy; the configuration consists of binary switching valves with pneumatic cylinders without any sensor elements. To enlarge the field of applications and allowing for higher accuracy, servo pneumatic valves and sensor for pressure position have been introduced.

However, if more accuracy on the performance is required, then nonlinear behaviour has to be taken

into account. Most contributions in this context focus on position control: Feedback linearization as control design method is broadly used [1; 7; 8], and since in this case the relative degree is lower than the system order, the cylinder chamber pressure has to be measured or the zero dynamics have to be compensated by feedforward compensation [4].

Fewer contributions focus on force control [2]. However, no matter whether position or force control is considered, the dominant nonlinearities are in the pneumatic part, and not in the mechanical part of the system. There is a fundamental need for a detailed modeling of the dynamic behaviour of the pneumatic actuator system.

This allows deriving system theoretic properties of the model which then lead to effective control strategies for the force control, such as force control of the inner part of the cascaded control concept.

The meanings of the symbols in Figure 1 are: $p_1(t), p_2(t)$ -pressure at time $t \geq 0$ in left/right chamber, resp., $x(t)$ -position of the piston at time $t \geq 0$, $F_p(t)$ -pressure force on the piston at time $t \geq 0$, $F_r(t)$ -resulting force at time $t \geq 0$, p_v -supply pressure, p_0 -ambient pressure, $b \in (0,1)$ -critical pressure fraction, $L > 0$ $[-L, L]$ -normal operation range of the cylinder, $L_0 > 0$ - additional length of piston, zone of end of travel absorbers

2. Model of a pneumatic actuator system

The aim of the present note is to control a desired force F_p on the piston rod by the pressures p_1 and p_2 in two cylinder chambers, see Figure 1. The pressures p_1 and p_2 are measured by two pressure sensors. The force on the piston F_p depends on the effective cross section areas A_1 and A_2 A_1 in the cylinder chambers, i.e.

$$F_p(t) = A_1 p_1(t) - A_2 p_2(t),$$

Note that due to friction effects, the resulting force F_r on the piston rod is not identical to the force F_p . However, in this paper we focus on the pneumatic dynamics and on controlling F_p .

To control the force F_p , i.e. the pressure difference, the differential cylinder is connected with

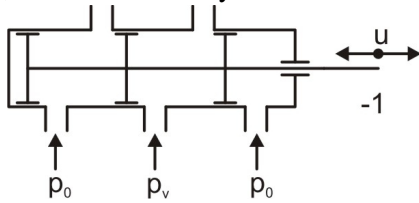
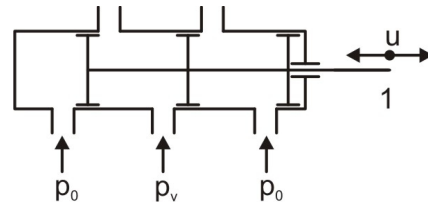


Figure 2

a 3/5-servo-valve. The notation of 3/5 means, that the valve has three different modes of operation and five ports (one for the supply pressure p_v , two for the ambient pressure p_0 , and two for the chambers of the cylinder). Between these three modes one may change continuously. The first mode is the zero-position of the valve as depicted in Figure 1; the second mode is filling chamber 1 and exhausting chamber 2 simultaneously; the third operation mode is deaerating chamber 1 and filling chamber 2. It will be assumed that the control input u is standardized such that $u = -1$ corresponds to maximum flow-rate filling chamber 2 and for $u = 1$ vice versa, Figure 2.



The mechanical dynamics are described by

$$\left. \begin{aligned} \dot{x} &= v & x(0) &= x_0 \in [-L, L], \\ \dot{v} &= a & v(0) &= v_0 \in R \end{aligned} \right\} \quad (1)$$

where x is the position, v the velocity and a the acceleration of the piston. We assume that the force compensation, which determines a , is realized such that

$$x(t) \in [-L, L] \quad \forall t \geq 0.$$

This assumption may be justified by the size of the cylinder and - possibly - an action of an external position controller; which is typically satisfied in such applications as assembling by force fitting.

The pressure in the cylinder chambers can be modeled [1; 3], invoking the principles of constant mass and conservation of energy, by the following differential equation:

$$\left. \begin{aligned} \dot{p}_1 &= \frac{k}{A_1(L_0 + L + x)} (RT\dot{m}(p_1, u) - p_1 A_1 \dot{x}), \\ \dot{p}_2 &= \frac{k}{A_2(L_0 + L - x)} (RT\dot{m}(p_2, -u) + p_2 A_2 \dot{x}). \end{aligned} \right\} \quad (2)$$

The mass flow rate \dot{m} depends on the flow rate function of the servo valve. The mass flow can be assumed to be a flow of a compressible fluid in a turbulent regime through a conical nozzle. In case of filling the cylinder chamber, a characteristic

depending on the pressure ratio and gas flow rate is described by a square root function. Let $b \in (0, 1)$ be the critical pressure fraction and define

$$\Psi_b : [0, 1] \rightarrow [0, 1], \quad q \rightarrow \begin{cases} 1, & q \leq b, \\ \sqrt{1 - \left(\frac{q-b}{1-b}\right)^2} & q \geq b \end{cases}$$

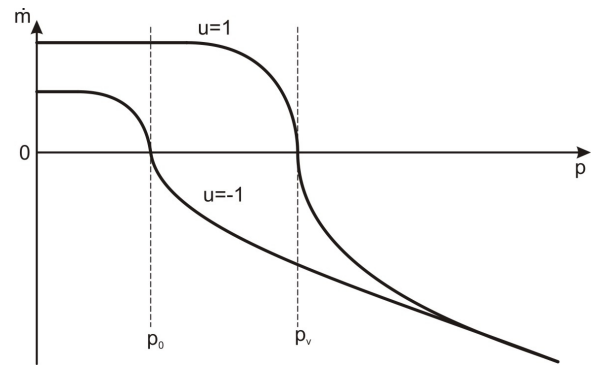


Figure 3

Neglecting the leakage of the valve, the mass flow rate can be described by the following equation [4, 5], Figure 3:

$$\dot{m} : R > 0[-1,1] \rightarrow R, \quad (p, u) \rightarrow \begin{cases} -\rho_0 C_m p \Psi_b(p_v / p) u, & \text{if } u > 0, p \geq p_v \\ \rho_0 C_m p_v \Psi_b(p / p_v) u, & \text{if } u > 0, p \leq p_v \\ 0, & \text{if } u = 0, \\ \rho_0 C_m p \Psi_b(p_0 / p) u, & \text{if } u < 0, p \geq p_0 \\ -\rho_0 C_m p_0 \Psi_b(p / p_0) u, & \text{if } u < 0, p \leq p_0 \end{cases} \quad (3)$$

3. Force control

In this section, it will be shown that the output, for cross sectional areas $A_1, A_2 > 0$ of the piston,

$$y(t) = A_1 p_1(t) - A_2 p_2(t) \quad \forall t \geq 0, \quad (4)$$

in combination with the simple proportional feedback controller, for $k > 0$, with saturation

$$\begin{aligned} u(t) &= \text{sat}_{[-1,1]}(-ke(t)) \text{ with} \\ e(t) &:= y(t) - y_{ref}(t) \quad \forall t \geq 0, \end{aligned} \quad (5)$$

achieves practical tracking in the following sense.

4. Experimental set-up and measurement results

The results of the previous sections have been verified by measurements using the experimental set-up depicted in Figure 5. A pneumatic cylinder of the manufacturer Festo has been used; the constants given in the table at the end of the Introduction are for this cylinder as follows: $p_v = 6000 \text{ hPa}$, $p_0 = 1000 \text{ hPa}$, $b = 0.3$, $L = 50 \text{ mm}$, $L_0 = 5 \text{ mm}$, $A_1 = \pi(d_1/2)^2$ and $A_2 = A_1 - \pi(d_1/2)^2$, (where $d_1 = 25 \text{ mm}$ and $d_2 = 10 \text{ mm}$), $C_m = 2.64 \cdot 10^{-9} \text{ l/(sPa)}$, $\rho = 1.185 \text{ kg/m}^3$, $k = 1$, $R = 287 \text{ Nm/(kg K)}$, $T = 293 \text{ K}$.

Two pressure sensors measure the chamber pressure p_1 and p_2 ; the position x of the piston rod is measured by a potentiometer. According to (5), the output $y(t)$ is a linear combination of the two pressures. Since the pressure measurement is corrupted by measurement noise, we implemented a low-pass filter of first order with the transfer function $s \rightarrow (1 + 2s/(\pi f))^{-1}$ and cut-off frequency $f = 20 \text{ Hz}$. Control and measurement data processing is implemented in Matlab/Simulink. The Simulink structure is downloaded via the Realtime Workshop to the controller board DS1103 of the manufacturer dspace.

All experiments illustrate how the feedback controller (4), (5) achieves tracking of given reference trajectories. Moreover, we also show how the controller compensates disturbances on the position

of the piston rod and how it follows piecewise constant reference forces; note that the latter cases are not covered by the theoretical results.

We apply the force control law (5) with gain parameter $k = 0.02$, i.e. $\lambda = 50$, and the experiments have a duration of 40 seconds. Certainly, the figures also show that the measurement data contain ‘‘real world’’ noise.

In the experimental test, a continuously differentiable reference signal y_{ref} as depicted in Figure 5 is used. The piston rod is fixed mechanically and so its position is constant (i.e. the piston velocity $v = 0$). As can be seen in Figure 5, whenever there is a continuously differentiable but fast change of the reference signal with 5 N or 40 N difference (for example at $t = 8$ or $t = 20$), the magnitude of the error between the output and the reference force is 4 N at most, and the control input has peaks about 0.08 large at most. However, within 1 second the error is close to a steady state; note that this steady state is positive, which may be due to the experimental set-up depicted in Figure 4, where:

1 is pneumatic cylinder, 2 - pressure sensor, 3 - servo valve, 4 - stroke sensor, 5 - force transducer.

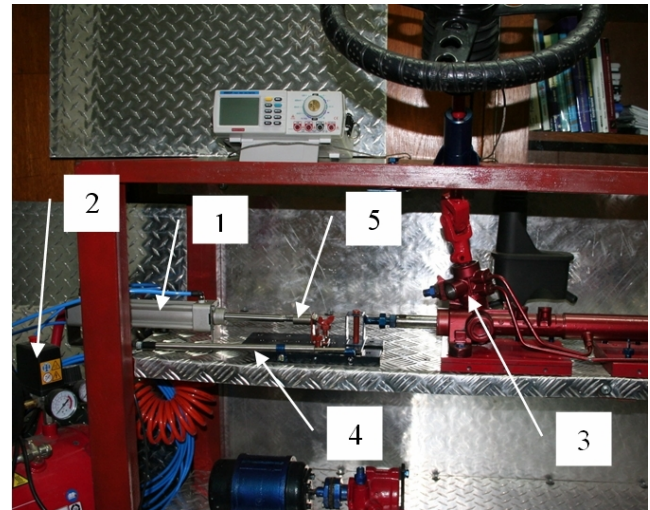


Figure 4

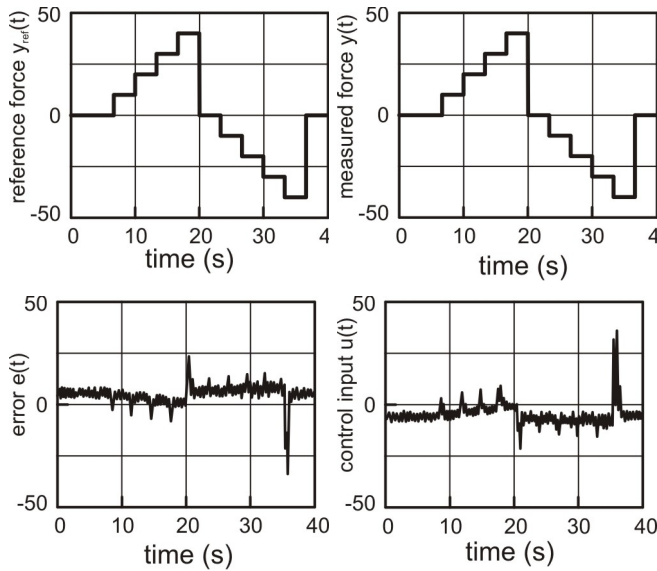


Figure 5

5. Conclusions

We have introduced a mathematical model for a pneumatic actuator taking into account essential nonlinearities. We have then investigated the mathematical properties of this model and have shown that the mathematical properties of the model coincide with the engineering understanding: the pressure values remain positive, the solution is unique and bounded. So, that we have investigated a proportional error feedback control with saturation. Although intuitively clear, it is mathematically not straightforward how to cope with the saturation and the underlying nonlinearities of the model.

References

- [1] A. Hildebrandt, O. Sawodny, R. Neumann, and A. Hartmann. A flatness based design for tracking control of pneumatic muscle actuators. In Proc. of the 7th Int. Conf. on Control, Automation, Robotics and Vision (ICARV02), pages 1156–1161, Singapore, 2002.
- [2] A. Hildebrandt, O. Sawodny, R. Neumann, and A. Hartmann. Cascaded tracking control concept for pneumatic muscle actuators. In Proc. of the European Control Conference (ECC), CD-ROM, Cambridge, 2003.
- [3] O. Ohligschl'ager. Pneumatische Zylinderantriebe - thermodynamische Grundlagen und digitale Simulation. PhD thesis, RWTH Aachen, DE, 1990.
- [4] O. Sawodny and A. Hildebrandt. Aspects of the control of differential pneumatic cylinders. In E. Shimemura and M. Fujita, editors, Proc. of German-Japanese Seminar, pages 247–256, Noto Hanto, 2002.
- [5] W. W. Thierheimer, *Sisteme tehnice din agricultur i industrie alimentara : ini iere i fundamente teoretice*, Editura Universitii "Transilvania" Brasov, Brasov, 2001
- [6] T. Wey, M. Lemmen, and W. Bernzen. Hydraulic actuators for flexible robots: A flatness based approach for tracking and vibration control. In Proc. of the European Control Conference (ECC), CD-ROM, Karlsruhe, 1999.
- [7] F. Xiang and J. Wikander. Block-oriented approximate feedback linearization for control of pneumatic actuator system. Control Engineering Practice, 12(4):387–399, 2004.

Vasile - Valerian COJOCARU, drd.-eng., Transilvania University of Brasov

Nicolae Tane, .prof.dr.-eng., Transilvania University of Brasov

Diana C. Thierheimer, drd.-eng., Transilvania University of Brasov

Mihai - Constantin CLINCIU, drd.-eng., Transilvania University of Brasov

Walter W. Thierheimer, assoc.prof.dr.-eng., Transilvania University of Brasov

SIMULATION OF THE BRAKING PROCESS AT THE STROKE END OF LINEAR HYDRAULIC MOTORS

Ioan Cristian

icristian@unitbv.ro

***Abstract.** The paper analyzes the transitory phenomena, which encounters at the braking at the stroke end of the hydraulic actuators from the structure of the hydraulic driving of the machines and industrial robotics. In order to point out, by numerical simulation, the transitory phenomena, which encounters at the braking at the stroke end of the hydraulic actuators, the mathematical model of the hydraulic actuator, in braking status, is first deduced. As a conclusion of the numerical simulation the motor response is analyzed and presented, for the particular case, when the braking is carried out by a hydraulic resistance.*

1. Introduction

The structure of many hydraulic driving of machine tools and industrial robots contain linear hydraulic motors, with simple or double driving. In order to prevent mechanical shocks occurred upon the piston hitting the side covers of the motor, it is recommended to provide a braking system at the stroke end. The most frequent solutions [4, 5, 6] are the use of braking throttles placed on the side cover and braking through the play between the cover bore and braking dowel which continues the motor piston.

The braking of the hydraulic motor at the stroke end is accompanied by pulsation of the pressures of its two chambers. Consequently, by knowing transient phenomena related to the hydraulic motor braking is necessary to establish the size of the braking throttle able to provide the fast loss of pressure pulsations, a small overshoot of this pressure and adjustment of the interval required for braking

2. Mathematical modeling of the hydraulic motor braking process

The linear mathematical model of the hydraulic motor under braking will highlight, as output size, the pressure P_B of the motors counter motor chamber. This will be done by accepting the following work hypothesis:

- the linear hydraulic motor is considered symmetrical,

- the adjustment of the hydraulic motor speed is done through the throttle \mathbf{Dr} (Fig.1) located at the exit,
- the force resistant to motor, prior and during braking, is null $F_{RM} = 0$:
- the clearance between cover and braking dowel is null, the braking is exclusively provided by the braking resistance \mathbf{DrF} ,
- to simplify the problem, both the motor speed adjustment throttle and the braking throttle are considered as being represented by flow laminar resistances,
- internal and external motor leakages are considered null $\alpha_M = 0$:
- The motor is considered fed at constant pressure $P_0 \approx const.$
- The return pressure is considered constant $P_{R0} \approx const.$
- The reference position of the motor is considered the position immediately near the point where the braking dowel which continues the piston enters the side cover. At this position the hydraulic motor speed is constant.

In Fig.1a the hydraulic motor is represented in the stage before braking, and in Fig.1.b the motor is represented in braking regime.

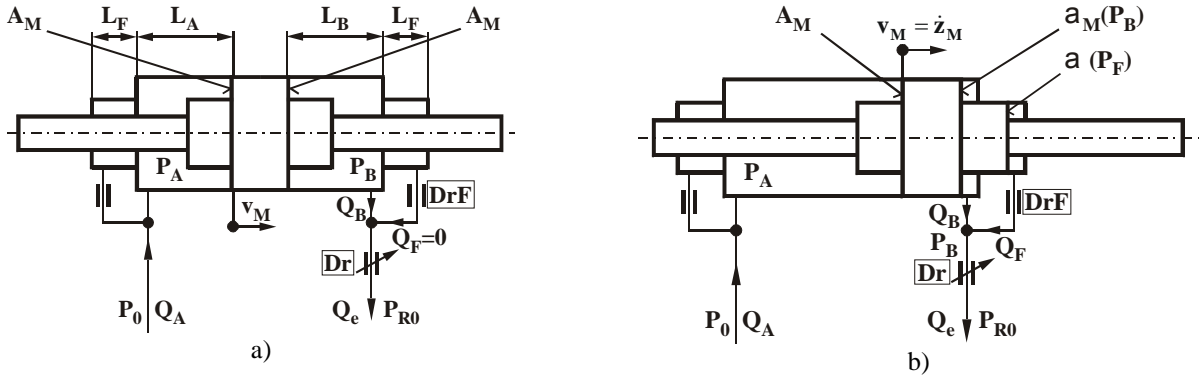


Fig.1 Braking stages

We will consider that prior the start of the braking process the motor is steady-state. Under these circumstances the flow through the braking throttle is null, and the flow crossing through the adjustment throttle is equal to the flow exiting from the hydraulic motor. Consequently the piston steady-state equilibrium and continuity of the flow to the motor and through the adjustment throttle:

$$\begin{cases} c_M v_M^* = A_M P_0 - A_M P_B^* \\ Q_A^* = Q_e^* = A_M v_M^* \\ Q_e^* = Y_{Hd} (P_B^* - P_{R0}) \end{cases} \quad (1)$$

Allow the calculation of the pressure steady-state values from the chamber of the counter motor and motor speed:

$$P_B^* = \frac{A_M^2 P_0 + c_{RM} Y_{Hd} P_{R0}}{A_M^2 + c_{RM} Y_{Hd}} \quad (2)$$

$$v_M^* = \frac{A_M}{c_{RM}} (P_0 - P_B^*) \quad (3)$$

In this relations A_M is the useful area of the hydraulic motor, Q_A - is the flow entering the motor chamber of the hydraulic motor, c_{RM} - low viscous friction coefficient of the hydraulic motor, and $Y_{Hd} = 1/R_{Hd}$, where R_{Hd} is the hydraulic resistance of the adjustment throttle. The asterisk marks the steady-state values of the variables in question.

When the braking dowel enters the suitable cavity of the motor side cover, starts the braking process, which is characterized by the following equations:

- the dynamic equilibrium equation of the motor:

$$A_M P_0 - a_M P_B - a P_F = m_{RM} \dot{v}_M + c_M v_M \quad (4)$$

- the equation of displacement of the motor piston,

$$z_M = \int v_M dt \quad (5)$$

- expression of calculation of the flow rate which enters the hydraulic motor,

$$Q_A \approx A_M v_M \quad (6)$$

- continuity equations of the flow associated to the counter motor chamber and cavity where braking dowel enters, respectively the knot upstream the adjustment dowel:

$$\begin{cases} -Q_B = -a_M v_M + C_{HB} \dot{P}_B \\ -Q_F = -a v_M + C_{HF} \dot{P}_F \\ Q_e = Q_B + Q_F \end{cases} \quad (7)$$

- expression of the laminar flow crossing through the adjustment dowel:

$$Q_F = Y_{HF} (P_F - P_B) \quad (8)$$

where a_M is the area of the counter motor chamber at braking stage, a - area of braking cavity, C_{HB} - hydraulic capacity of the counter motor chamber, C_{HF} - hydraulic capacity of the braking chamber, $Y_{HF} = 1/R_{HF}$, where R_{HF} is the hydraulic resistance of the braking throttle, Q_F - laminar flow through the braking throttle.

With these considerations, the dynamic, in terms of time, of the hydraulic motor is described by the following equations:

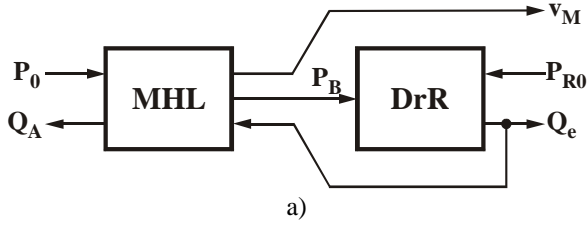
$$\begin{cases} m_{RM} \dot{v}_M + c_M v_M = A_M P_0 - a_M P_B - a P_F \\ z_M = \int v_M dt \\ Q_A = A_M v_M \\ C_{HF} \dot{P}_F = (a_M + a) v_M - C_{HB} \dot{P}_B - Q_e \\ C_{HB} \dot{P}_B + Y_{HF} P_B = a_M v_M + Y_{HF} P_F - Q_e \end{cases} \quad (9)$$

When speaking of the linear hydraulic motor system -

adjustment throttle, to the above equations the expression of adjustment throttle located on the exit is added:

$$Q_e = Y_{Hd} (P_B - P_{R0}) \quad (10)$$

One can note that the dynamic of the linear hydraulic motor – adjustment throttle, in the field of time, is



described as a system of six equations. At the same time, in the structural diagram of Fig.2a, one can note the flow feedback transmitted to the throttle over the hydraulic motor.

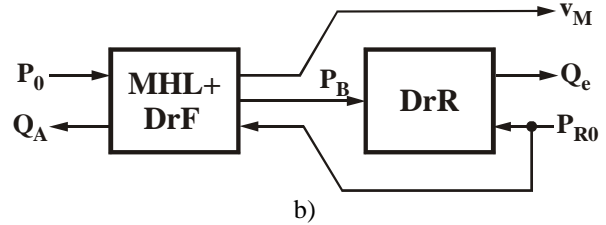


Fig.2 System structural diagrams

By replacement of the relation (12) in the system of equations (11), the number of variables and implicitly the number of equations describing the system dynamics is decreased:

$$\begin{cases} m_{RM} \dot{v}_M + c_M v_M = A_M P_0 - a_M P_B - a P_F \\ z_M = \int v_M dt \\ Q_A = A_M v_M \\ C_{HF} \dot{P}_F = (a_M + a) v_M - C_{HB} \dot{P}_B - Y_{Hd} P_B + Y_{Hd} P_{R0} \\ C_{HB} \dot{P}_B + (Y_{HF} + Y_{Hd}) P_B = a_M v_M + Y_{HF} P_F + Y_{Hd} P_{R0} \end{cases} \quad (11)$$

According to the structural diagram of Fig.2.b, drawn up based on these equations, the previous flow feedback was replaced by the return pressure feedback P_{R0} .

By applying the Laplace transformation, the dynamics, in complex, of the system hydraulic motor – speed adjustment throttle is described by the following system of equations:

$$\begin{cases} v_M(s) = \frac{K_7}{T_3 s + 1} [P_0(s) - K_5 P_B(s) - K_6 P_F(s)] \\ z_M(s) = \frac{1}{s} v_M(s) \\ Q_A(s) = K_8 v_M(s) \\ P_F(s) = \frac{1}{T_4 s} v_M(s) - \frac{T_5 s + 1}{T_6 s} P_B(s) + \frac{1}{T_6 s} P_{R0}(s) \\ P_B(s) = \frac{1}{T_7 s + 1} [K_9 v_M(s) + K_{10} P_F(s) + K_{11} P_{R0}(s)] \\ Q_e(s) = K_{12} [P_B(s) - P_{R0}(s)] \end{cases} \quad (12)$$

where:

$$\begin{aligned} K_5 &= \frac{a_M}{A_M}; & K_6 &= \frac{a}{A_M}; & K_7 &= \frac{A_M}{c_M}; \\ K_8 &= A_M; & K_9 &= \frac{a_M}{Y_{HF} + Y_{Hd}}; \\ K_{10} &= \frac{Y_{HF}}{Y_{HF} + Y_{Hd}}; & K_{11} &= \frac{Y_{Hd}}{Y_{HF} + Y_{Hd}}; & K_{12} &= Y_{Hd}; \\ T_3 &= \frac{m_{RM}}{c_M}; & T_4 &= \frac{C_{HF}}{a_M + a}; & T_5 &= \frac{C_{HB}}{Y_{Hd}}; \\ T_6 &= \frac{C_{HF}}{Y_{Hd}}; & T_7 &= \frac{C_{HB}}{Y_{HF} + Y_{Hd}} \end{aligned}$$

The block-diagram disclosed by Fig.3 reveals the internal connections within the system. One can note that in the case of the hydraulic motor controlled by the throttle placed at exit, the input size in the hydraulic motor is represented by the feeding pressure P_0 of the hydraulic motor, as a difference from the case the motor is controlled by servovalve and the input size is represented by the motor input flow. Moreover the speed v_M influences both directly and indirectly the counter- motor pressure P_B , which leads to the emergence of two direct ways of transmission of the information.

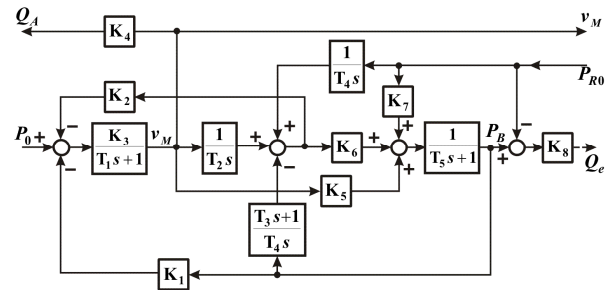


Fig.3 System block diagram

3. Simulation of the braking transient process

Based on the above and on the mathematical model of the linear hydraulic motor for the stage prior the braking [2] the simulation diagram was done, using Simulink language within the programming environment Matlab. Fig.4 discloses the evolution, prior and during braking, of pressure P_B from the motor's counter motor chamber, of speed v_M of the hydraulic piston and its position z_M . The following constructive - functional parameters of the hydraulic motor were considered: $D_M = 62$ [mm], $d_M = 40$ [mm], $L_M = 400$ [mm], $L_A = 0,355$ [mm], $L_B = 0,050$ [mm], $L_F = 0,040$ [mm], $\alpha_{iM} = 0$, $D_{dR} = 1$ [mm], $D_{dF} = 0.5$ [mm], $P_0 = 50$ [bar], $P_{R0} = 3$ [bar].

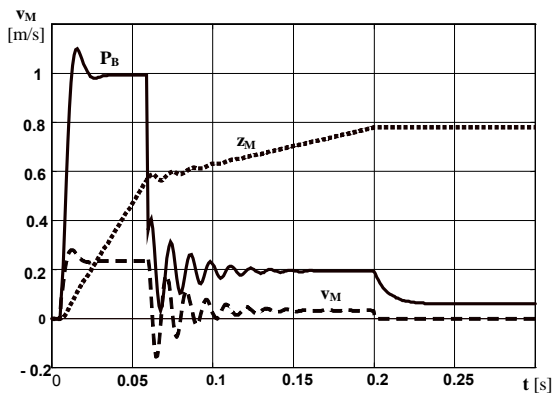


Fig.4 Numerical simulation of braking process

Upon the supply of hydraulic motor with pressure at $P_0 = 50$ [bar] and in presence of counter pressure $P_{R0} = 3$ [bar] and in the absence of the force resistant to motor, its speed will stabilize at the value $v_M = 0,225$ [m/s]. This is the speed when the braking process begins, the speed of input of the braking dowel entering the side cover. The transient braking process lasts approximately 0.1 seconds and is characterized by the following parameters:

- the speed represents negative overshoot of approximately 0.2 [m/s],
- the piston makes small absorbed oscillations, with initial amplitude of $\approx 0,3$ [mm].
- the transient braking process is continued by the steady-state displacement at the speed of $\approx 0,04$ [m/s]; at this speed the piston will hit the side cover and will stop.

4. Conclusions

Knowing the transient braking regime at the stroke end of hydraulic motors and its connection with the mathematical model supplies important details related to the establishment of the size of the braking throttle, able to provide the requested dynamic and steady parameters: duration and braking speed, pressure overshooting, speed and force of the piston hitting the side cover, etc.

References

1. B l oiu, V., Cristian, I., Bordea u, Il. *Echipamente i sisteme hidraulice de automatizare*, Vol. 1+2, Ed. Orizonturi Universitare, ISBN 978-973-638-313-7, Timi oara, , 2008 (in romanian)
2. Cristian, I., *Modelarea i simularea sistemelor mecanice*, Ed. Univ. Transilvania, ISBN 973-635-160-2, Bra ov, 2004 (in romanian)
3. Cristian, I., *Servosisteme electrohidraulice analogice*, Ed. Univ. Transilvania, ISBN 973-635-178-5, Bra ov, 2004 (in romanian)
4. Ivan, M., M niu , P., Cristian, I., Dobrea, Gh. *Hidraulica Ma inilor Unelte - Curs*, Universitatea din Bra ov, Bra ov, 1989. (in romanian)
5. Meritt, H.E., *Hydraulic Control Systems*, John Wiley and Sons Inc., New York, 1967
6. Oprean, A. *Hidraulica Ma inilor-Unelte*, Ed. Tehnic , Bucure ti, 1977 (in romanian)
7. *** *Matlab 6.5, Simulink – User‘ Guide*, MathWorks, Natick, MA., 2005

Calculation of Natural Elastic Compensators Configurations

Mihaela Urdea
urdeam@unitbv.ro

Emilia Scheibner
emiliascheibner@yahoo.com

Abstract: This paper is focused on the development of applicable software with C++ language, to process the database of the compensating device in L form. The compensating device for construction of heat networks approached by this paper takes the form L. The main objective of the project is to create a database, to prepare the application with all the calculus, to design the relation between the sketch and the data. The initial sketch, drawn in AutoCAD, called pattern sketch, for the compensating device form L, was associated to some groups of compensating device. Finally, the final drawings result, for the given compensating device. C++ is the best example to organize the database for reading, for improving and processing.

Key Words: C++, Script file, AutoCAD, compensating device, elastic configuration.

1. Introduction

The processing of useful database in constructive design needs an intense management and supervision activity. For this purpose it was necessary to use a complex and modern programming language such as C++, that allowed the database reading, its processing, the achievement of decision blocks, results interpretation, print of results on the screen or printer, as list for one item or as table for several items [1].

This paper develops a C++ application for compensator's database processing, intended to calculate all configurations for natural elastic compensators in „L” form. Besides all related calculation, necessary to determine a compensator, the maximum bending tensile stress for the elastic configuration is checked resulting in a Script file necessary to obtain the detail engineering for the processed compensator.

2. About the compensating device

Compensators are used to take over pipes' dilatation due to variations in temperature of the heating agent. Generally, for heat networks construction the following compensators are used: curved "U" shape (Fig.1), equipped with stuffing box, natural elastic and lenticular.

Natural elastic compensators are made by changing the direction of the heating pipes lay-out. These are delimited by fixed arresters on both sides of the direction change, at convenient distances from the

angle vertex point. Thus, compensators of "L" or "Z" form, able to contort in elastic field under influence of the heating agent's temperature variations, can be delimited.

The following recommendations are valid for delimiting such configurations:

- sides ratio: $L2/L1 = 1...5$;
- $\alpha = 90...135^\circ$ material dilatation coefficient;
- for $\alpha = 90^\circ$; $L2_{max} = 70...80$ m;
- for $\alpha > 90^\circ$; $L2_{max} = 35...40$ m;

After choosing the length of the arms, the configurations are checked by calculations.

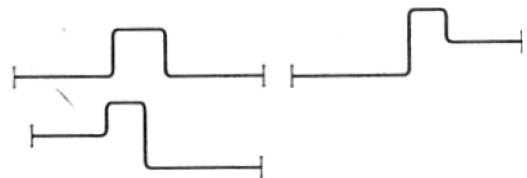


Fig. 1 Natural elastic compensators in U shape

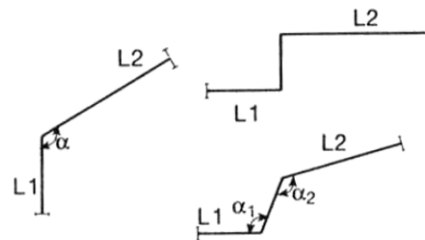


Fig. 2 Natural elastic compensators in "L" and "Z" shape

3. Preparing the pattern drawing in AutoCAD

According to the information supplied the figure 3 drawing was made, representing the calculation diagram of the elastic configuration in "L" shape.

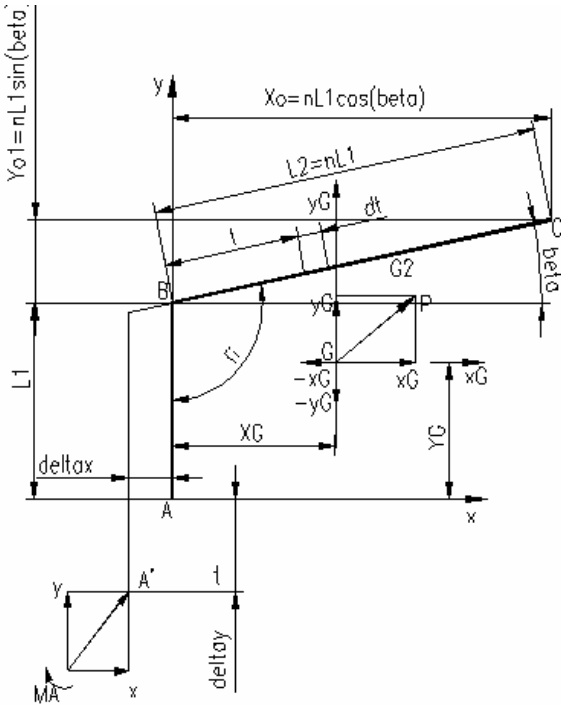


Fig. 3 Calculation diagram of elastic configuration in "L" shape

Input data for natural elastic compensators in form L are presented below:

- the duct is in steel pipe (OL38, OL42, OLT45);
- duct's diameter D_n ;
- length of the arms of the configuration L_1, L_2 ;
- sides of the configuration ratio ($n = L_2/L_1$);
- f_i, β angles, the shape of the elastic compensator
- heating agent temperature t_f [degrees];
- assembly temperature t_0 [degrees];
- α – coefficient for dilatation of the material employed [mm/mm·K] is enclosed in the tables.

The figure 4 is transformed in pattern drawing by exploding sizes and erasing their values. Each size coordinates will be written down for the purpose of developing a Script files in C++ application, completing all unknown data of the pattern drawing.

3. CNE application

The application called CNE in C++ programming language was made to calculate natural elastic configurations, according to the specific formula. This program reads the input data of the table CNE.txt, processes the data, lists the data, checks the maximum bending tensile stress for the elastic

configuration under observation and generates the script.scr. file.

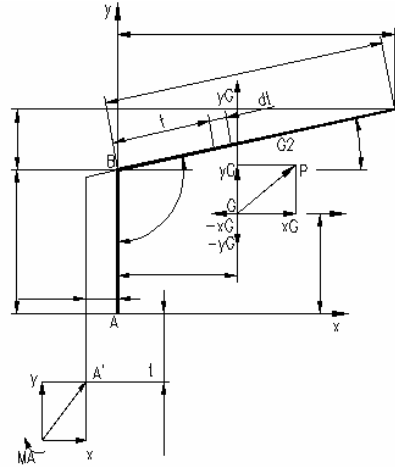


Fig. 4 Pattern drawing

Script files complete the pattern drawing for the calculation diagram of the elastic „L” form configuration, made in AutoCAD. The calculation refers to the following output data:

- Components of point A displacement because of δ_{xax} , δ_{yay} heat deformation;
- Static moments of the system in relation to axes x and y M_{sx}, M_{sy} [cm²];
- Maximum side displacements in the area of bend ducts D_1, D_2 [cm];
- Gravity center coordinates of the system G_X, G_Y [cm];
- System's moments of inertia in relation to x and y axis I_x, I_y [cm³];
- System's moments of inertia in relation to x_G and y_G axis, I_{xG}, I_{yG}, I_{xyG} [cm²];
- Bending moments at A, B, C points, M_A, M_B, M_C [daN·m].

CNE application creates an optimal calculation technology for natural elastic configurations. Several goals were considered for this purpose:

- A pattern drawing was made in AutoCAD, representing the calculation diagram of „L” shape elastic configuration, valid for several dimensions. In this drawing a layer **text** and a text style **ISO** were created.
- Definition of a CNE.txt file with fixed datas (Fig. 5);
- Running the program and creation of SCRIPT files;
- Completion of the template with variable dimensions, processed in C++ application by opening the SCRIPT file;

File	Edit	Format	View	Help				
V500	521	0.8	3000	3000	30	165	10	0.000012
V600	620	0.8	4000	4000	20	150	0	0.000012
V700	720	0.9	5000	5000	20	150	5	0.000012
V800	835	0.9	5500	5500	25	155	5	0.000012

Fig. 5 CNE.txt file

- The pattern drawing was made in AutoCAD according to standards in force. In the end, specific dimensions are completed in AutoCAD, in the pattern drawing by loading the adequate Script file [1,2].

In achieving this application several functions C++ specific participate, suggestively named and allowing input data entering, reading of the existent database, and choice of work branches by summarizing the decision blocks, printing of results and creation of Script files adequate to the chosen branch.

The structure of CNE application is schematically presented by captures from figures 6 and 7.

```

cout<<"\n sigma=" <<sigma;
if (Mmax/W <1000) cout<<"\n Conducta REZISTA";
else cout<<"\n ATENTIE Conducta NU rezista!!!";
}

void fisier(void) //completeaza datenoi.txt
{ FILE *fr;
fr=fopen("datenoi.txt","a");
if(fr==NULL) {printf("\n Nu se poate scrie in date.txt"); return;}
fprintf(fr, "\n\n %2.1f %2.1f %2.1f %2.1f %d %d %2.1f", Vn, Dn, g, L1, L2, beta, tf, t0, alfa);
cout<<"\n Ati completat tabelul datenoi.txt";
fclose(fr);
}

void alegerescript(void)
{
do{cout<<"\n Alegeti generarea fisierelor SCRIPT";
cout<<"\n 1-Fisiere Script, \r\n 2-Renuntare";
cout<<"\n Alegere:";
scr=getche();
switch(scr)
{ case '1':cout<<"\n Fisiere Script"; script(); break;
case '2':cout<<"\n Renuntare"; break;
}
while(scr!='1' && scr!='2');
}

void script(void)
{ cout<<"\n Se creeaza fisiere SCR pentru fiecare desen de executie";
FILE *bl;
bl=fopen("script1.scr","w");
if(bl==NULL) {cout<<"\n Nu se deschide"; return;}
fprintf(bl, "LAYER S text \n");
fprintf(bl, "TEXT S RS 53,159.8 90 %2.0f\n", L1);
fprintf(bl, "TEXT S RS 149,223.5 11 %2.0f\n", L2);
fprintf(bl, "TEXT S RS 124,143 0 %2.2f\n", GX);
fprintf(bl, "TEXT S RS 156,142 90 %2.2f\n", GY);
fprintf(bl, "TEXT S RS 64,134 0 %2.2f\n", deltax);
fprintf(bl, "TEXT S RS 117.3,76 90 %2.2f\n", deltax);
fprintf(bl, "TEXT S RS 120,147 51 %2.0f\n", E4);
fprintf(bl, "TEXT S RS 210,193 276 %2.0f\n", beta);
fprintf(bl, "TEXT S RS 156,240.5 0 %2.2f\n", X0);
fprintf(bl, "TEXT S RS 53,192 90 %2.2f\n", Y01);
fprintf(bl, "TEXT S RS 377,12.6 0 %s\n", Vn);
cout<<"\n Sa creac fisiereul script1.scr ";
fclose(bl);
}
    
```

Fig. 7 CNE application capture – function script ()

```

//CNE.txt
//Vn Dn, g, L1, L2, beta, tf, t0, alfa;
//V500 521 8 30 30 30 165 10 0.000012

main()
{
password();
help();
int ml;
ifstream fp("CNE.txt"); //tabel de date
if (fp==NULL){cerr<<"\n Nu se poate deschide";return 1;}
cout<<"\n ";
cout<<"\n Introduceti date:"; // date intrare
cout<<"\n =====";
cout<<"\n Reper teava:"; cin>>Vn;
cout<<"\n Material teava:"; cin>>Mat;
cout<<"\n Coef. de dilatare liniara alfa :"; cin>>alfa;
cout<<"\n Momentul de inerție I (cm4)"; cin>>I;
cout<<"\n Modulul de elasticitate longitudinala E (daN/cm2)"; cin>>E;
cout<<"\n Modulul de rezistenta al sec. conductei (cm3)W:"; cin>>W;

do{ fp>>Vna>>Dn>>g>>L1>>L2>>beta>>tf>>t0>>alfa; //citire tabel
//bucia de, while pentru verificarea datelor din prima coloana
ml=memcmp(Vn, Vna, 6); //compara datele introduse cu cele din tabel
if (fp.eof())
{cout<<"\n NU sunt valori din fisier! ";
cout<<"\n Doriti sa continuati astfel ?";
cout<<"\n (d/n)";
if (getche()=='d')
{cout<<"\n Val Dn:"; cin>>Dn;
cout<<"\n Val g:"; cin>>g;
cout<<"\n Val L1:"; cin>>L1;
cout<<"\n Val L2:"; cin>>L2;
cout<<"\n Val beta:"; cin>>beta;
cout<<"\n Val tf:"; cin>>tf;
cout<<"\n Val t0:"; cin>>t0;
cout<<"\n Val alfa:"; cin>>alfa;
fisier();
calcule();
rezultate();
alegerescript();
if (sfarsit()==0) return 0;
else return 0;
}while(ml!=0);
calcule();
rezultate();
}
    
```

Fig. 6 CNE application capture – function main ()

The function **calculus()** covers all calculus necessary for the development of script.scr file and for the maximum bending moment. A part of calculus () function is presented below:

```

void calculus(void)
{n=L1/L2; fi=90+beta;
betar=(beta/180)*pi; fir=(fi/180)*pi;
D1=alfa*(tf-
t0)*L1*(n+sin(betar))/cos(betar);
D2=alfa*(tf-
t0)*L1*(1+n+sin(betar))/cos(betar);
deltax=alfa*n*L1*cos(betar)*(tf-t0);
deltay=alfa*L1*(1+n*sin(betar))*(tf-
t0);
AA=deltax*deltax+deltay*deltay;
X0= n*L1*cos(beta);
Y01= n*L1*sin(beta);
xG1=0; yG1=L1/2;
xG2=0.5*n*L1*cos(betar);
yG2=L1+0.5*n*L1*sin(betar);
Msx=yG1*L1+yG2*L2;
Msy=xG1*L1+xG2*L2;
GX = Msy/(L1+n*L1);
GY= Msx/(L1+n*L1);
Iy=1/3*(pow(L1,3)*pow(n,3)*cos(betar)*
cos(betar));
IXG=Ix- ((L1+L2)*pow(GY,2));
IYG=Iy- (GX*GX*(L1+L2));
IXYG=IXy- (GY*GX*(L1+L2));
NumX=E*I*(deltax*IYG +deltay*IXYG);
X=NumX/(IXG*IYG-(IXYG*IXYG));
MA = (X*GY-Y*GX)*0.01;
MB = (X*(GY-L1)-Y*GX)*0.01;
    
```

```

MC1= Y*(n*L1*cos(betar)-GX)*0.01;
MC2 = X*(L1*(1+n*sin(betar))-GY)*0.01;
MC= MC1-MC2;
cout<<"\r\n MC (daN.m):" <<MC;
z = max(MA, MB); Mmax = max (z,MC);
sigma = Mmax/W; }

```

3.1 Running CNE.CPP application

The CNE application is focused on the organization of database for reading, for organizing, for improving and processing the database of the compensating device form L (Fig. 3) using C++ language.

The variable data will be entered during the running of user-friendly programs, most of which are elaborated by means of high level languages such as C++. Especially designed to process data, these programs work with a part of the constant data and make calculations, have decisional blocks, provide information and lists on the screen or prints data. The final step is to generate a script file.

The script file loaded in AutoCAD in the adequate pattern drawing completes the variable dimensions resulting in the detail engineering for the calculus diagram of the L-form elastic configuration.

Upon running, the program requests a password to open the program, calls the database, with the possibility to enter data in the case of new items. The program initially includes information concerning how data are entered and how decision blocks are completed.

To provide an example, one presented captures during CNE.exe file running in the case of item V600.

Fig. 8 displays the input data window, in this case, data for item V600.

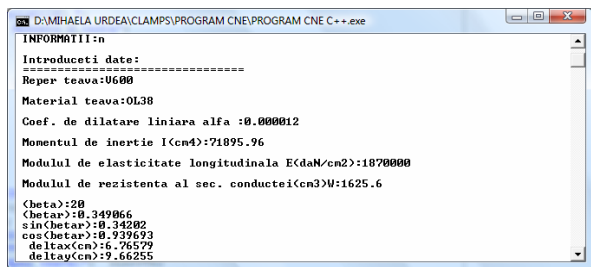


Fig. 8 Input data

If the program running window displays the warning "Data file cannot open!", means that the CNE.txt file is not in the catalogue that generated the file CNE.exe.

The next capture (Fig. 9) represents the results

print. Input data are listed from the data table CNE.txt and the calculated data too.

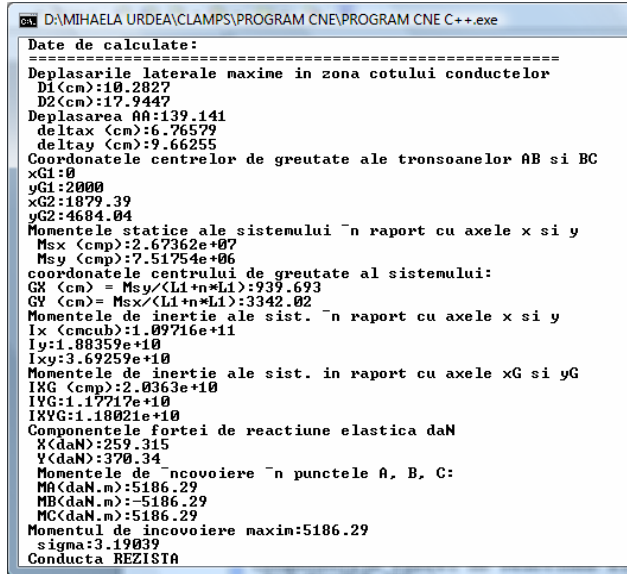


Fig. 9 Data listing

The Script decision block allows the generation of the script file. Script1.scr file is obtained. This file contains a sum of Layer and Text commands, writing the calculated values in the defined positions.

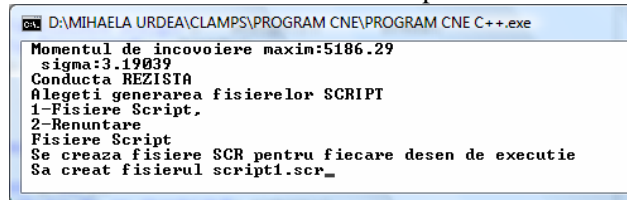


Fig. 10 The dialog box for script file

Figure 11 displays the script file obtained when running the program. These files could be recognized by AutoCAD or other CAD programs. The Script files are text files and this method could be used to the simple representations without scale [1,2].

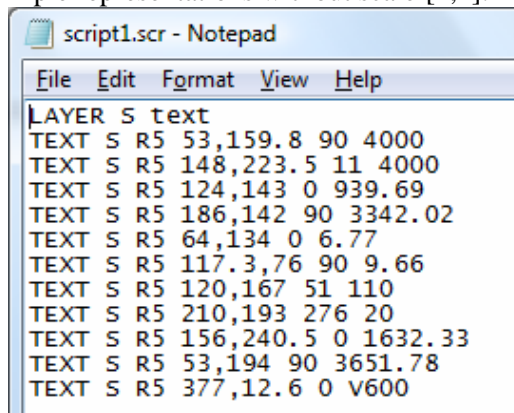


Fig. 11 Script1.txt file

In case the data proposed by the user are not in the CNE.txt database, there is the possibility to enter data from the keyboard. Figure 12 capture displays this possibility.

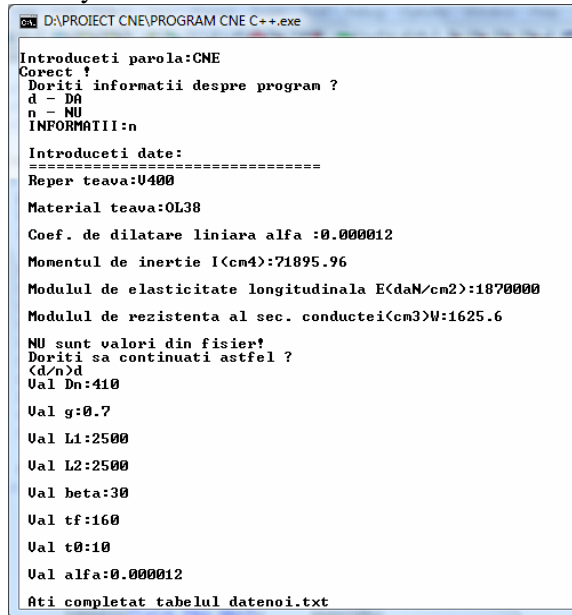


Fig. 12 Data not existent in the CNE.txt database

A newdatas.txt file results when the program is run, including all the new data proposed by the users. Figure 13 displays the newdatas.txt. file

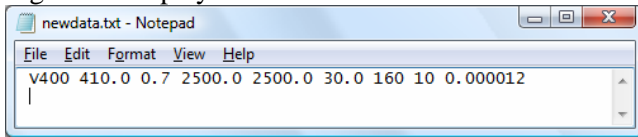


Fig. 13 Newdatas.txt files

3.2. Generation of the final drawing

Using the SCRIPT command activated in AutoCAD in the pattern drawing, the missing

dimensions are completed with value. At the end, the final drawings result (Fig. 14) for V600, conduct's diameter $D=600$.

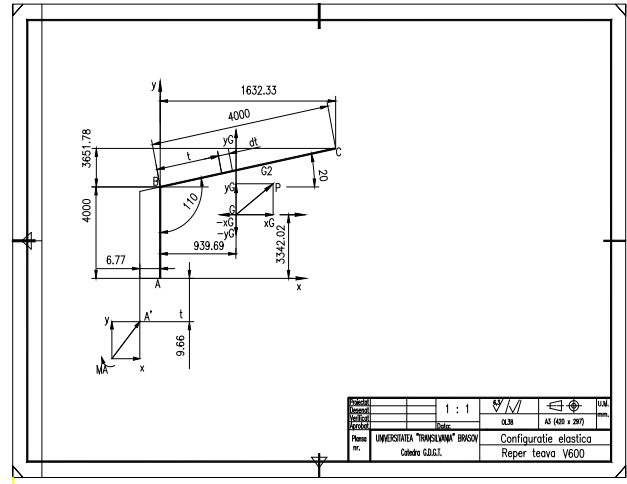


Fig. 14 The final drawing

4. Conclusion

The use of computers in the conception activity and the achievement of technological processes confers numerous material advantages:

- reducing the costs of preparing the manufacture, either directly or indirectly, by significantly saving the time for planning the technological process, special devices;
- high quality design work by accelerating the flow of information and eliminate routine;
- possibility to store a large amount of information and accessing such in a short time;
- coordination with other sectors of design, using network connected common database;

References:

- [1]Urdea, M., C++ Application for organizing, improving and processing the database International Conference "Mechanic and Machine Elements", Technical University of Sofia, Bulgaria, 2005, pp. 240-243.
- [2]Urdea M., Computer-Aided Design. Technological Design Software Libraries, Creation and Operation of Database, Publishing University 'Transilvania' Bra ov, 2006.

Mihaela Urdea , Transilvania University of Bra ov

Emilia Scheibner , Transilvania University of Bra ov

MATHEMATICAL MODELING OF THE EXPERIMENTAL DATA FOR THE DEEP DRAWING FORCE

Ion Neagoe
neagoe_ion@unitbv.ro

Alexandru Filip
filipal@unitbv.ro

Abstract: *The calculus of the deep drawing force is one important stage in the manufacturing design process. This paper aims to offer a new method for an accurate calculus of the force, based on the experimental data, collected during real experiments conducted by the authors. The values of the force were recorded with digital measurement equipment, together with the corresponding values of the punch stroke. After the experiments, a mathematical modeling in MathCAD was done, based on four types of regressions, most used in the field. There were considered three main parameters on which the force depends, namely the part's diameter and thickness and the deep drawing coefficient. The comparative analysis of the mathematical model with the experimental data has shown its accuracy.*

1. Introduction

The manufacturing process by deep drawing is very useful in industrial fields such as automotive, home appliances, electrical equipment, due to its very high efficiency. On the other part, the optimization of the process is hard, because of the many parameters of influence, which often create instability.

In the case of deep drawing of cylindrical products have been carried out many studies regarding the variables of the deformation process. One of them is the forming force, usually called the punch load [1], [2], [8].

The correct estimation of the forming forces is one important issue which leads directly to the success of the manufacturing process. These values decide the type of press which will drive the forming die and also will be used for the strength calculus of the die components.

Most of the technical literature [1], [2], [4], [8], [10] present for the calculus of the deep-drawing forces both analytical and empirical equations, but still, their results are not as accurate as needed. Usually, the results of these equations give higher values than the real ones, conducting to an overload prediction of the forming device. The fact imposes researches in the field to try to establish some more accurate equations for the calculus of those forces.

This paper uses a new method for assessing the correct mathematical model for the calculus of the

punch load by using experimental data which are modeled with suitable regressions. The accuracy of the method is high and the equations proposed are easy-to-use for manufacturing design and simulation purposes.

A modern equipment for experimental research was used, including a digital system for measuring and recording the process parameters, as well used in today modern experimental research, [3], [4], [6], [9]. Such a system was developed by the authors of this paper, under the frame of the national research platform *PlaDeTIno* [9], developed in the authors' department.

The experimental data was then modeled in MathCAD software, with the most appropriate regressions and a mathematical model is proposed, in the case of soft steel, named DC04 Am, SR EN 10130+ A1.

2. The experimental methodology

The experiments were realized in the research lab of "Cold Forming Technologies", at Transilvania University of Brasov. The manufacturing equipment (fig.1) was driven by a hydraulic press (pos.1), with the nominal force $F_n=100\text{ kN}$. The deep-drawing die (pos.2) is provided with several sets of tools, having different values of the die hole diameter d . Each die has a set of punches, according to the sheet thickness,

to assure the same punch-die clearance for all the tests.

The recording and measuring system is composed by a resistive transducer for tensile/compressive forces (pos.3) with the range 0...250 kN, an inductive transducer for movements (pos.4), with the range 0...200 mm and a digital measurement unit for data acquisition (DAQ), type HBM® Spider 8, with four channels. The unit was connected to a computer, which recorded the experimental data.

The measurement tasks with the Spider Pack system are relatively easy to carry out. The specialized software, catman® Easy, quickly recognizes the measuring devices connected to the computer and offers a wide range of visualization, recording and analysis of the data. The software can manage two major types of projects: data acquisition (DAQ) or data analysis. For each type, one can design its own configuration of the tasks and their visualization or can use previous designed ones.

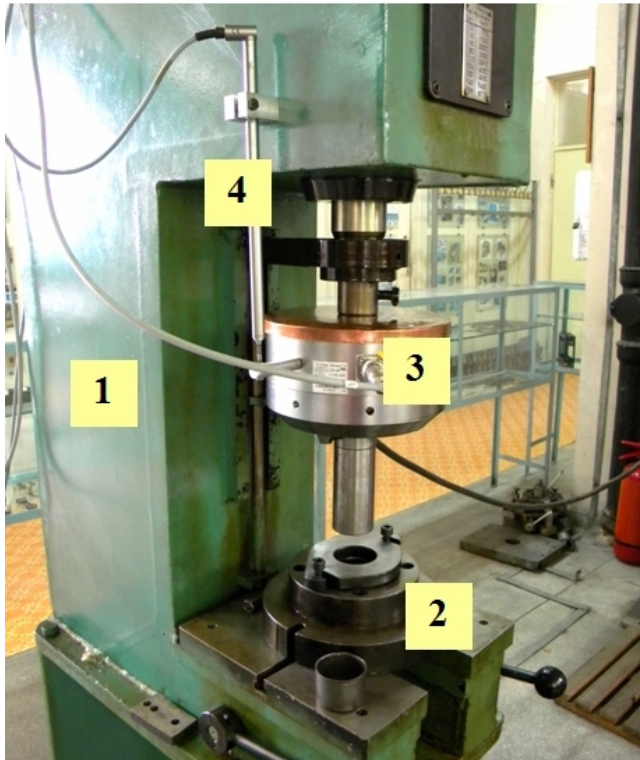


Fig.1 Experimental equipment used for the tests

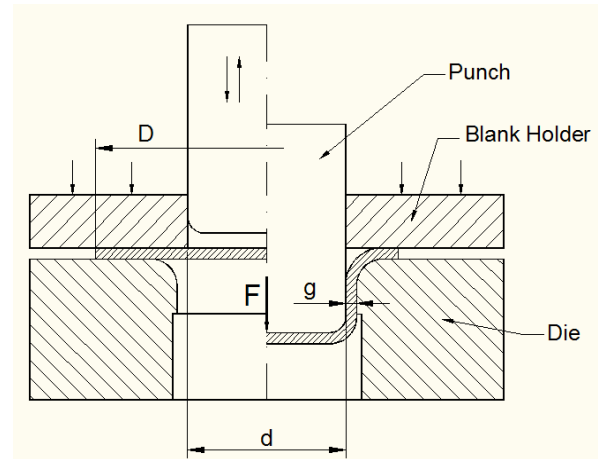


Fig.2 Principle of deep drawing of cylindrical parts, using planar blank holder

The experiments were realized when manufacturing cylindrical flangeless parts, made of soft steel sheet, type DC 04 Am, SR EN 10130+ A1. The range of the parameters used is the following:

- for the part's diameter d : 30, 40, 50 and 60 mm;
- for the sheet thickness g : 0.6, 0.8, 1.0 and 1.2 mm;
- for the drawing coefficient m : 0.5, 0.6, 0.7 and 0.8.

The notations are according to fig.2, where the deep-drawing principle is presented. The deep drawing coefficient was calculated with the well-known equation:

$$m = \frac{d}{D} \quad (1)$$

The working die had a planar holding ring and mineral oil was used as lubricant. The blank holder force was supposed invariant as it was realized by clamping with a screw-nut system.

The catman® Easy software can display the recorded data in several ways, such as table of all values or special ones like min, max or average or under the shape of graphs $F=f(\text{time})$ or $F=F(h)$, where h is the punch travel. For example, for a certain test, the recorded data is presented such in fig.3.

In fig.4 there are presented some of the parts which were manufactured, having different values of the geometrical parameters.

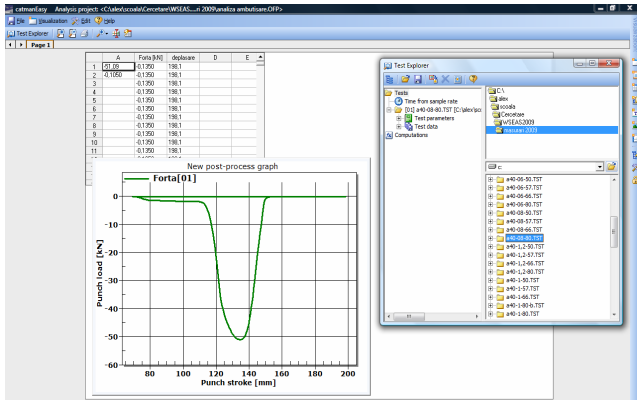


Fig.3 Dependence of punch load on the punch stroke, recorded with catman® Easy software



Fig.4 Parts manufactured during the experiments

The experimental data was analyzed by drawing some graphics, to present the laws of variation of the maximum values of the deep drawing force, depending on the main process parameters.

As shown in figs. 5 and 6, the values of the forces rise with the thickness g and with the diameter d , due to cross-sectional area increase of the part.

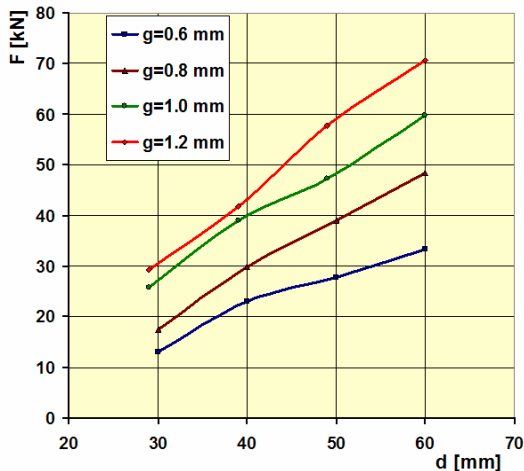


Fig.5 Deep drawing force depending on the diameter d , for several values of the thickness g , for $m=0.6$

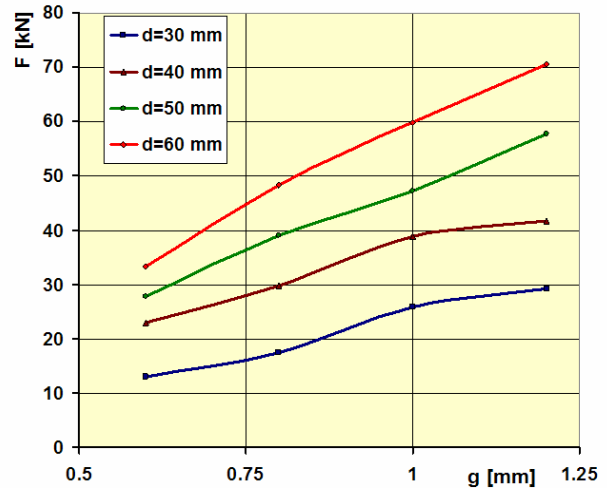


Fig.6 Deep drawing force depending on the thickness g , for several values of the diameter d , for $m=0.6$

The influence of the deep drawing coefficient is as expected, meaning the force increases with the decrease of m , which intensifies the deformation process. The law of variation is presented in fig.7.

As the digital equipment records also the punch stroke variation in time, the punch load depending on the punch stroke can be analyzed. A comparison between the different shapes of this diagram, for different values of the deep drawing coefficient, in a certain case of part's diameter and thickness, is presented in fig.8.

The use of diagrams presented in figs.5 to 7 for estimating the deep drawing force during the design stage of the manufacturing process is rather difficult.

Technical literature, [1], [2], [7], [10] propose empirical equations, using a correction coefficient to adjust the theoretical model of the maximum strain values which determines the values of the deep drawing forces.

This paper proposes a new approach, the mathematical modeling of the experimental data by regressions, aiming to obtain a simple, but more accurate equation for the calculus of the maximum value of deep drawing force.

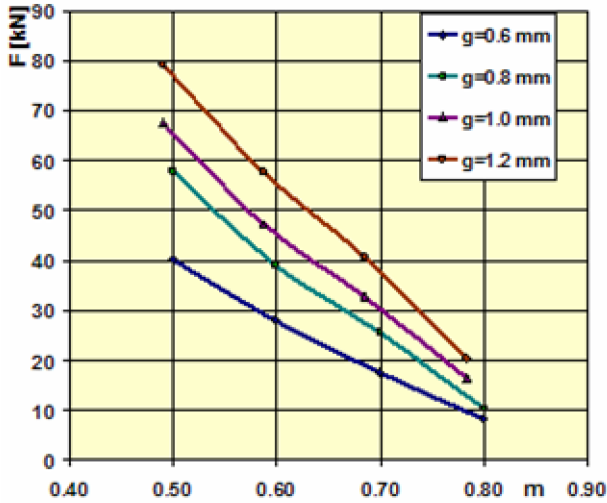


Fig.7 Deep drawing force depending on the deep drawing coefficient m , for a certain diameter, $d=50\text{ mm}$

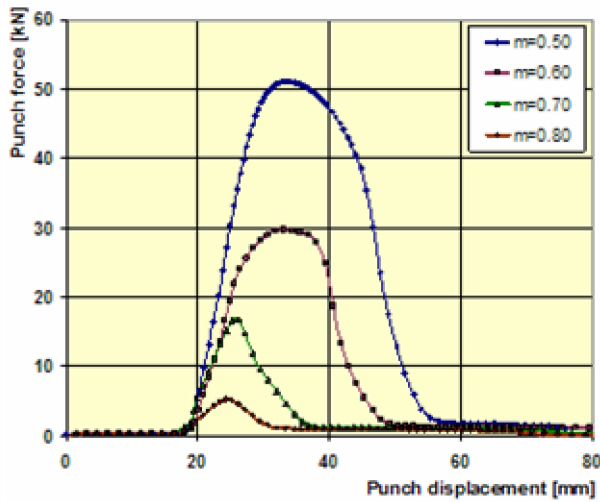


Fig.8 Punch load depending on the punch stroke, for $d=40\text{ mm}$ and $g=0.8\text{ mm}$

3. Mathematical modeling of the experimental data

Usually, the dependence between the parameters of a manufacturing process can be represented [5] like a matrix:

$$T = \begin{pmatrix} x_1 & y_1 & \dots & t_1 \\ x_2 & y_2 & \dots & t_2 \\ x_3 & y_3 & \dots & t_3 \\ x_4 & y_4 & \dots & t_4 \end{pmatrix} \quad (2)$$

meaning that parameter T is depending on the parameters x, y, \dots and t .

In the case of the present research, the values of the deep drawing force F is considered to depend on the part's diameter d and thickness g and the drawing coefficient m , calculated with the equation (1), meaning three parameters of influence.

To assess the mathematical equation which stays behind the matrix (2), a method of modelling with a suitable software can be used.

For the present research an application created under the MathCAD® environment [5], specially designed for the task was created. The application can test four types of regressions, the power, the exponential and the 2nd and 3rd degree polynomial ones.

The application calculates the parameters of each type of regression and the correlation ratio,

$$R_c = \sqrt{1 - \frac{\sum_{i=0}^{n-1} (w_i - f(x_i, y_i, z_i))^2}{\sum_{i=0}^{n-1} (w_i - m(w))^2}} \quad (3)$$

where w_i are the data values to be modelled and $m(w)$ is the mean value of the data series.

As shown during the experiments, the deep forces depend on three parameters,

$$F = f(d, g, m) \quad (4)$$

After running the MathCAD application, the results were analyzed, considering a minimum acceptable value of the correlation ratio

$$R_{c_{\min}} = 0.95 \quad (5)$$

which is usually recommended in such situations [4].

Among the four types of regressions analyzed, there was chosen the power type, as it passed the correlation ratio test and it is enough simple to be used by specialists during the design stage of the manufacturing process.

The general shape of the power regression is:

$$F(d, g, m) = c_1 \cdot d^{c_2} \cdot g^{c_3} \cdot m^{c_4} + c_5 \quad (6)$$

and considering the values of the coefficients c_1, c_2, \dots, c_5 , given by the MathCAD modeling, the equation is

$$F(d, g, m) = 0.083 \cdot d^{1.253} \cdot g^{0.903} \cdot m^{-2.521} + 0.2515 \quad (7)$$

To check the precision of the eqn.(7), a comparative graphical representation was done, between the experimental and the modelled data, for a certain set of parameter values. As shown in fig.9, the

modelled values are quite near to the experimental ones.

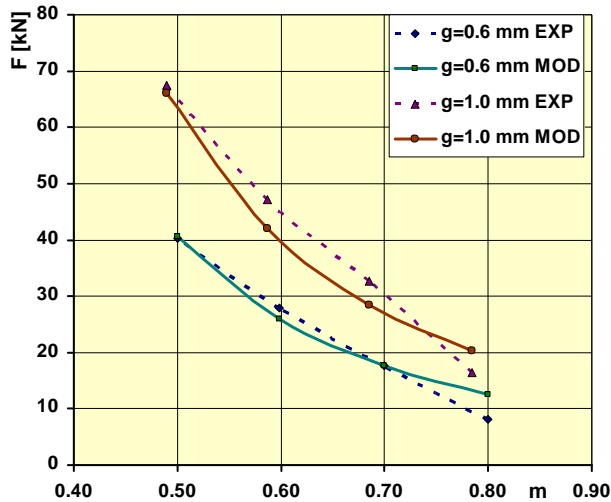


Fig.9 Comparative values of the experimental and the modelled data, for $d=50\text{ mm}$

The use of eqn.(7) is more convenient than using the diagrams presented in figs.5 to 7 and surely more

accurate than the empirical equations given by the most technical literature.

4. Conclusions

The correct calculus of the deep drawing force is an important issue during the design stages of a manufacturing process by cold forming.

The method of determination of a suitable model for this calculus, proposed in this paper, gives more accurate results, also easy to apply in industrial environment.

The eqn.(6), assessed for DC 04 Am SR EN 10130+ A1 steel sheet, can be surely and successfully used by the design engineers to calculate the estimated value of the deep drawing force. The equation was determined by mathematical modeling with regressions of the experimental data, recorded during the tests conducted by the authors.

Further research can assess similar equations for different sheet materials or for different types of the blank holder system.

References

- [1] Boljanovic, V., *Sheet Metal Forming Processes and Die Design*. Industrial Press, 2004.
- [2] Iliescu, C. (1990), *Cold Pressing Technology*. Elsevier Publishers, London, 1990.
- [3] Karabegovic, I., E. Husak, Mathematical modeling of deep drawing force with double reduction of wall thickness. *Mechanika* no.2(70), 2008.
- [4] Martinescu, I., Filip, A.C., Neagoe, I. *Researches on the recording of the functional parameters at the cup-drawing of cylindrical parts*. Proceedings of the International symposium REV – Remote Engineering and Virtual Instrumentation, 2004, Carinthia Tech Institute, Kassel University Press, Villach, Austria.
- [5] Morariu, C.O., T. Paunescu *Informatic aplicat în inginerie – MathCAD*. Editura Universit ii Transilvania, Bra ov, 2004.
- [6] Neagoe, I., Filip, A.C. Digital system for measuring and recording the forces during the cold pressing operations. *Proceedings of the 2nd International Conference “Computing and Solutions in Manufacturing Engineering – CoSME’08”*, 2008, University Transilvania of Brasov, Romania.
- [7] Neagoe, I., Filip, A.C. Experimental research on digital measuring and recording of the deep drawing forces, *Proceedings of the 2nd International Conference “Computing and Solutions in Manufacturing Engineering – CoSME’08”*, 2008, University Transilvania of Brasov, Romania.
- [8] Park, D.H., Yarlagadda, K.D.V. Effects of punch load for elliptical deep-drawing product of automotive parts. *International Journal of Advanced Manufacturing Technology*. Vol. 35:814–820, 2006, Springer Verlag Limited.
- [9] PlaDeTIno, *Research Platform for Innovative Technological Developments* (2007). Available from <http://www.unitbv.ro/it/TCM/Platforma/index.htm>, accesed May 2009.
- [10] Stoughton T.B., Model of drawbead forces in sheet metal forming. *Proceedings of the 15th IDDRG*, 1988, Dearborn, USA and Toronto, Canada, Pp. 205-215.

Ion Neagoe, University “Transilvania” of Brasov

Alexandru C. Filip, University “Transilvania” of Brasov

IMPROVING ENERGY EFFICIENCY OF THERMAL TO THE NEIGHBORHOOD BY MOUNTING OF SOLAR COLLECTORS INTENDED FOR THE DOMESTIC HOT WATER

Cristian Mugea

Buzatu Constantin

Lepadatescu Badea

Abstract: *The paper presents a simple and efficient solution to reduce energy consumption (gas) for producing hot water in the neighborhoods of blocks. It is proposed mounting points on the roof of solar panels heat the neighborhood, which through a heat exchanger plate, will perform pre-heating water from network entry in the boiler water heating. In this way is done during a year savings in gas consumption by up to 60%.*

1. Actual State

Expanding use of renewable energy is a major component of EU energy policy, aimed at reducing dependence on imports and reduce greenhouse gas emissions with greenhouse effect.

In 2020, the share of renewable energy resources in the balance of primary resources should reach 20% compared to 8% today.

It can accurately calculate that by investing and implementing water heating systems using solar radiation may be a fuel economy that can exceed 60% of current consumption.

Romania, in terms of energy from the sun, is 6.1 kWh/m²/zi summer, up from 5.5 kWh/m²/zi, which is the average energy received from Germany and Austria, countries that have implemented wide-scale use of solar collectors.



Fig. 1 Solar collectors mounted on a flat roof.

2. Description of functional and technological solutions proposed

On the flat roof of the heating stations will be mounted on concrete plates which provide some stability for wind, solar collectors are a number of 80-90, which will circulate a fluid mixture antigel.

This circuit called "primary circuit, is coupled to a plate heat exchanger, which transfers to solar heat received from the network and stores water in hot water accumulation tanks menajera. Masa total roof-mounted solar installation will be 3150 kg for solar (90 panels x 35 kg / panel), which will add weight concrete props needed fixing their roof. Manufacturer of solar collectors installed, depending on the surface is roof assembly plant and the conditions to ensure the best conditions for exposure to ami direction "South". Thus, the collector works in a good yield and spread radiation of the sun, which represents 50% of the total radiation.

Figure 2 presents a diagram of principle of how the installation operates with the ACM preparation with solar energy.

The primary circuit of solar collectors, circulating an antifreeze liquid, which the pumping system is sent to the primary circuit of a heat exchanger plates. Water from the network is passed through the secondary circuit of the shift to peace, where the thermal energy received over the hotel roof-mounted solar collectors.

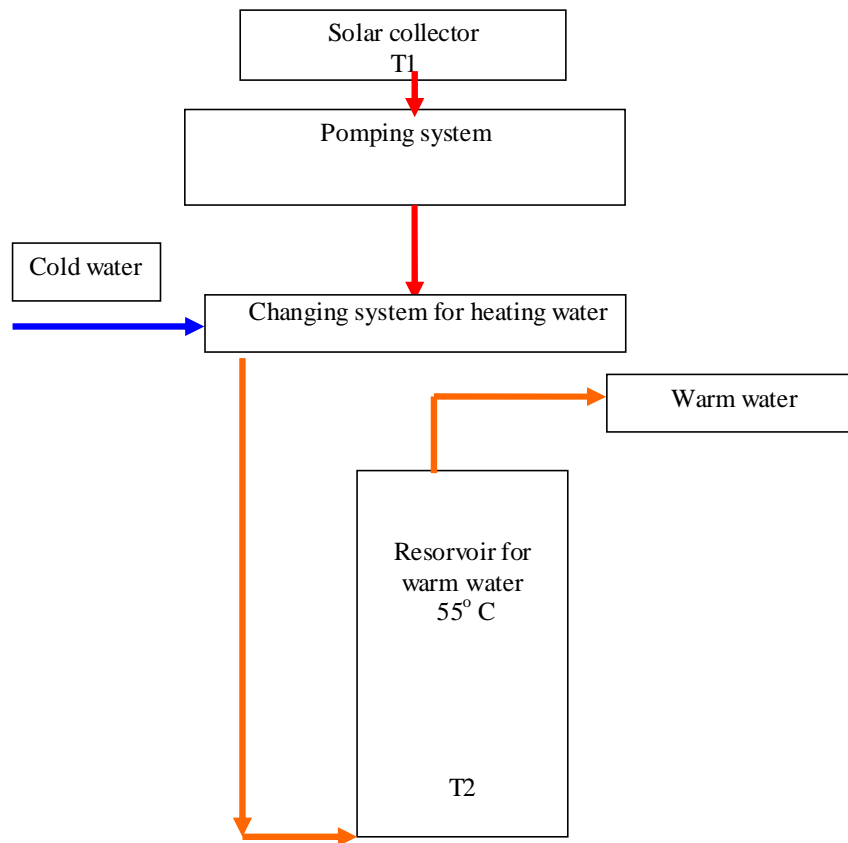


Fig.2 The principle scheme of the installation of solar-DHW preparation

The plant became operational at the time when the primary in solar collector temperature is 50C higher than that of the storage tank. Instalataia is designed to secure solar DHW temperature of 550 C, which will be stored in existing storage tanks to some large hotels.

To be effective as a large installation by secondary flow, water storage tanks will be recycled during the sunlight through plate heat exchangers, which are mounted separately from existing now.

The moment when the collector temperature is lower than that of storage tanks, pump stops and the recirculation of the primary circuit. In these conditions, will start in automatic heating system for DHW preparation.

Should be mentioned that during the summer and diffuse radiation from the sun get 50% of the total radiation received, can provide pre-heating water in good conditions in the network.

References

- [1] N. Muge. Economic aspects of renewable energy, agro tourism complexes in Romania. Mechanization of Agriculture. No.9-2005.
- [2] B. Lepadatescu, N. Muge. "Increasing energy efincieny of touristic buildings by mounting solar collectors for warm water preparing Sofia 2-4 Noiembrie 2006-Machine & Machine Elements.
- [3] N. Mugea, B Lepadatescu. Microfarm Ecological energy independent by using renewable energies "- Sofia 2-4 Noiembrie 2006-Machine & Machine Elements

Energy Efficiency and Sustainable Development

Energy efficient material in a building system with real example

Crutescu Ruxandra Crutescu Marin Nicolaie Costache Ismail Ozgur Viorel Badescu
Dragos Hera Florin Iordache Liviu Drughean Gabriel Ivan Anica Ilie Nadine Laaser
ruxandra.crutescu@passiv.ro

1. Planning the first romanian passive office building.

We have demonstrate that it is possible to create an innovative, sustainable office building by respecting the passive house standard with a very easy to build efficient energy technology. That means neopor insulated concrete forms -ICF- produced in Romania, at Bragadiru, for the envelope and excellent work areas for headquarters of Amvic Group. This building is the **first passive office building in Romania** which was planned in year 2007 and built in 2008, in BRAGADIRU. We want to give an example for everyone, most of all for romanian people and authorities, to show in reality the very big advantages of the passive house standard. We have the hope that this will increase the courage of the romanian architects, engineers and especially of authorities to follow our example. For the participants at the 13 Conference we want to present how good

the sustainable efficient energy concept was put in value in this first passive romanian office building. What should be emphasized here is that we considered all conditions of the real estate for maximum benefit of its advantages. We wish to share our experience with all the specialists who are interested to get to know this concept. Further we want to point out that the passive house standard is an ongoing success story if you know how to take it into account in an intelligent way. Starting from the planning of an energy efficient and sustainable solution and continuing with the building process which was very simple, we have obtained an environment- friendly result by using the ICF energy efficient building system. The PHPP was a real help for planning.



Fig.1 – Plain view of Amvic Building



Fig.2 – Facade of Amvic Building

2. Energy Efficient Solutions

We try to put in value and speculate the local conditions in our advantage, to make the most efficient possible the energy saving for all the processes in this building.

The insulated concrete forms –ICF- fabric offer partial protection for this building. We have a heat-earth recovery in the garden who offer preheating or precooling of the fresh air for the entire building. The building is oriented with its main facade towards South. Within the space of the building with commercial and office purpose, the cold and hot water consumption being usually reduced. The lighting will be made by electric lamps with reduced consumption and sensitive system related to the illumination opportunity. Equipments like heating pumps, regenerative heat exchangers (between introduced air and evacuated air, fresh earth-air), solar panels and all equipments are with a low energy consumption (fans, pumps).

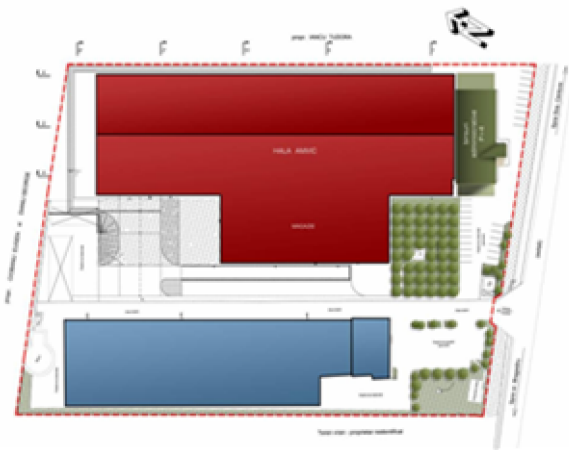


Fig.3 – Site plan

The heating system of the building is made with hot air generally prepared with unconventional sources: soil heating taking over, pre-heating in a battery with heat carrier from a surface of solar receptor from an industrial process, heating recovery from the air exhausted, final heating being accomplished with heating pump water - water.

During summer, the interior air –conditioning is accomplished, that is its cooling by means of a reversible heating pump. The electric power necessary to generate the cooling task will be

approximately three times lower than the heating effects.

For the air-conditioning dimensioning and the hot water preparation necessary for the functioning of the building, an assessment of the necessary heating and, respectively, of cold for the administrative house was accomplished under different challenging climatic conditions , summarized under the form of some equivalent temperatures.

In wintertime we use steam from the production process of insulated concrete forms as a source for the additional heating system. This offers gratis energy to be used in the building.

Other important aspects are:

- for envelope and structure of the building we have used Neopor ICF with an additional thermal insulation of Polystyrene (24kg/m³) to the exterior and Thermofloc to the interior

- for the thermal insulation of the roof we used Thermofloc and Polystyrene

- the U-value of glazing is 0,5 W/ (m² K),of the whole window (incl.aluframe)0,8 W/ (m² K)

- jalousie for solar protection

- for preheating/ precooling of the fresh air we have a awaduct (Rehau) in the garden nearby

- the building has a good protection on the north side , consisting of the production hall

- using renewable energy of sun

- heatpumps for floor heating system

Due to the technological processes within the plant that is located close to the passive house the flow of hot technological water with an approximate temperature of 70 °C that totalize a maximal volume of 120 mc for a three hours interval, for the day period and for approximately 9 months each year. During the very cold period of the year, this heating source is reduced as a consequence of the reduction of the technological process for producing expanded polystyrene. This source of energy is used in order to increase the temperature of the fresh air at the output of the switch with soil and before entering the filtration stage. The heating pump is the key equipment of this appliance and it functions in the cooling mode or in the heating mode, according to the season.



Fig.4 – Solar vacuum installation on Amvic Building



Fig.5 – Solar vacuum panels on the roof

Waste energies represent the energy sources of the heating pump; these types of energy can be renewable or with low heat potential and they are freely disposed in the nature.



Fig.6 – Interior optimal confort in Amvic Building



Fig.7 – current level plan

Moreover, in order to increase the energetic efficiency of the building, by means of reducing the power consumption in the warm period of the year, the cooling down the space with external air (free cooling) can be accomplished, according to the necessities; the flow of air can increase for a greater efficiency of the cooling process until a maximal value of 150% of the value of the nominal flow.

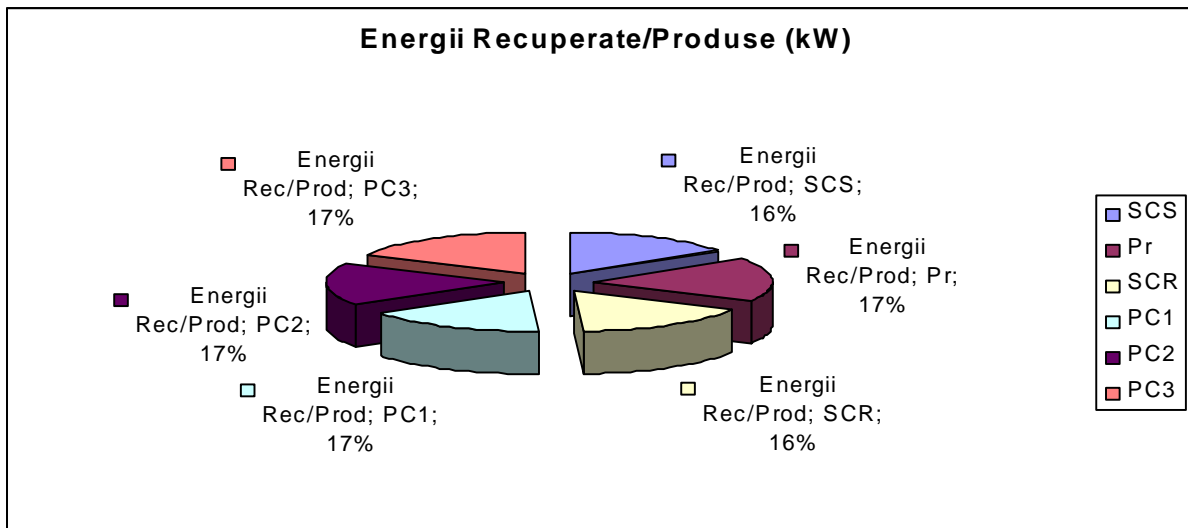
Thus, heating accumulated over a day in the inertial elements of the building will be evacuated by

means of free cooling phenomenon the next day the cooling unit being only used to eliminate the heating and humidity gains due to human activity as well as to the heating gains due to the equipment used. It is not recommended to accidentally open the windows for a natural ventilation because this action must be very well correlated with the external temperature as a random usage can lead to supplementary energetic consumptions.

4. Conclusions

Graphic 1 presents the energy saving for each equipment as well as the global saving that is accomplished using the energetic loops developed in the functional scheme. Moreover, an approximate value of 50% is represented by the energy recovered from the environment (soil, sun) and from the energy of the interior air, thus resulting only the necessary quantity for producing 50% of the total power. The isolation degree is highlighted once again by the energy need for the heat pump 3 that only covers the power losses to the exterior.

At the present, the building described is finished and Passivhaus Proiect and Amvic Ltd are doing their activities as well inside of the very beautiful building; during cold period and also warm period ,the building is in process to monitoring of the energetic consumptions and to the analysis of their improvements.



Graphic 1. Recovered energy/ Products for attaining the indoor heat comfort

This monitoring as well as the entire building is part of the program “INOVARE”, in collaboration with Politechnical University of Bucharest based on the

European Union Grands Projects and the Research Department of Amvic Group Romania.

References

[Feist 2007] Feist, Wolfgang, Protokollband Nr. 18 – Qualitaetssicherung beim Bau von Passivhausern (2007)

[Feist 2005] Feist, Wolfgang, Protokollband Nr. 31 – Energieeffiziente Raumkuhlung (2005)

[Feist 2004] Feist, Wolfgang, Protokollband Nr. 27 – Waermeverluste durch das Erdreich(2004)

[Feist 2003] Feist, Wolfgang, Protokollband Nr. 22- Lueftungsstrategien fuer den Sommer (2003)

[Feist 2001] Feist, Wolfgang, Gestaltungs-grundlagen Passivhauser (2001)

- [Schnieders 2007] Schnieders, Jurgen, CEPHEUS-Wissenschaftliche Begleitung und Auswertung (2005)
- [Hera 2006] Hera, Radu – Usage of the heating pumps for dwelling heating, an ecological solution and power efficient, rev. The plumber, no 9/2006, ISSN 1223-7418, pag. 26-37 (2006)
- [Hera 2004] Hera R., Mateescu, I., Ivan, G – Optimization of power consumption within buildings by using heating pumps systems (Conf. a XI-a a Installation Fac. With international participation „, Efficiency, confort, power conservation and environmental protection’’, Buc. 25-26 nov. 2004), publ. CD. conf. 6 p. (2004)
- [Badescu 2005] Badescu V., 2005, Use of soil thermal energy for passive house heating, 2nd International Symposium, "Renewable Energies And Sustainable Development", 24 – 26 September, Tulcea, Romania. (2005)

AN ALGORITHM FOR OPTIMIZATION OF A POWER DISTRIBUTION NETWORK

Gheorghe-Dan Sorea

gheorghe.sorea@unitbv.ro

The actual increasing demand for energy requires a lot of research efforts to be invested in finding of better solutions. One way is to optimize the existing resources and equipment based on new IT technologies. This paper presents an algorithm for optimization of a power distribution network by taking into account more parameters than the classical approach of the problem being closer to the real practical aspects which occur in such networks.

1. Introduction

The optimization of the power transportation and distribution networks is one of the most important research directions of our society in the actual increasing demand for energy. In this context, the optimization means the obtaining of the minimum power losses between sources and consumers, having all other quality aspects fulfilled.

The aim is to increase the exploitation performances of the existing networks based on the same resources or less, and to find the best solution when further development is necessary. For that reason, an algorithm for calculation of a dynamic network was developed and adapted to the specific characteristics of these networks.

For greater networks the distributed calculation is also possible by dividing the original network in several subnetworks and each one of them can be viewed as a calculation cell.

2. The Optimization Algorithm

2.1. The calculation of the network

The network is calculated when all electrical sizes are known (currents, voltages, powers). In the real cases of the distribution networks, the voltages of the nodes corresponding to the stations are known, and all the other sizes must be calculated.

The network can be associated with an oriented graph in which the nodes are the stations and, respectively, the transformation posts. Each line represents an edge of the graph. The best way of the graph representation in mathematical form is the matrix representation.

A matrix based method for solving the networks is the nodes potentials method[1]. This method is based on the first Kirchhoff theorem and uses the A matrix, the admittance matrix Y and the sources matrix U .

The A matrix is called the reduced incidence matrix of the graph and its lines correspond to the node whereas the columns correspond to the edges. The terms can have the values:

+1 - if the edge leaves the node;

-1 - if the edge enters into node;

0 - if the edge does not belong to the node.

The Y matrix is called the admittance matrix and it is a square matrix in which the diagonal contains the complex admittances of the edges. The U matrix contains the voltages of the sources, in this case the voltages from the secondary windings of the transformers from power stations.

This method has the advantage that the matrix A of the graph can be modified automatically very easy according to the modification of the network, thus it is suitable for dynamic networks.

The matrix of the currents I can be calculated with the following formula:

$$I = Y \cdot U + Y \cdot A^t \cdot V' \quad (1)$$

where the V' matrix is a column matrix called the nodes potentials matrix. If one replaces the above formula in the first Kirchhoff theorem:

$$A \cdot I = 0 \quad (2)$$

some substitutions can be made:

$$I' = A \cdot Y \cdot U \quad (3)$$

$$Y' = A \cdot Y \cdot A^t$$

and one can obtain the following equivalent equation system:

$$-Y'V' = I' \quad (4)$$

The system can be solved by using the specific numerical methods such as Gauss elimination method or Gauss-Seidel method[2], and the V' column matrix is obtained. After that one can evaluate the voltage drops, the currents, the powers and the power losses[1].

Each line of the network can be considered as in the following figure:

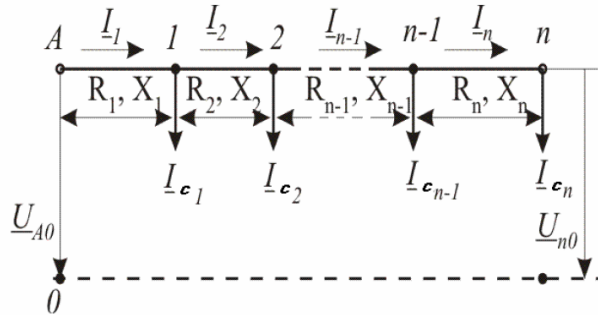


Figure 1. Electrical schema of a distribution line

For each transformation post the charge is variable during the day, according to the type of consumers, and one possible current vs. time charging characteristic is represented in the following figure:

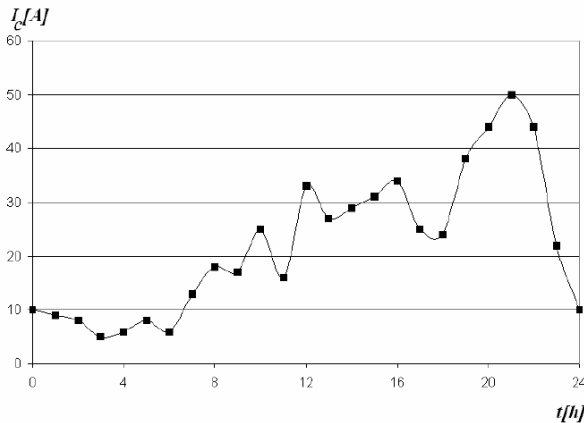


Figure 2. The load characteristic in a transformation post (current vs. time)

2.2. The Basics of Optimization Algorithm

The function that must be kept to its minimum value is the total power losses. An example of a distribution network in which all possible links between nodes are made is presented in the figure 3.

The empty nodes are the sources nodes, whereas the others are the nodes corresponding to the posts. Some of the lines are active and some of them are not active.

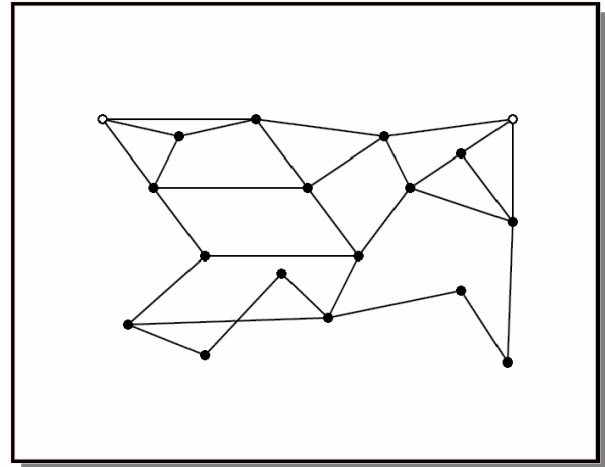


Figure 3. The Network

The optimized schema will contain only those lines that will supply all the nodes with the minimum of the power losses. An example of such a network can be seen in the next figure:

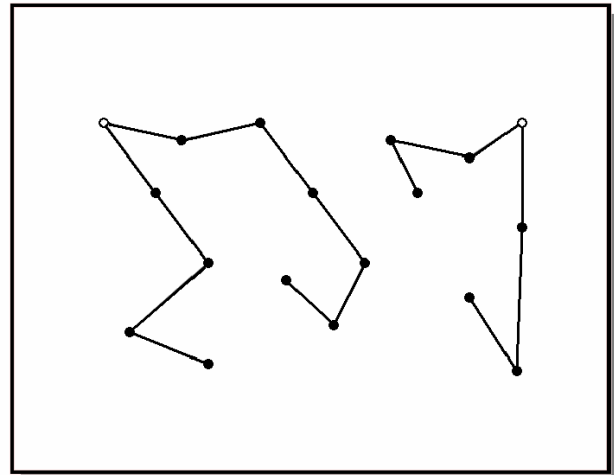


Figure 4. The Optimized Network

One can see that the power losses in the lines are proportional with the length of the lines if the level of the voltage is already established. According to this rule, the mathematical condition that must be satisfied is:

$$\sum l_k = \min \quad (5)$$

Another factor that has a great influence is the square of the current I . Using the classical approach of the network optimization methods, this factor

influence is neglected because it is very difficult to predict the values, as in figure 2. If the currents are taken into account better results will be obtained. The new approach lead to the following formula:

$$\sum I_k^2 \cdot l_k = \min \quad (6)$$

2.3. Results

A comparison will be made between three configurations of the same network:

- A. in the first case the network was optimized using (5) as optimization condition and is presented in figure 4.
- B. in the second case the network was optimized using optimization condition {6}, but condition (5) was neglected – figure 5.

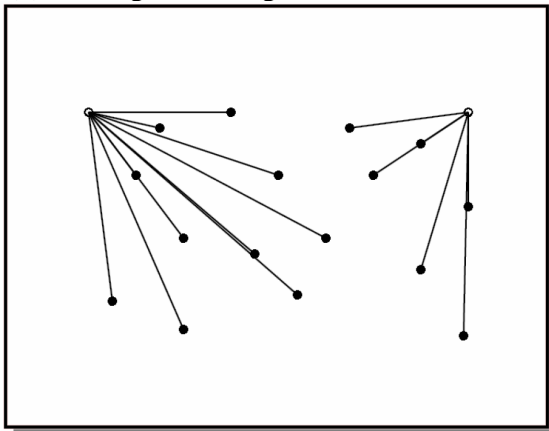


Figure 5. The optimized network using condition {6}

- C. In the third case both conditions {5} and {6} were used for optimization of the network – figure 6.

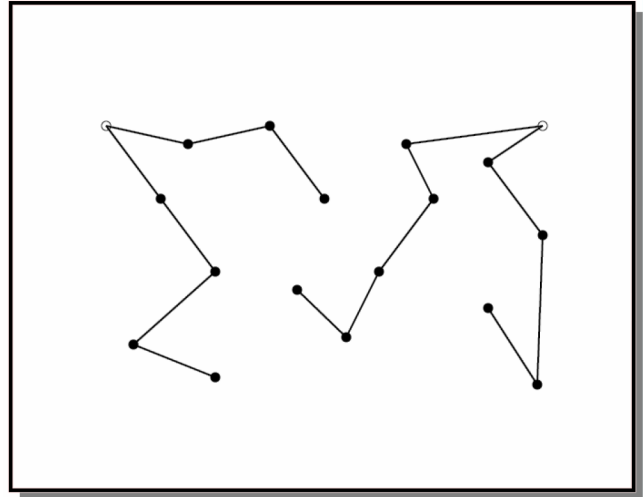


Figure 6. The optimized network using both conditions {5} and {6}.

The results of the comparison are presented in the table 1.

Table 1

Network	A	B	C
Power [kVA]	14872.26	15172.82	15000.82
Power Losses [kW]	820.23	236.81	710.80
Power Losses [%]	5.52	1.56	4.74

From the above table the case B can lead to the less power losses, but, because the condition {5} is not satisfied, this case is more difficult and more expensive to be implemented. The case C can lead to better results for a longer period regarding the power losses than the case A.

3. Summary

References:

[1] N. Balabanian. Electrical Network Theory. John Wiley and Sons Inc, New York, 1969.

An algorithm and a computer program for optimization of a power distribution network which takes into account more parameters than the classical approach was presented. In this way more parameters than the classical approach of the problem were involved, and the situation became closer to the real power distribution networks.

[2] M. N. Sadiku. Numerical Techniques in Electromagnetics - 2nd. ed. CRC Press LLC, Boca Raton, 2001.

Gheorghe Dan SOREA – Lecturer ,PhD ,Engineer, “Transilvania” University of Brasov

3D

**A
E**

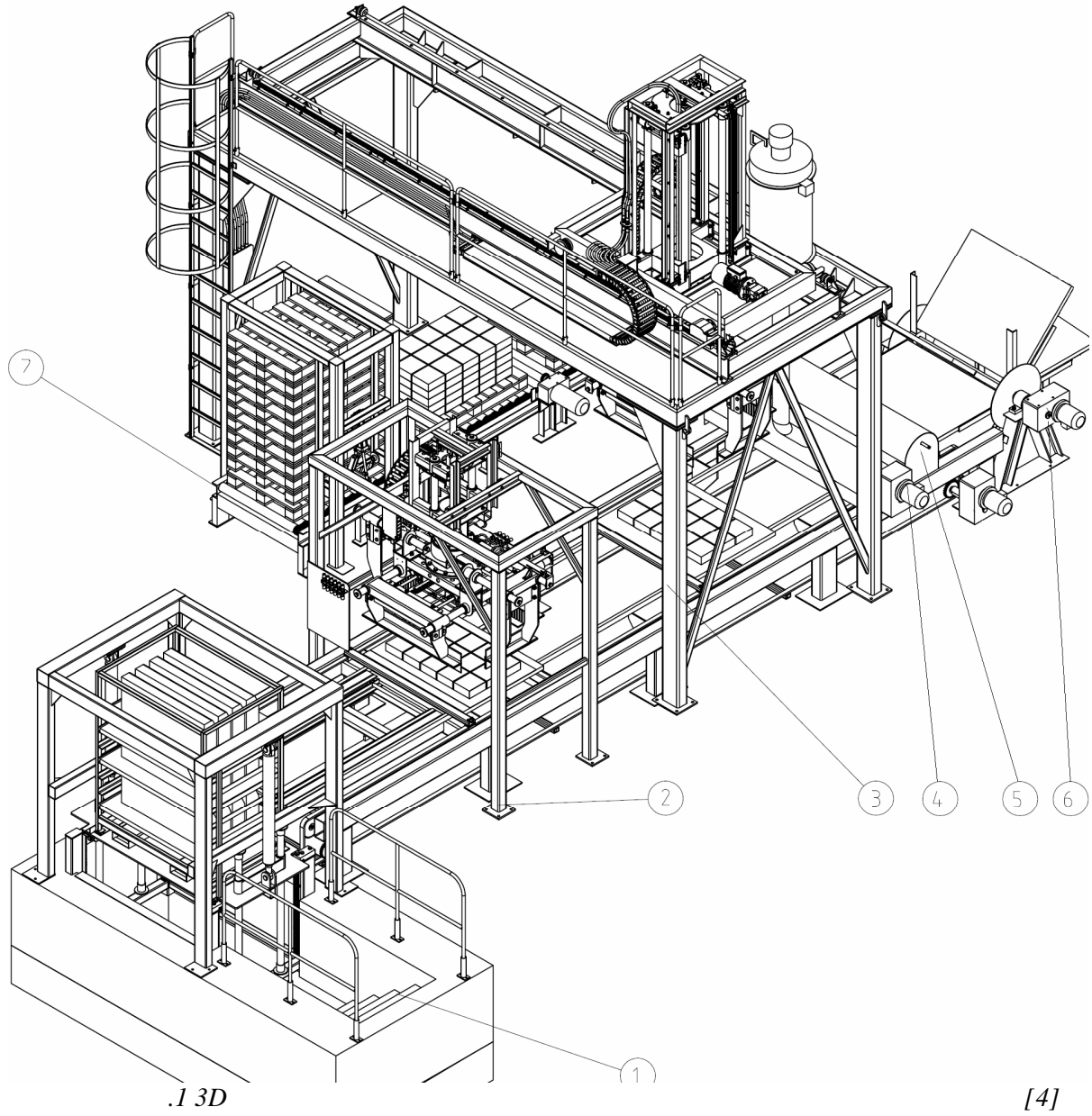
ivoianakiev@mail.bg

e 3D

: CAD/CAE, 3D

I.

), -
, -
, -
, -
70 XX , , -
- [9,10]. -
-
CAD - , -
, - /
CAD () [1,2]. (-
3D -) [4], 3D
[7],
.. [6,7].
2.
[4].
[5,8]. 80-90 30-35 ²
-
, -
, ..
280 ²
3D () 2D (- 1400 ².



3D

.1.

(3)

1

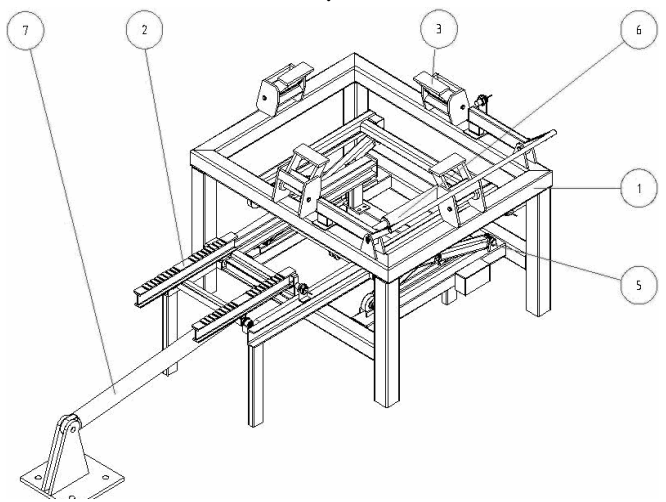
(2),

7 , (5), (7), (6) (5) (4). (3), 10,2 (6) (5). - 12), (

3D

CAD

3D



2. 3D

– CosmosMotion 2008.

(2),

(7)

(2)

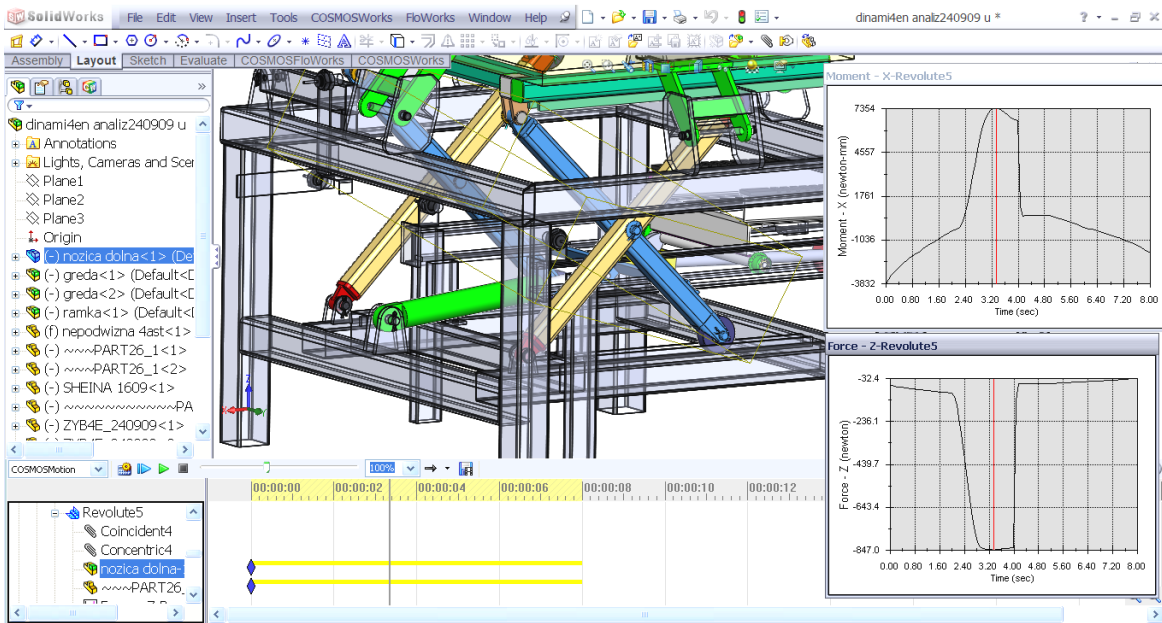
FFE () CAE
(CosmosWorks 2008)

4

CAE,

3.

e
3D



. 4.

3D

1. A. SolidWorks / CosmosWorks 2006/2007.
2. A. SolidWorks 2007/2008.
3. „, 2005, „, XIV
4. „, 2005”, , 440 – 445 .
5. „, 2009.
6. „, 2000 .
7. „, 2005
8. CAD
9. „, 2004 .
10. Bedworth, D., M. Henderson, P. Wolfe Computer-Integrated Design and Manufacturing, McGraw-Hill, Inc. New York 1991.
11. Moaveni, S., Finite Element analysis. Theory and Application with ANSYS, Prentice Hill, New Jersey, 1999.
12. Oden, T., Nonlinear Finite Element Analysis of Elastomers, MSC. Software Corporation, Los Angeles, 2001.

ENGINEERING SIMULATION AND ANALYSIS 3D MODEL OF GATHER MACHINE AS A PART OF AUTOMATIC LINE FOR CONCRETE PARTS

I. Ianakiev

Abstract

In the present work are made simulation of the movement on a 3D model of gather machine as a part of automatic line (AL) for concrete parts. There are chosen optimal displacement, velocity and acceleration for the flexible parts of the machine. There are made force analysis of particular mechanisms on the determinately static positions. Part of construction is modified to avoid collision between parts during the work.

Keywords: CAD/ CAE, 3D model, simulation, gather machine

Assist.prof. Ivo Ianakiev, Ph.D, Technical University-Sofia

СИНТЕЗИРАНЕ НА СИСТЕМА ОТ ГРАФИЧНИ СИМВОЛИ ЗА РАЦИОНАЛИЗИРАНЕ ПРОЕКТИРАНЕТО НА ПРОИЗВОДСТВЕНИ СИСТЕМИ

Радка Петкова
petkova@tu-sofia.bg

Анализиран е системният подход при избор на оптимален вариант на производствени системи за автоматизирано нанасяне на покрития. Направена е класификация на устройствата за изпълнение на частични функции. Разработена е библиотека от графични символи за построяване схеми на производствени клетки за нанасяне на прахови материали. Прилагането ѝ позволява да се рационализират процесите на анализ и синтез..

Ключови думи: *системен подход, производствени системи, изпълняващи устройства, графични символи, автоматизирано нанасяне на покрития.*

1. Въведение

Съвременното производство се характеризира с непрекъснато повишаване степента на автоматизация. Това се отнася и за процесите за нанасяне на покрития, които се осъществяват като крайни, завършващи процеси в производството на практически почти всички изделия. В този аспект е от особено значение да се търси оптимално решение при създаването на производствени системи за осъществяване на тези процеси.

При проектирането на комплекси или линии за автоматизирано нанасяне на покрития чрез автоматични /и ръчни/ уреди за нанасяне е съществено да се определи оптималният вариант на съоръжението, в което се извършва основната технологична операция, в случая – нанасяне на покритие от течен или прахов материал върху обекта на производство. Това дава възможност и е предпоставка за оптимизиране на цялостната производствена система, за повишаване на технологичността и на икономическата ѝ ефективност.

2. Изложение

2.1. Класификация на градивните елементи на производствена система.

За целта обектът на проектиране – производствената система (клетка, участък, линия) се разглежда като “техническа система” [1], притежава-

ща определена функция, структура и дефинирани отношения със своята околна среда.

Структурата на техническата система представлява множество на градивните ѝ елементи и отношенията между тях. Това множество в зависимост от нивото на сложност може да включва различни елементи. При по-сложните производствени системи градивни елементи са отделните производствени клетки (съоръжението, в което се извършва основната технологична операция), транспортните средства и др. технологични съоръжения.

За да се определят градивните елементи на отделна производствена клетка за нанасяне на покритие, първо се формулира нейната обща функция, която се разлага на частични функции.

Общата функция на тази производствена клетка е: нанасяне на определен материал като покритие със зададени параметри върху конкретен обект, при дадени изисквания за качество и производителност.

В Таблица 1 са обобщени формулираните частични функции - I, респективно са класифицирани съответните устройства/ системи, които ги изпълняват – II.

Таблица 1.Класификация на устройствата изпълняващи частични функции.

	I. ЧАСТИЧНИ ФУНКЦИИ	II. ВИДОВЕ ИЗПЪЛНЯВАЩИ УСТРОЙСТВА / СИСТЕМИ			
		1	2	3	4
1	зареждане с нов / свеж прах	Вибромаса със сонда	Система BIG-BAG	Прахов център	...
2	пресяване на новия прах	Вибросито	Ротационно сито	Барабанно сито	...
3	флуидизиране на праха	Флуидизиращ съд	Вибро-Флуидизиращ съд	Съд с разбъркване	...
4	транспортиране на свеж прах	Прахова помпа	Вакуумен транспортър	“Dense-Phase” транспортър	...
5	смесване на свеж и отработен прах	Бункер/съд за прах			...
6	транспортиране на смесен прахов материал	Инжектор	Инжектор с автоматичен контрол	Винтов транспортър	...
7	електростатично зареждане на праха	Електростатичен “Корона” пистолет	“Tribo” – пистолет	Aerobell	...
8	нанасяне устойчив прахов слой				...
9	контрол/управление процеса на нанасяне	Съответни управляващи устройства и обща система за контрол и управление			
10	манипулиране нанасящите устройства	Манипулатор 1 ос	Манипулатор 2 оси	Робот	...
11	събиране/отвеждане на неполепналия върху обекта прах	Транспортираща лента	Система”ракел” с флуид. канал	Кабини с кон- стр. Наклони	Комбинирана система
12	разделяне на възд. - праховата смес - рециклиране на прах	Мултициклон	Мини-/Моноциклон	Лентови филтри	Филтър-патрони
13	пресяване отработен /рециклиран/ прах	Вибросито	Ротационно сито	Барабанно сито	...
14	флуидизиране на отработен /рециклиран/ прах	Флуидизиращ съд	Вибро-Флуидизиращ съд	Съд с разбъркване	...
15	транспортиране на отработен /рециклиран/ прах	Прахова помпа	Вакуумен транспортър	“Dense-Phase” транспортър	...

2.2. Библиотека от графични символи за синтезиране на производствени системи

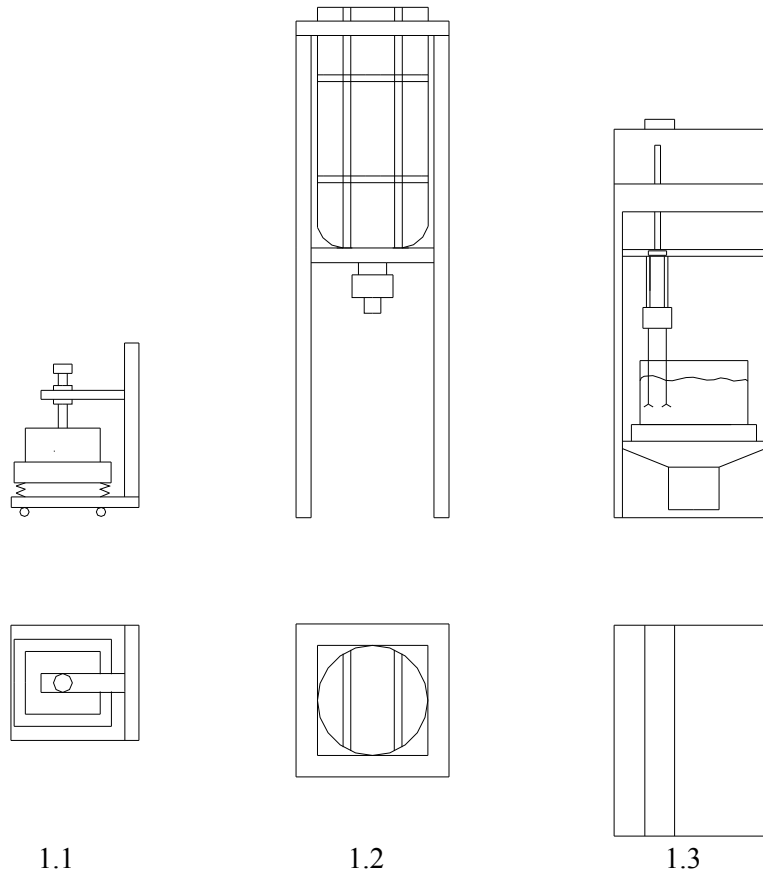
Посочените устройства за изграждане на производствени клетки за нанасяне на прахови покрития се предлагат в практиката от различни

фирми-производители и могат да се представят с обобщени графични символи, базирани на най-разпространените за тях конкретни фирмени схемни изображения.

Разработените по този начин чрез продукта AutoCAD обобщени графични символи, изразяват най-съществените характерни отличия на устройствата, с оглед частичните функции, които изпълняват. Така е разработена една библиотека от унифицирани символи, които могат да се използват от различни потребители – проектантски организации или екипи, конструктори и т.н. независимо от фирмената им принадлежност. Това позволява значително съкращаване на времето и разходите за проектиране на производствените клетки.

На фиг. 1 са показани графични символи от библиотеката на устройства, изпълняващи частична функция 1 – “зареждане с нов/свеж прах”: 1.1 – вибромаса със сонда; 1.2 – система “BIG-BAG”; 1.3 – прахов център.

Графични символи за функция 12 – “разделяне на въздушно-праховата смес (рециклиране на прах)” са представени на фиг.2: 12.1 – мултициклон; 12.2 – моно-циклон; 12.3 – лентови филтри; 12.4 – филтър-патрони.



Фиг. 1 Графични символи на устройства за частична функция 1.

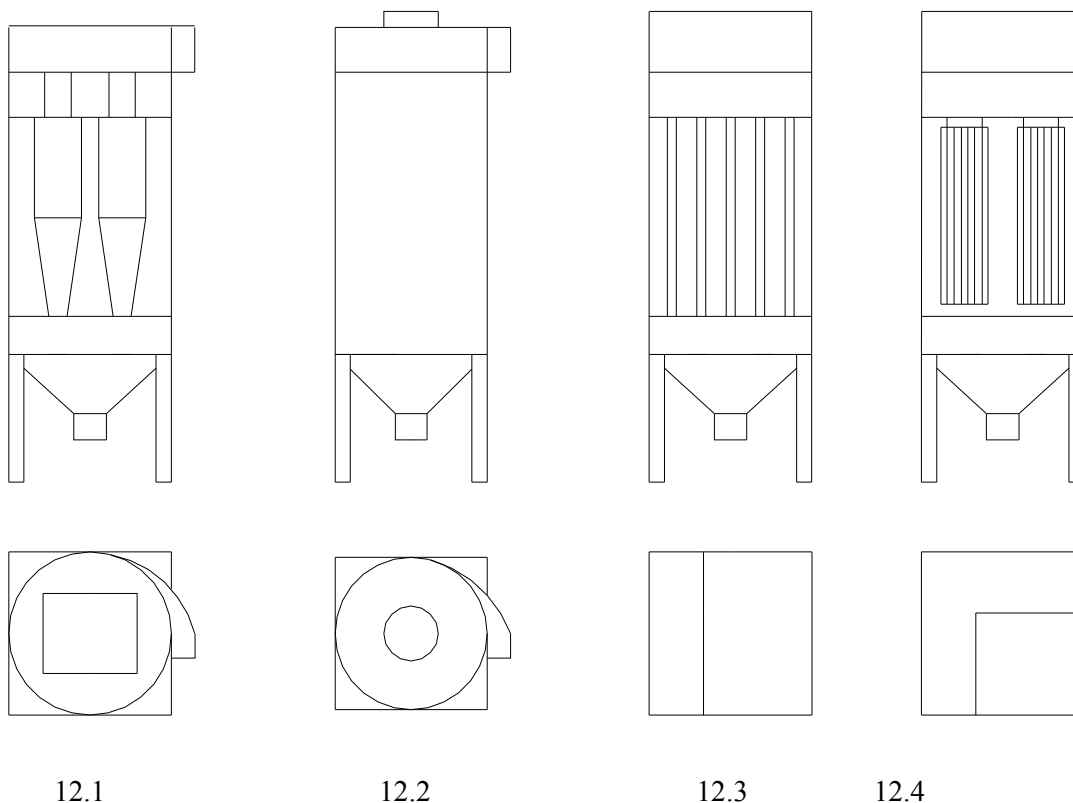
Устройствата, показани на фиг.3 изпълняват повече от една функция – функции 7 и 8, съответно “електростатично зареждане на праха” и “нанасяне на устойчив прахов слой”: |7&8|.1 – електростатичен “Корона” пистолет; |7&8|.2 – “Tribo” пистолет; |7&8|.3 - Aerobell.

Така предлаганата библиотека от графични символи може да бъде допълвана и да се разширява постоянно, съобразно непрекъснато появяващите се в практиката нови устройства за изпълнение на дадена частична функция или при формулирането на нова такава – при развитието

на конкретния технологичен процес за нанасяне на покритие.

Тук трябва да се отбележи, че в библиотеката са включени и графични символи за редица спомагателни устройства, вкл. за съответни енергийни или материални връзки между устройствата, осигуряващи обмен на материали, енергия

и информация, като например кабели и свързващи елементи (съответно управляващи устройства) за високо и управляващо напрежение, маркучи и съответните свързки за материала или за пневмо-/ и хидро-системите и т.н.

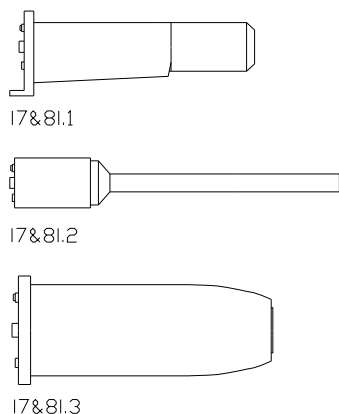


Фиг. 2 Графични символи на устройства за частична функция 12.

3. Заключение

Използването на групирани в бази данни унифицирани графични символи рационализира процесите на анализ и синтез на различни по йерархично ниво на сложност производствени системи за нанасяне на покрития. Т.е. предложената библиотека, съответно допълнена и обогатена може да се използва и при проектирането на цялостни производствени системи – на ниво автоматизирани комплекси и линии или да служи като основа за създаването на по-обща база за осъществяването на тази задача.

Същевременно формулираната основна функция на производствената клетка за нанасяне на покрития е валидна въобще, включително и за производствените системи за нанасяне на покрития от течен материал върху обекта на производство. Това означава, че след формулирането на частични функции за производствените клетки в тези системи, които не се отличават много съществено и по принцип са по-малобройни от вече показаните в Таблица 1, аналогично могат да се класифицират съответните изпълняващи ги устройства.



Фиг. 3 Графични символи на устройства за частична функции 7&8.

Литература:

- [1]Pahl G. & Beitz W., Engineering Design – A Systematic Approach, Springer-Verlag London Limited. 1996, 3 rd printing 2001.
- [2]www.itwgema.com
- [3] www.nordson.com
- [4]www.wagner.de

Доц.д-р.инж.Радка Петкова, Технически университет-София

SYNTHESSYS OF A SYSTEM OF GRAPHICAL SYMBOLS FOR RATIONALIZING THE DESIGN OF MANUFACTURING SYSTEMS

Radka Petkova,

Abstract

Analyzed is the systematic approach in choosing the optimal variant of manufacturing systems for automated coating. A classification of the devices for performing sub-functions is made. Developed is a library of graphical symbols for constructing schemes of production cells for coating with powder materials. Its application allows the processes of analysis and synthesis to be rationalized.

Keywords: *systematic approach, manufacturing systems, performing devices, graphical symbols, automated coating.*

Assoc.prof.Radka Petkova, Ph.D, Technical University-Sofia

kradlov@abv.bg

nkotzev@tu-sofia.bg

3D

3D

12

I.

ANSYS

3D

ANSYS

ANSYS
ANSYS WORKBENCH,

[3].

2.

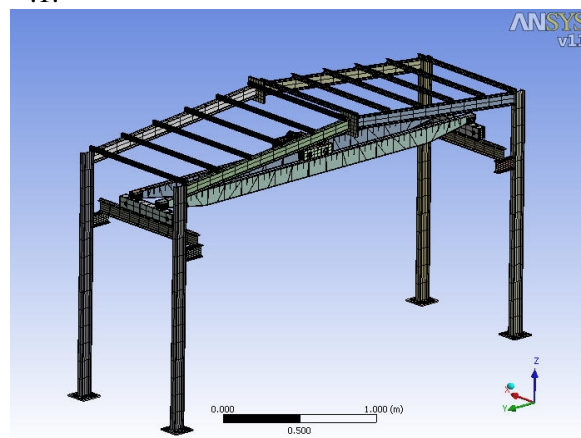
ANSYS WORKBENCH

3D

196

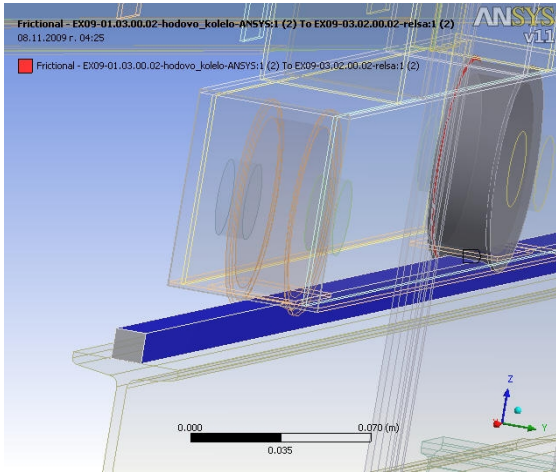
3D

3D



.1

” (frictional)- .2



.2

3D

1.
.1.

	8.8 Hz

ANSYS

WORKBENCH
3D

3D

3D

3D

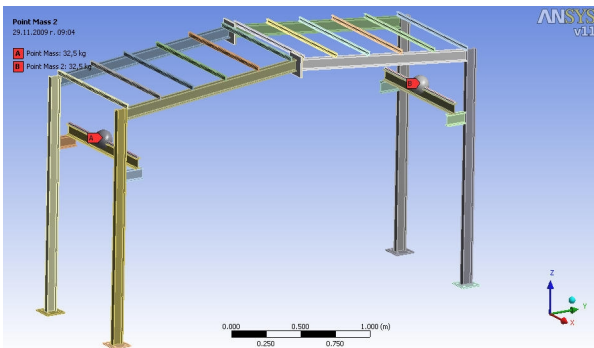
2

.4.

.2.

+ 65 ..

32,5 .- .3.

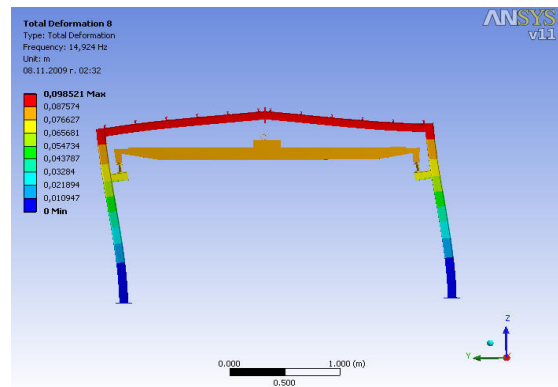


.3

3D

	14.92 Hz

.4



.4

3D

[2]

3D

3D

.5. ” 3 ”

’ ” - ”

.3.

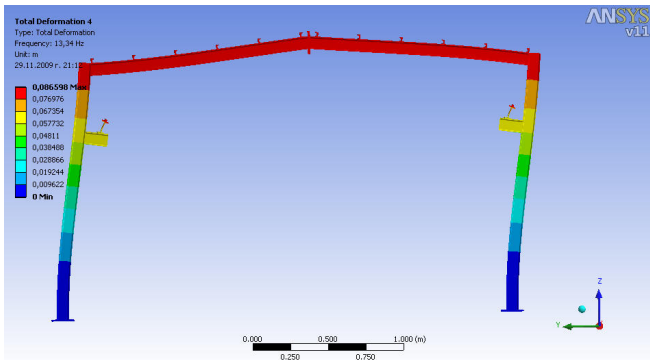
	13.34 Hz
.6	

ANSYS WORKBENCH

.5.

5.

	[Hz]
1.	3,47
2.	10,69
3.	12,32
4.	14,92
5.	26,4
6.	29,74
7.	34,10
8.	34,76
9.	37,60
10.	38,74
11.	61,29
12.	72,16



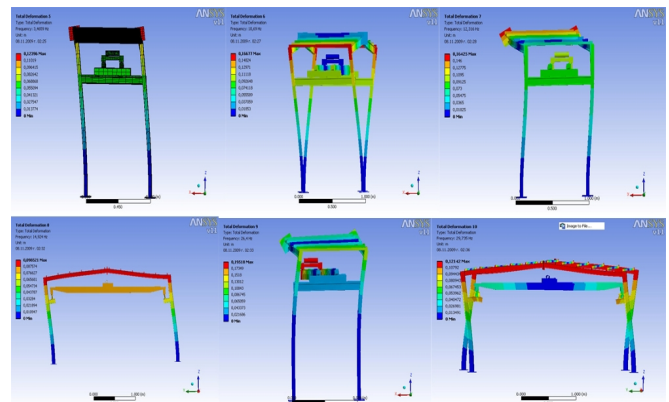
.5

” - ”

4.

.4.

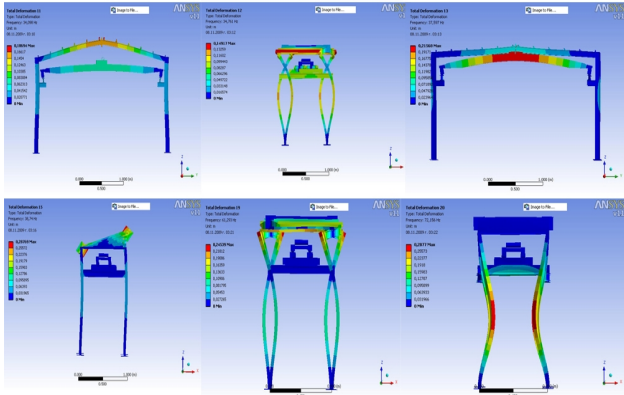
1	59%
2	66%



.6.

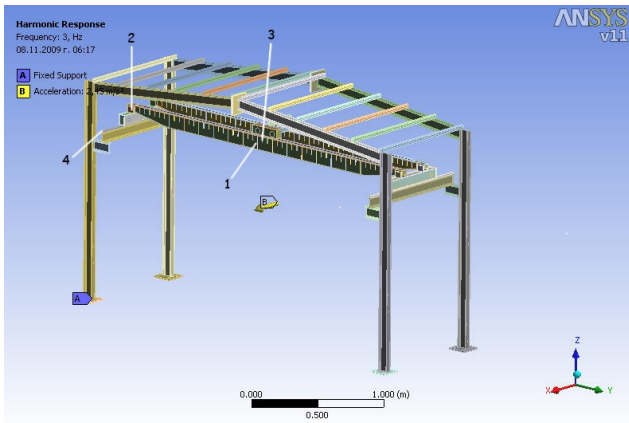
3D

” - ”



.6

"y"- .7



.7

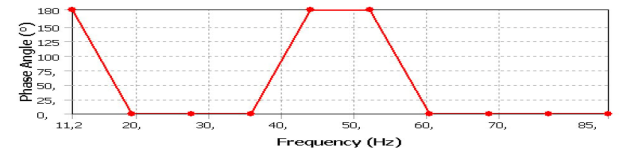
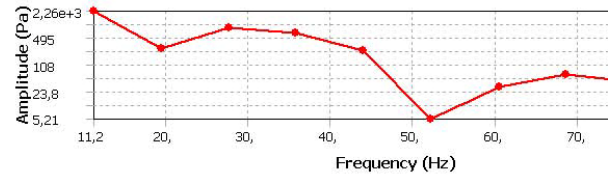
.7.-
2,45[m/s²],
80Hz.
WORKBENCH

- .5:
- 1.
- 1;
- 2.
- 2;
- 3.
- 3;
- 4.
- 4.

=0,25g=
3 Hz
ANSYS

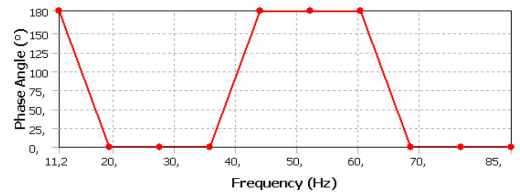
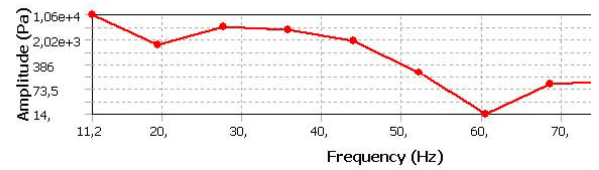
.8, .9, .10, .11

Frequency Response



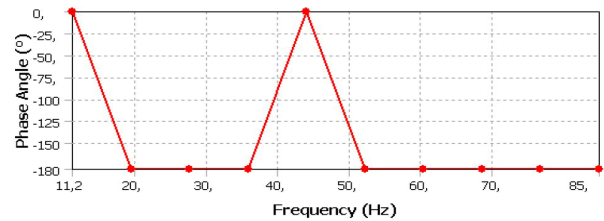
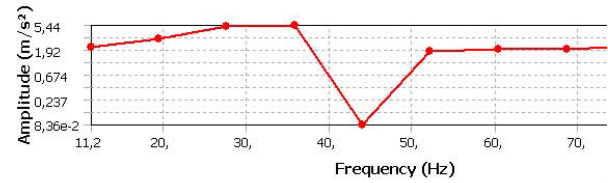
.8

Frequency Response



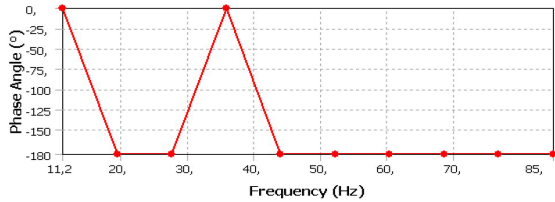
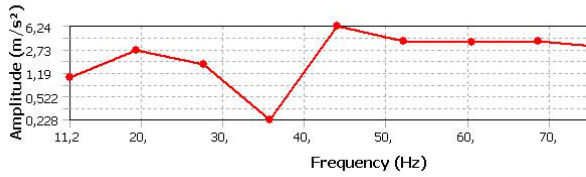
.9

Frequency Response



.10

Frequency Response



.11

3.

“ ”
3D

091 021-06.

1. “ ” ,1987
2. “ ” ” ,2009 .
3. Lawrence. K., Ansys Workbench Tutorial, 2006

SYSTEM “GIRDER CRANE- BUILDING” DYNAMIC ANALYSIS BY USING THE FINITE ELEMENTS METHOD

. Radlov N. Kotzev

Abstract

The present work suggests dynamic analysis of the system “girder crane- building” by using the finite element method. There are developed two kinds of system “girder crane- building” 3D computer models, and an correctness estimation is performed for each of them, by criteria “correspondation to the results from an experimental researchment”. There are also modal analysis performed and the first 12 frequencies and modal forms are obtained. There is a harmonic analysis performed for four parameters: stresses in the main beam middle section; stresses in the main beam end section; acceleration in the main beam middle point; acceleration in the main beam end point in case of external harmonic accelerative actuation.

Keywords: girder crane, finite element method, computer model

Eng. Kalin Radlov, Technical University-Sofia
 Assoc.prof.Nikolay Kotzev, DSc., Technical University-Sofia